LIBRARY & INFORMATICS
NIST(CSIR) TRIVANDRUM
G2877

ESIS AND PHOTOPHYSICAL STUDIES OF LENEETHYNYLENE BASED MOLECULAR SYSTEMS

THESIS SUBMITTED TO
THE UNIVERSITY OF KERALA
FOR THE DEGREE OF
DOCTOR OF PHILOSOPHY
IN CHEMISTRY
UNDER THE FACULTY OF SCIENCE

By

JAMES P. V.

PHOTOSCIENCES AND PHOTONICS
CHEMICAL SCIENCES AND TECHNOLOGY DIVISION
REGIONAL RESEARCH LABORATORY (CSIR)
TRIVANDRUM-695019
KERALA, INDIA

DECEMBER 2006

SYNTHESIS AND PHOTOPHYSICAL STUDIES OF PHENYLENEETHYNYLENE BASED MOLECULAR SYSTEMS

THESIS SUBMITTED TO

THE UNIVERSITY OF KERALA

FOR THE DEGREE OF

DOCTOR OF PHILOSOPHY

IN CHEMISTRY

UNDER THE FACULTY OF SCIENCE

By

JAMES P. V.

PHOTOSCIENCES AND PHOTONICS

CHEMICAL SCIENCES AND TECHNOLOGY DIVISION

REGIONAL RESEARCH LABORATORY (CSIR)

TRIVANDRUM-695019

KERALA, INDIA

AUGUST 2006

STATEMENT

I hereby declare that the matter embodied in the thesis entitled, **"Synthesis and Photophysical Studies of Phenyleneethynylene based Molecular Systems"** are results of investigations carried out by me at the Photosciences and Photonics, Chemical Sciences and Technology Division, Regional Research Laboratory (CSIR), Trivandrum, under the supervision of Dr. K. George Thomas and the same has not been submitted elsewhere for a degree.

In keeping with the general practice of reporting scientific observations, due acknowledgement has been made wherever the work described is based on the findings of other investigators.

James P. V

Dr. K. George Thomas
Scientist EII

Photosciences and Photonics
REGIONAL RESEARCH LABORATORY
(Council of Scientific and Industrial Research)
TRIVANDRUM – 695 019, INDIA

Telephone: 91-471-2515364; Fax: 91-471-2490186
E-Mail: kgt@vsnl.com
Web: http://w3rrlt.csir.res.in

December 06, 2006

CERTIFICATE

This is to certify that the work embodied in the thesis entitled, **"Synthesis and Photophysical Studies of Phenyleneethynylene based Molecular Systems"** has been carried out by Mr. James P. V. under my supervision and the same has not been submitted elsewhere for a degree.

K. George Thomas

Thesis supervisor

ACKNOWLEDGEMENTS

I have great pleasure in placing on record my deep sense of gratitude to Dr. K. George Thomas, my thesis supervisor, for suggesting the research problem and for his guidance, constant support and encouragement, leading to the successful completion of this work.

I would like to express my sincere thanks to Prof. M. V. George for his encouragement, inspiration and useful discussions during the tenure of this work.

I also thank Prof. T. K. Chandrashekhar, Director, Regional Research Laboratory, Trivandrum for providing necessary facilities for carrying out this work.

I extend my heartfelt thanks to Dr. C. H. Suresh, Computer Simulations and Modeling group, for his help and suggestions in my theoretical studies.

I also thank Dr. Nicola Armaroli, ISOF-CNR, Via Gobetti, Bologna, Italy for the help and encouragement I received from him during my stay there. I would also like to thank Dr. P. V. Kamat, Radiation Laboratory, Notre Dame for the femtosecond transient measurements and pulse radiolysis studies.

I sincerely thank Dr. Suresh Das, Head, Chemical Sciences and Technology Division for the useful discussions with him. I would also like to thank Dr. A. Ajayaghosh, Dr. D. Ramaiah and Dr. K. R. Gopidas, scientists of Photosciences and Photonics, for all their help and support. I would also like to thank Prof. P. Ramamurthy, National Centre for Ultrafast Processes, Chennai for

allowing access to the Picosecond Time Correlated Single Photon Counting facilities. I thank all the members of Photosciences and Photonics, in particular Dr. P. K. Sudeep, Dr. Binil Itty Ipe, Mr. Shibu Joseph, Mr. K. Yoosaf, Mr. P. Pramod, Mr. A. R. Ramesh, Mr. Vinayakan, Mr. Robert Philip and Ms. Sarada Nair for their cooperation. I also thank friends in other divisions of Regional Research Laboratory, Trivandrum for their help. I would also like to express my thanks to Ms. Soumini Mathew for NMR analysis and Ms. Viji. S. for mass spectrometry analysis.

I deeply express my gratitude to my parents and family members for their constant encouragement, valuable support and understanding.

James P. V.

CONTENTS

Statement i

Certificate ii

Acknowledgements iii

Preface viii

Chapter 1. **A Brief Review on Phenyleneethynylene based Molecular Systems**

1.1. Introduction to π-conjugated molecular systems 1

1.2. Synthesis of OPE based molecular systems 2

1.3. OPE based molecular wires and electronic devices 5

1.4. OPE based sensors 12

1.5. Objectives of the present work 16

1.6. References 16

Chapter 2. **Photophysical and Theoretical Investigations of Oligo (p-phenyleneethynylene)s: Effect of Alkoxy Substitution and Alkyne–Aryl Bond Rotations**

2.1. Abstract 20

2.2. Introduction 21

2.3. Experimental section 24

2.3.1. Materials and methods 24

2.3.2. General method of synthesis 24

2.3.3.	Purification of compounds **2** and **3**	**28**
2.4.	Results and discussion	**29**
2.4.1.	Photophysical investigation	**29**
2.4.2.	Theoretical investigation	**45**
2.5.	Conclusions	**55**
2.6.	References	**56**

Chapter 3. **Effect of *meta* Substitution on the Electronic Properties of Donor-π-Acceptor Systems**

3.1.	Abstract	**64**
3.2.	Introduction to donor-π-acceptor systems	**65**
3.3.	Experimental section	**73**
3.3.1.	Materials and methods	**73**
3.3.2.	General method of synthesis	**73**
3.4.	Results and discussion	**82**
3.4.1.	Photophysical investigation	**82**
3.4.2.	Theoretical investigation	**94**
3.5.	Conclusions	**104**
3.6.	References	**105**

Chapter 4. Synthesis and Photophysical Studies of Phenyleneethynylene Based Bipyridine Ligands and an Iridium Complex

4.1.	Abstract	**109**
4.2.	Introduction	**110**
4.2.1	Photophysical properties of bipyridines	**111**
4.2.2.	Introduction to iridium complexes	**113**
4.3.	Experimental section	**116**
4.3.1.	Materials and methods	**116**
4.3.2.	General method of synthesis	**117**
4.4.	Results and discussion	**120**
4.4.1.	Photophysical investigation	**120**
4.4.2.	Effect of complexation with H^+ and Zn^{2+} ions	**124**
4.4.3.	Photophysical characterization of $Ir(Phbpy)_2Cl_2$ complex	**133**
4.4.4.	Theoretical investigation	**136**
4.5.	Conclusions	**143**
4.6.	References	**144**

PREFACE

Newer synthetic strategies based on Sonogashira cross coupling reaction and s modifications have provided numerous possibilities for the design of rigid nolecular systems based on phenyleneethynylene spacer groups. The major dvantages of using the oligo(phenyleneethynylene)s (OPEs) unit as a bridge for lectronic communication compared to oligo(phenylenevinylene)s (OPVs) unit may e attributed to (i) its rigid structure which do not involve any possibility of isomerization and (ii) the cylindrical symmetry of acetylene unit which maintains the π-electon conjugation at any degree of rotation. These properties make OPEs an attractive candidates for various optoelectronic applications. However, the photophysical properties of this class of molecules are less understood. The main objectives of our studies have been (i) to investigate the primary photophysical and theoretical aspects of a few model phenyleneethynylene systems which can be used as a potential bridge in molecular devices; (ii) to examine the charge-transfer ability of phenyleneethynylene based donor-acceptor systems and (iii) to investigate the luminescence properties of bipyridine based ligands possessing phenylene-ethynylenes and their iridium complexes.

The first chapter of the thesis provides general introduction on phenyleneethynylenes; their synthesis and applications in various molecular devices. The potential applications of phenyleneethynylenes as molecular sensors and as components in molecular electronic devices (wires and interconnectors) are discussed in this chapter.

In the second chapter, the photophysical, conformational, and electronic properties of two model phenyleneethynylene based rigid rod molecules possessing

dialkoxy substitution have been investigated. Twisting of the phenyl rings along the carbon-carbon triple bond is almost frictionless in these systems giving rise to planar as well as several twisted conformations in the ground state resulting in broad absorption bands. In the case of the unsubstituted compound the broad absorption band observed is due to HOMO-LUMO transition whereas the dialkoxy substitution in the 2,5-position of the central phenyl ring in phenyleneethynylenes modifies the MOs and these aspects are investigated in detail. The excited state properties of phenyleneethynylenes have been characterized by various spectroscopic techniques. The highly structured emission spectra observed in these systems results from the planarization of the molecules in the excited state. Singlet as well as triplet excited state characteristics and the excited state reactions of these model systems were investigated in detail.

The third chapter involves the synthesis and photophysical studies of phenyleneethynylene based donor–acceptor systems possessing N,N-dimethylaniline as the donor and pyridine as acceptor in terminal positions. A series of compounds having different conjugation lengths as well as different connectivity (*meta* or *para*) between the donor and acceptor groups was synthesized. The absorption spectral features of the compounds do not vary with solvent polarity and emit with high quantum yields in nonpolar solvents. Interestingly a large bathochromic shift in emission maximum accompanied by a decrease in quantum yield was observed with increase in solvent polarity. The ground as well as excited state properties of the quarternized derivatives of phenyleneethynylene based donor–acceptor systems has also been examined. Based on these studies it is concluded that the *meta* linkage acts as an insulator in the ground state and

electronic communication open up in the excited state leading to charge transfer transition.

Two bipyridine derivatives possessing phenyleneethynylene units (unsubstituted and methoxy substituted at the terminal position) at the 4,4'-positions were synthesized and their photophysical properties are discussed in the fourth chapter. Based on various experimental and theoretical investigations, we have concluded that the absorption in these systems originate from π-π^* transition and any involvement of n-π^* transition is ruled out. The methoxy substituted compound possess high fluorescence yield (0.12) as compared to the unsubstituted compound (fluorescence yield = 2.4×10^{-3}). The protonated as well as the zinc ion complex of the unsubstituted compound is highly emissive due to the existence of a locked *cis* conformation which prevents the deactivation through non-radiative channels. Interestingly a nonemissive charge transfer state was observed in the case of **2** on adding H^+/Zn^{2+} ions, the excited state charge transfer ability of donor-acceptor increases for methoxy substituted compound and emission yield decreases due to enhanced decay through nonradiative channels. A new iridium complex $[Ir(Phbpy)_2Cl_2)]$ has also been synthesized. This compound possesses excellent luminescent properties (luminescence quantum yield of 0.30 and lifetime of 0.9 microseconds) and has potential application in optoelectronic devices.

CHAPTER 1

A Brief Review on Phenyleneethynylene Based Molecular Systems

1.1. Introduction to π-conjugated Molecular Systems

Pioneering work of Nobel laureates, Alan J. Heeger, Alan G. MacDiarmid and Hideki Shirakawa on the conductivity of *trans*-polyacetylene has opened a plethora of scientific activity on the development of semiconducting and conducting polymers.[1] More recently, π-conjugated molecular systems such as oligo(phenylenevinylene)s and oligo(phenyleneethynylene)s have been proposed as elements in various optoelectronic devices. Extensive reviews are available on the synthesis and the possible applications of these systems as organic light-emitting diodes,[2] field-effect transistors,[3] sensors,[4] photovoltaic and nanoelectronic systems.[5] As compared to oligo(phenylenevinylene)s (OPVs), molecular structure of oligo(phenyleneethynylene)s (OPEs) is totally rigid and do not involve any possibility of isomerization. These properties make OPEs an attractive candidate for various device applications. Recent advances on the synthesis of phenyleneethynylene based molecular systems and their potential applications are summarized below.

. Synthesis of OPE Based Molecular Systems

Newer synthetic strategies based on Sonogashira cross coupling reaction l its modifications have provided numerous possibilities for the design of rigid lecular systems based on phenyleneethynylene spacer groups. In general, ıogashira reaction involves the coupling of terminal alkynes with aryl or vinyl ides in the presence of a palladium catalyst, a copper(I) co-catalyst, and an ine as base. Although the palladium catalyzed reaction occurs through several ps, the overall scheme can be represented as a reaction between a 'sp' carbon m of alkynes and 'sp^2' carbon atom to which halide ion is attached (Scheme 1.1).

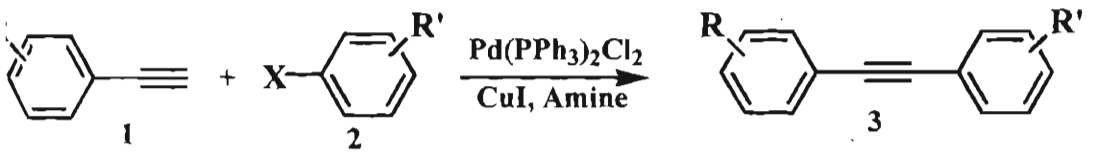

Scheme 1.1. Sonogashira cross coupling reaction.

The first step of the palladium catalysed reaction involves the generation of active catalyst, wherein the Pd possesses a zero oxidation state, through a :s of steps as shown in Scheme 1.2 (oxidation state of Pd in the added reagent $Ph_3)_2Cl_2$ is +2). In presence of amine, the acetylenic hydrogen of the reactant :st displaced by Cu^+ ion to form Cu-acetylide complex (**I** in Scheme 1.2). smetallation of **I** with the Pd catalyst results in the formation of acetylide-Pd)lex (**II** in Scheme 1.2) with the elimination of two molecules of CuCl. This

unstable complex reductively eliminates butadiyne and generates the active Pd catalyst, $(PPh_3)_2Pd(0)$.

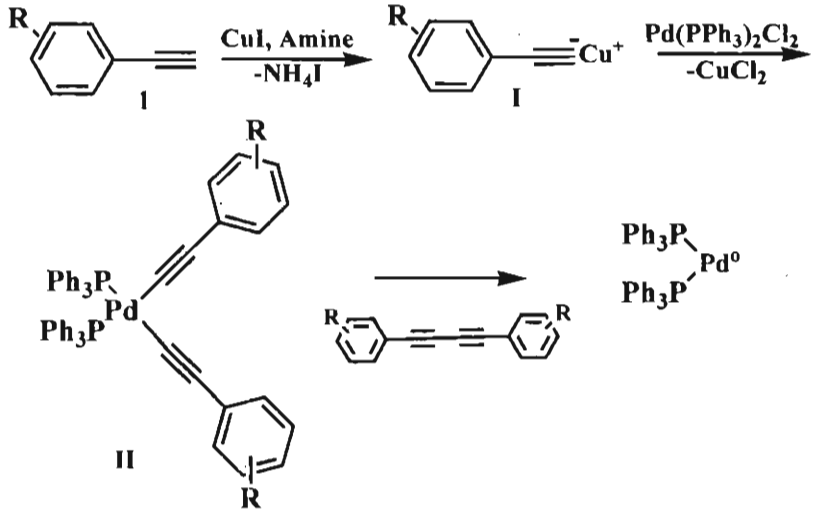

Scheme 1.2. Generation of the active Pd(0) catalyst.

In the reaction step (Scheme 1.3), addition of aryl halide to $(PPh_3)_2Pd(0)$ results in the formation of a complex **III** (oxidation state of Pd in the complex is +2). Further the reaction of **III** with acetylide-Cu complex (**I** in Scheme 1.2) leads to the formation of an unstable complex **IV**, which dissociate to yield the desired tolane derivative (**3**) regenerating the active catalyst.

Several parameters can influence the rate and yield of palladium catalysed reaction and these aspects are summarized in an earlier review.[6] Since the active Pd catalyst is electron rich in nature, the presence of electron withdrawing substituents at the *ortho* or *para* positions of the aryl halide can accelerate the rate of reaction. The nature of the halide can also influence the reaction rate: the iodide group being a better leaving group, reaction usually proceeds at room temperature

conditions whereas reaction with bromo substituted reagents occur only at elevated temperatures. The presence of CuI as co-catalyst is essential as it assists

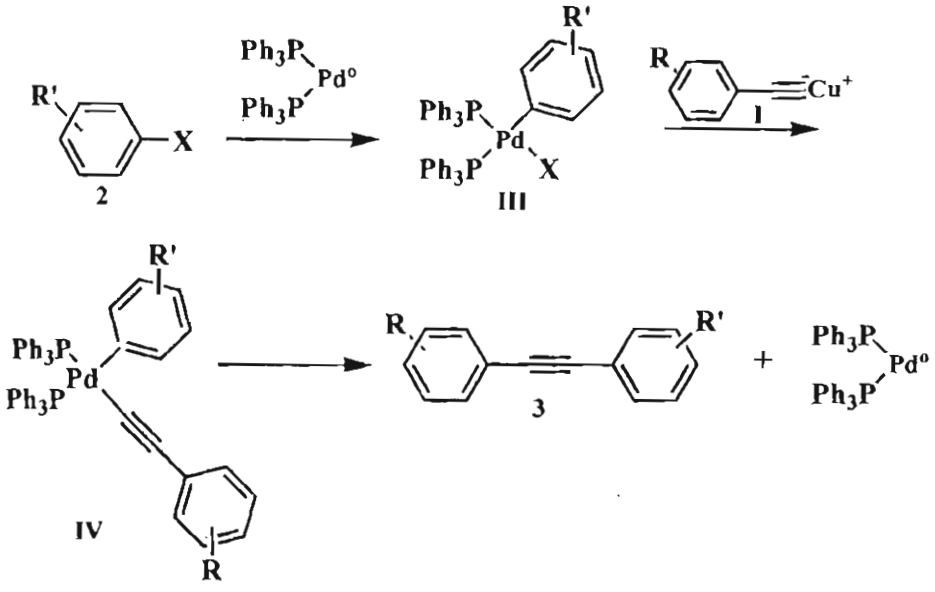

Scheme 1.3. Formation of product and regeneration of catalyst.

the activation of alkynes through the formation of the Cu-acetylide complex.[7] The choice of the amine is found to be crucial and generally used amines are triethylamine, diethylamine and diisopropylamine. In most cases amines can also act as solvent and in cases where the substrates are insoluble, cosolvents such as toluene, THF and diethyl ether are used.[8] However, halogenated solvents should be avoided and excess amounts of methanol can hamper the reaction. Amount of the catalyst plays an important role and usually varies from 0.1-5.0 mole percentage of the reactant used. It is also reported that by adding small quantities of triphenylphosphine, it is possible to reduce the amount of Pd catalyst thereby decreasing the amount of biproduct formed (diyne in Scheme 1.2).[9] A variety of

OPE based functional molecular systems have been recently synthesized by adopting cross coupling reaction and the potential applications of these systems are presented in the following sections.

1.3. OPE Based Molecular Wires and Electronic Devices

In the mid of 1970's, Ratner and Aviram put forward the idea of using few molecules or a cluster of molecules in place of semiconductor devices in electronic equipments to perform various functions such as rectification, amplification and storage. However, suitable technologies to connect individual molecules to form electronic circuits have not been completely achieved. The major advantage of using the OPE core unit as a bridge for electronic communication may be attributed to its rigid rod structure and cylindrical symmetry of acetylene unit which maintains the π-electron conjugation at any degree of rotation. Efforts have been initiated by various groups on the design of OPE based molecules which can integrate the elementary functions and interconnections required in molecular electronic devices. It has been reported that the OPE derivatives can exhibit negative differential resistance,[10] bistable conductance and controlled switching under an applied electric field.[11]

Tour and coworkers designed a molecular diode in 1999 by sandwiching a monolayer of 2'-amino-4-ethynylphenyl-4'-ethynylphenyl-5'-nitro-1-benzenethiol (4 in Chart 1.1) between two Au electrodes and observed negative differential resistance (NDR) behavior, i.e., an initial rise in current followed by a steep

decrease when the voltage is progressively increased. The device showed an on/off peak to valley ratio (PVR) of 1030:1 at 60 K, which decreases with increase in temperature[10] (Figure 1.1). A possible mechanism as suggested by Tour

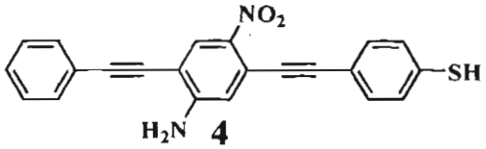

4

Chart 1.1. Structure of 2'-amino-4-ethynylphenyl-4'-ethynylphenyl-5'-nitro-1-benzenethiol.

and coworkers, involves a two stage reduction process. As the bias voltage is increased between the electrodes, electrons are injected to the molecule, resulting in the formation of a conducting monoanion and the charge is distributed all over the molecule. On further increasing the voltage, second reduction occurs and the current flow is blocked. (Figure 1.2) The mechanism was further supported by theoretical calculations by Seminario et al.[12] They showed that the current flow over

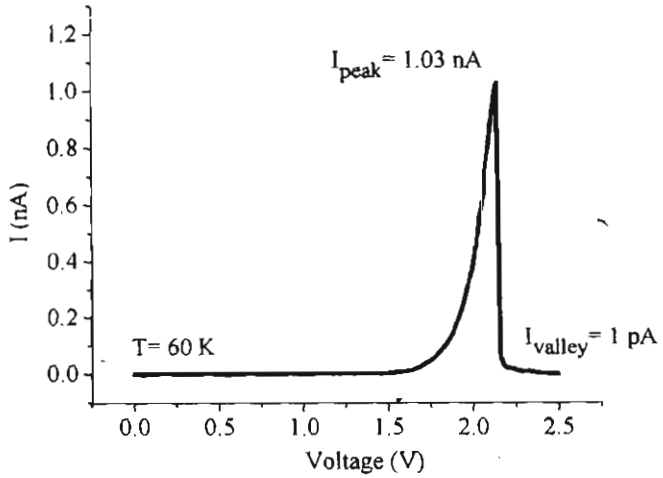

Figure 1.1. I-V characteristics of a Au-4-Au device at 60 K. The peak current density is ~50 A/cm^2, the NDR is ~400 μohm^{-1}cm^2, and the PVR is 1030:1 *(adapted from reference 5).*

the molecule is possible only in its one electron reduced state where in the LUMO extends all over the molecule. At higher voltages the LUMO corresponding to two electron reduced state gets localized and the current drops to zero. However, similar results were not observed for monofunctionalized OPEs containing nitro as well as amino functionalities. OPE based molecular systems showing NDR behaviour have gained a lot of attention in recent years. Several theoretical and experimental attempts have been made to explain conductance changes through a variety of schemes (conformational changes, hydrogen bond formation in the packing layer etc.); however the mechanism of this process is not fully understood.[13, 14]

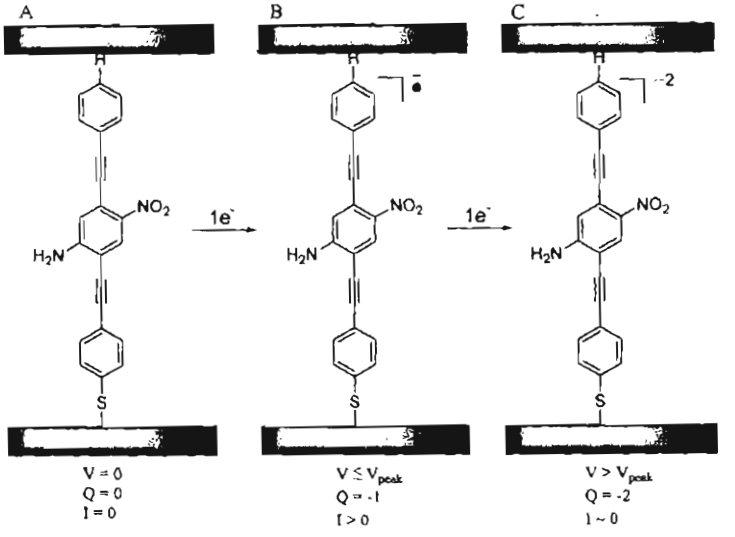

Figure 1.2. Mechanism of NDR. As the applied voltage across the SAM (A) increases, **4** undergo reduction to form monoanion which is conducting (B); futher increase in voltage results in the formation of nonconducting dianion (C) *(adapted from reference 5)*.

The future of molecular electronics depends mainly on the development of molecular wires of higher conductivity. Ideally, molecular wire should be able to

communicate distant centres at a faster rate through strong coupling between the electrodes and the assembled molecules. A tunnelling mechanism has been proposed for explaining the transfer of charge over long distance through the molecule. Creager and coworkers investigated the electron transfer kinetics, using AC voltametry technique, by attaching ferrocene groups to gold electrodes through phenyleneethynylene bridges (Figure 1.3.) containing three to six repeating units (corresponding to distances of 22 to 43 Å).[15] They calculated the β values of 0.36 $Å^{-1}$ for phenyleneethynylene based bridges by plotting log k versus distance of separation (note: lower β value implies a higher conductivity; k denotes electron transfer rate constant). When linked through aliphatic bridges the corresponding β value was obtained as 0.9 $Å^{-1}$, a value three times lower than the phenylenethynylene units[16] indicating that OPEs are better conductors.

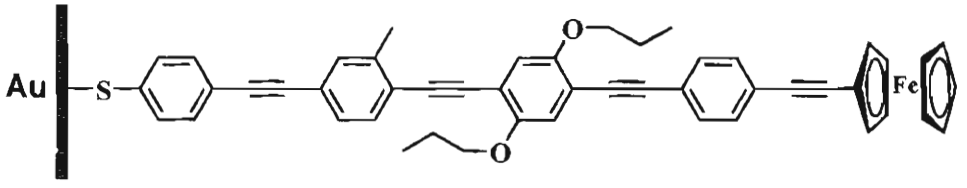

Figure 1.3. Ferrocene molecule linked to gold electrode through four phenylenethynylene units *(adapted from reference 10).*

Oligo(phenyleneethynylene)s are ideally suited as molecular wires due to their extended π-conjugation.[17-20] Tour and coworkers have synthesized a series of molecular wires based on OPEs (commonly known as Tours wires) and one of the longest wires of this type, having a length of 128 Å, is shown in Chart 1.2.[17, 21]

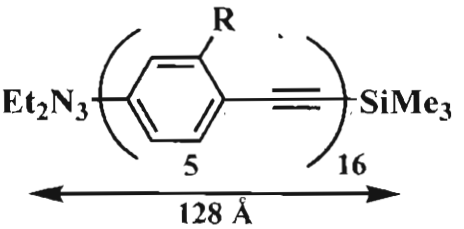

Chart 1.2. Longest molecular wire based on phenylenethynylenes.

Blumm and coworkers reported the conductivity of an OPE derivative, namely 4,4'-di(phenyleneethynylene)benzenethiolate, by inserting them as self assembled monolayers along with nonconducting n-dodecanethiol.[22] The conductivity was probed using the STM tip and found that these systems were more conducting than the corresponding alkyl thiol derivatives. These experiments also supported the view that phenyleneethynylenes are good conductors having potential applications as molecular wires. In contrast, Ramachandran et al. have observed stochastic on-off conductivity switching in phenyleneethynylene oligomers when inserted into self-assembled monolayers of alkanemonothiol on Au(III) and the conductivity was probed using STM.[23] These results were explained in terms of changes in ring conformations or electron localization or both. It may be noted that the techniques used for the conductance measurements are highly sensitive to several factors such as preparation of SAM, packing of the molecules on the monolayer, strength of the contact between STM tip and the molecule. More controlled experiments are essential to obtain a better insight on the mechanism of conductance switching.

Investigation on the electronic transport through single molecules, sandwiched between two metal contacts, has been realized recently by using mechanically controlled break junction (MCBJ) technique and STM. 1,4-bis(phenylethynyl)anthracene molecule possessing thiol groups on the *meta* as well as *para* positions were synthesized and these molecular systems were immobilized between gold electrodes of a mechanically controlled break-junction (Figure 1.4).[24] When linked through *para* position the current measured was found to be 100 fold higher than the *meta* substituted system under same conditions.

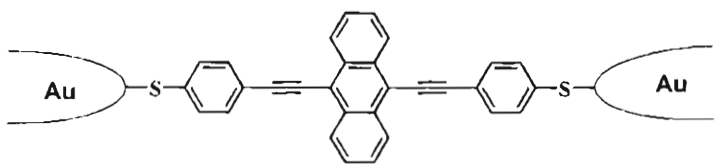

more conducting when linked through "*para*" positions

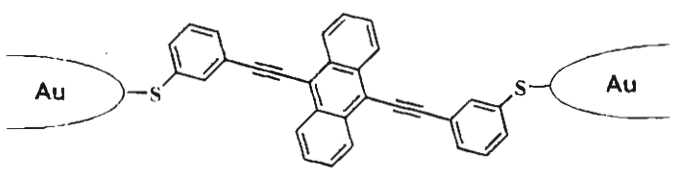

less conducting when linked through "*meta*" positions

Figure 1.4. Schematic representation showing the "*para*" and "*meta*" thio linked anthracene derivatives on the gold electrode of MCBJ *(adapted from reference 19).*

More recently, Hummelen and coworkers have prepared an anthraquinone based molecular wire possessing phenylethynyl moieties on both ends (Figure 1.5).[25] The authors have demonstrated that the model system substituted with tert-butylthio groups, can be electrochemically switched in a reversible fashion, from cross conjugated form having low conductance ("off state") to linearly conjugated form (high conductance; "on state") *via* two electron reduction/oxidation reaction.

Such systems are proposed as redox controlled switches in molecular electronic devices when linked between Au electrodes (Figure 1.5).

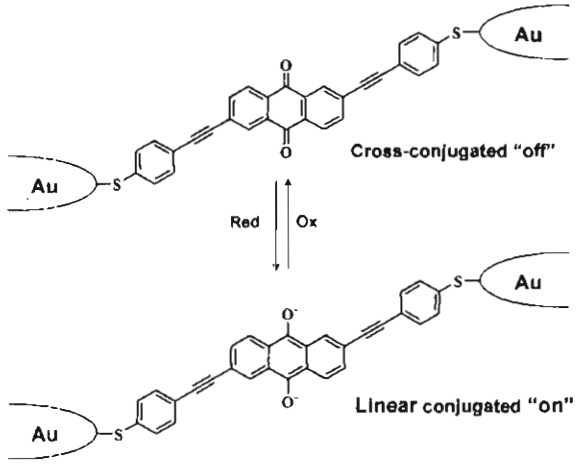

Figure 1.5. Proposed switching of conjugation and conductivity of anthraquinone derivative via oxidation/reduction reactions *(adapted from reference 24).*

An optically active molecular electronic wire containing chiral 1,1'-binaphthyl system with terminal aryleneethynylene unit have been synthesized and incorporated into nanowell devices by self-assembly on the gold surface[26] (Figure 1.6). Authors have demonstrated that the chirality of the molecules strongly influence their electrical transport properties. In the nanowell device, median current from the molecules containing both *S* and *R* enantiomers were found to be significantly smaller than those from the pure *S* or *R* molecule. This may be attributed to the difference in packing between the homochiral and heterochiral molecules in the monolayer. However, the conductivity of these wires is found to be much lower than pure oligophenyleneethynylene wires.

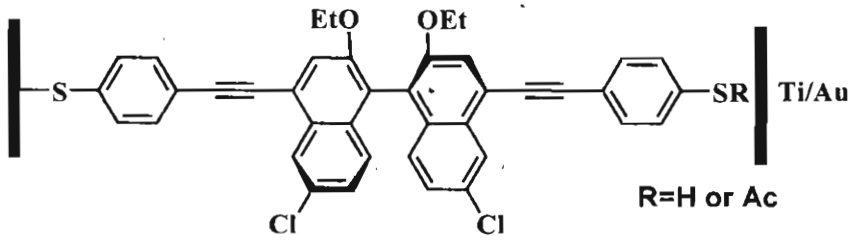

Figure 1.6. Schematic representation of a chiral binaphthyl derivative assembled between two electrodes. The current flow through the monolayer containing both R and S isomer is less than those containing pure *R* or *S (adapted from reference 25).*

1.4. OPE Based Sensors

By combining the high fluorescence quantum yield of phenyleneethynylene based molecular systems and the unique characteristics of polyelectrolytes (for example, solubility in aqueous media and processability), Whitten and coworkers have developed conjugated polyelectrolyes (CPE) for sensing biological targets. Representative examples of phenyleneethynylene based cationic and anionic CPEs are illustrated in Chart 1.3. Sensing strategy in these systems adopts a fluorescence superquenching mechanism, which involves an electron/energy transfer process on association of a quencher with CPE. By adopting this methodology several conjugated polyelectrolytes have been developed for biosensing [27-34]

A novel biosensing strategy, termed as quencher tether ligand (QTL) approach, was recently developed by Whitten and coworkers by taking advantage of fluorescence superquenching mechanism. In this methodology, a quencher molecule was first linked to a complexing molecule (QTL). The receptor for a

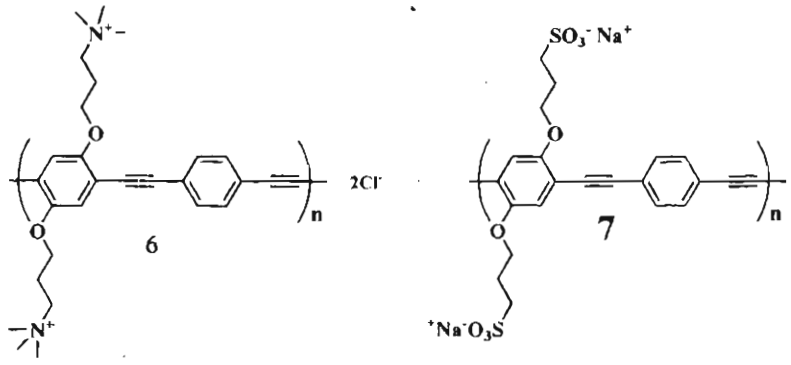

Cationic PPE **Anionic PPE**

Chart 1.3. Phenyleneethynylene based conjugated polyelectrolytes (CPEs) having cationic and anionic pendant groups *(adapted from reference 28).*

specific analyte was first attached on poly(phenyleneethynylene)s (PPE) which was further coated on the surface of latex microspheres. The competition between the analyte and a synthetic QTL conjugate, for complexing with receptor sites, forms the basis of sensing. When the ligand attached to the quencher (QTL) recognizes the receptor sites on a fluorescent polymer, quenching of the fluorescence occurs. On addition of an analyte, having comparable binding properties, fluorescence regains due to the displacement of QTL by the analyte.

A modified version of QTL approach was used for the detection of proteolytic enzymes, namely enterokinase, caspase-3/7, and β-secretase using different peptide sequence as tether.[29] The PPE based polymer containing a biotin binding protein was coated over polystyrene microsphere. QTL was designed in such a way that it contains a reactive peptide sequence with a quencher on one side and biotin on the other. The peptide binds to the conjugate polymer through biotin-biotin protein interaction and the quenching of the fluorescence occurs.

When reactive enzymes are introduced into the system, cleavage of the peptide sequence occurs and the fluorescence is regained. Same group have also developed an assay for the detection of a 20mer-DNA sequence for the anthrax lethal factor based on PPE.[30,31]

Synthesis of novel cruciform molecules (Chart 1.4) and their application as sensors of metal cation have been demonstrated by Bunz and coworkers.[34,35] The optical properties of the cruciforms can be tuned by binding with various metal cations and the authors observed that the pyridyl functionalised cruciform molecules could selectively detect Ca^{2+} and Mg^{2+}.

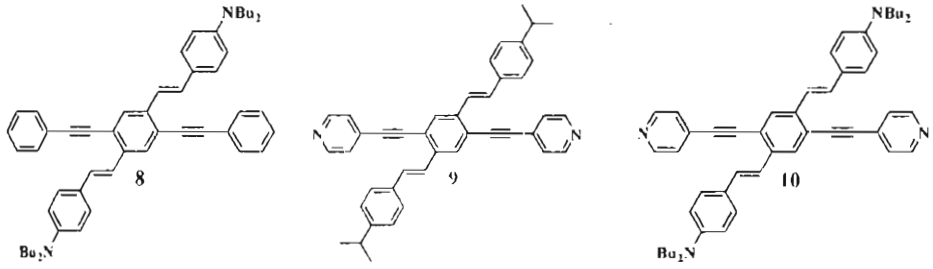

Chart 1.4. Phenyleneethynylene based cruciform as cationic sensors *(adapted from reference 33).*

A new method for detection of bacteria based on water soluble fluorescent poly(phenyleneethynylene) (PPE), functionalized with glycosides, has been developed by Disney et al.[36] Authors have demonstrated that the PPE functionalized glycosides effectively bind to bacteria *(E. coli)* and form bright fluorescent cell aggregates. The aggregation is due to multivalent interactions between the mannosylated polymer and mannose receptors located on the bacterial pili, which was confirmed by confocal microscopy and binding studies.

Carbohydrate-functionalized PPEs has an obvious advantage that it can detect the presence of a pathogen in approximately 10 to 15 min where as conventional methods (selective growth in liquid media or on plates) takes several days. This methodology can be further extended for sensing of a wide range of pathogens by exploiting the preference of different bacteria to bind with specific carbohydrates.

Another interesting application that has been envisaged using pentiptycene-derived poly(phenyleneethynylene) for the detection of vapours of explosives such as 2,4-dinitrotoluene (DNT) and 2,4,6-trinitrotoluene (TNT).[37] Authors have observed that the thin films of pentiptycene polymer (**11** in Chart 1.5) possess enhanced fluorescence compared to the planar model polymer (**12**). The rigid three-dimensional pentiptycene moieties in the molecular framework prevent both π-stacking and excimer formation leading to enhanced emission. The polymer coated thin film of 25 Å when exposed to TNT vapours showed strong quenching ~50 % within 30 s and to ~75 % at 60 s. The response of the same film to DNT vapour was found to be even faster (~91 % fluorescence quenching at 30 s).

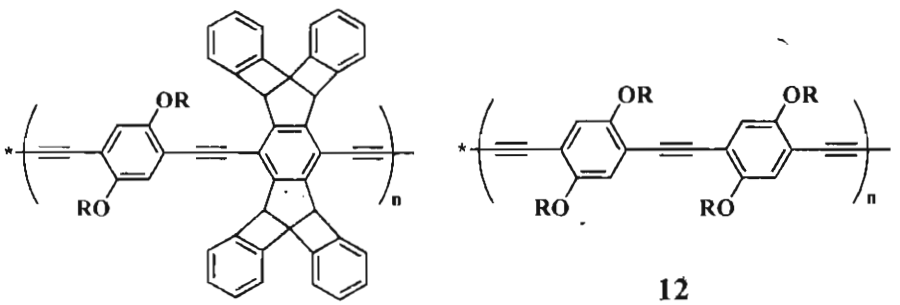

11 **12**

Chart 1.5. Phenyleneethynylene derivatives for the detection of explosive vapours *(adapted from reference 36)*

1.5. Objectives of the Present Work

OPE based system has emerged as attractive candidate for various optoelectronic applications, however the photophysical properties of this class of molecule is less understood. The objectives of the present work are to (i) investigate the primary photophysical and theoretical aspects of a few model phenyleneethynylene systems which can be used as a bridge in molecular devices (Chapter 2); (ii) examine the charge-transfer ability of phenyleneethynylene based donor-acceptor systems (Chapter 3) and (iii) investigate the luminescence properties of bipyridine based ligands possessing phenyleneethynylenes and their iridium complexes (Chapter 4).

1.6. References

1. Chiang, C. K.; Fincher, C. R.; Park, Y. W.; Heeger, A. J.; Shirakawa, H.; Louis, E. J.; Gau, S. C.; McDiarmid, A. G. *Phys. Rev. Lett.* **1977**, *39*, 1098.
2. Arno Kraft, Grimsdale, A. C.; Holmes, A. B. *Angew. Chem. Int. Ed.* **1998**, *37*, 402.
3. Muccini, M. *Nat. Mater.* **2006**, *5*, 605.
4. Swager, T. M. *Acc. Chem. Res.* **1998**, *31*, 201.
5. Tour, J. M. *Chem. Rev.* **1996**, *96*, 537.
6. Bunz, U. H. F. *Chem. Rev.* **2000**, *100*, 1605.
7. Osakada, K.; Sakata, R.; Yamamoto, T. *Organometallics* **1997**, *16*, 5354.

8. Alami, M.; Ferri, F.; Linstrumelle, G. *Tet. Lett.* **1993**, *34*, 6403.

9. Harald Häger, W. H. *Macromol. Chem. Phys.* **1998**, *199*, 1821.

10. Chen, J.; Reed, M. A.; Rawlett, A. M.; Tour, J. M. *Science* **1999**, *286*, 1550.

11. Reed, M. A.; Chen, J.; Rawlett, A. M.; Price, D. W.; Tour, J. M. *Appl. Phys. Lett.* **2001**, *78*, 3735.

12. Seminario, J. M.; Zacarias, A. G.; Tour, J. M. *J. Am. Chem. Soc.* **2000**, *122*, 3015.

13. Cornil, J.; Karzazi, Y.; Bredas, J. L. *J. Am. Chem. Soc.* **2002**, *124*, 3516.

14. Moore, A. M.; Dameron, A. A.; Mantooth, B. A.; Smith, R. K.; Fuchs, D. J.; Ciszek, J. W.; Maya, F.; Yao, Y.; Tour, J. M.; Weiss, P. S. *J. Am. Chem. Soc.* **2006**, *128*, 1959.

15. Creager, S.; Yu, C. J.; Bamdad, C.; O'Connor, S.; MacLean, T.; Lam, E.; Chong, Y.; Olsen, G. T.; Luo, J.; Gozin, M.; Kayyem, J. F. *J. Am. Chem. Soc.* **1999**, *121*, 1059.

16. Weber, K.; Hockett, L.; Creager, S. *J. Phys. Chem. B* **1997**, *101*, 8286.

17. Pearson, D. L.; Tour, J. M. *J. Org. Chem.* **1997**, *62*, 1376.

18. Wang, C.; Batsanov, A. S.; Bryce, M. R. *J. Org. Chem.* **2006**, *71*, 108.

19. Tour, J. M.; Rawlett A,. M.; Kozaki, M; Yao, Y.; Jagessar, R. C.; Dirk S. M.; David W. Price, D. W.; Reed, M. A.;. Zhou, C.-Wu.; Chen J.; Wang, W.; Campbell I. *Chem.-Eur. J.* **2001**, *7*, 5118.

20. Sorensen, J. K.; Vestergaard, M.; Kadziola, A.; Kilsa, K.; Nielsen, M. B. *Org. Lett.* **2006**, *8*, 1173.

21. Jones, L.; Schumm, J. S.; Tour, J. M. *J. Org. Chem.* **1997**, *62*, 1388.

22. Bumm, L. A.; Arnold, J. J.; Cygan, M. T.; Dunbar, T. D.; Burgin, T. P.; Jones, L., II; Allara, D. L.; Tour, J. M.; Weiss, P. S. *Science* **1996**, *271*, 1705.

23. Ramachandran, G. K.; Hopson, T. J.; Rawlett, A. M.; Nagahara, L. A.; Primak, A.; Lindsay, S. M. *Science* **2003**, *300*, 1413.

24. Mayor, M.; Weber, H. B.; Reichert, J; Elbing, M.; Carsten von Hänisch; Beckmann D.; Fischer, M. *Angew. Chem. Int. Ed.* **2003,** *42*, 5834.

25. vanDijk, E. H.; Myles, D. J. T.; vanderVeen, M. H.; Hummelen, J. C. *Org. Lett.* **2006**, *8*, 2333.

26. Zhu, Y.; Gergel, N.; Majumdar, N.; Harriott, L. R.; Bean, J. C.; Pu, L. *Org. Lett.* **2006**, *8*, 355.

27. Pinto, M. R.; Schanze, K. S. *Proc. Natl. Acad. Sci.* **2004**, *101*, 7505.

28. Rininsland, F.; Xia, W.; Wittenburg, S.; Shi, X.; Stankewicz, C.; Achyuthan, K.; McBranch, D.; Whitten, D. *Proc. Natl. Acad. Sci.* **2004**, *101*, 15295.

29. Kumaraswamy, S.; Bergstedt, T.; Shi, X.; Rininsland, F.; Kushon, S.; Xia, W.; Ley, K.; Achyuthan, K.; McBranch, D.; Whitten, D. *Proc. Natl. Acad. Sci.* **2004**, *101*, 7511.

30. Kushon, S. A.; Bradford, K.; Marin, V.; Suhrada, C.; Armitage, B. A.; McBranch, D.; Whitten, D. *Langmuir* **2003**, *19*, 6456.

31. Kushon, S. A.; Ley, K. D.; Bradford, K.; Jones, R. M.; McBranch, D.; Whitten, D. *Langmuir* **2002**, *18*, 7245.

32. Heeger, P. S.; Heeger, A. J. *Proc. Natl. Acad. Sci.* **1999**, *96*, 12219.

33. Wosnick, J. H.; Mello, C. M.; Swager, T. M. *J. Am. Chem. Soc.* **2005**, *127*, 3400.

34. Wilson, J. N.; Bunz, U. H. F. *J. Am. Chem. Soc.* **2005**, *127*, 4124-4125.

35. Wilsona, J. N.; Hardcastleb, K. I.; Josowicza, M.; Bunz, U. H. F. *Tetrahedron* **2004**, *60*, 7157.

36. Disney, M. D.; Zheng, J.; Swager, T. M.; Seeberger, P. H. *J. Am. Chem. Soc.* **2004**, *126*, 13343.

37. Yang, J. S.; Swager, T. M. *J. Am. Chem. Soc.* **1998**, *120*, 5321.

CHAPTER 2

Photophysical and Theoretical Investigations of Oligo(*p*-phenyleneethynylene)s: Effect of Alkoxy Substitution and Alkyne–Aryl Bond Rotations

2.1. Abstract

The unique photophysical, conformational and electronic properties of two model phenyleneethynylene rigid rod molecular systems, possessing dialkoxy substitutions were studied in comparison with an unsubstituted system. Twisting of the phenyl rings along the carbon-carbon triple bond is almost frictionless in these systems giving rise to planar as well as several twisted ground state conformations and this results in broad structureless absorption in the spectral region of 250-450 nm. In the case of 1,4-bis(phenylethynyl)benzene, a broad absorption band was observed due to HOMO-LUMO transition whereas dialkoxy substituted compounds possess two well separated bands. Dialkoxy substitution in the 2,5-position of the phenyl ring in phenyleneethynylenes alters its central arene π-orbitals through the resonance interaction with oxygen lone pairs resulting in similar orbital features for HOMO and HOMO-1/HOMO-2. Electronic transition from the low lying HOMO-1/HOMO-2 orbital to LUMO results in the high energy band and the red shifted band originates from HOMO-LUMO transition. The first excited state transition energies at different dihedral angle, calculated by

TDDFT method indicate that the orthogonal conformation has the highest excitation energy with an energy difference of 15 kcal/mol than the low lying planar conformation. The emission of these compounds originates preferentially from more relaxed planar conformation resulting in well defined vibronic features. The fluorescence spectral profile and lifetimes were found to be independent of excitation wavelengths, confirming the existence of a single emitting species. The transient spectrum of **2**, recorded immediately after laser pulse showed depletion at 390 nm and absorption at 520 nm was characterized as the triplet excited state. Interestingly, in the case of higher homologue (**3**), the absorption of the triplet excited state is red shifted to 660 nm.

2.2. Introduction

Oligo(phenyleneethynylene) based molecular systems[1] possess a well defined architecture and are widely used in the design of functional molecular materials such as conjugated polymers,[2-12] donor-acceptor systems,[13-21] sensors,[22-30] and self-assembled monolayer on metal surface.[31-34] The major advantage of using the oligo(phenyleneethynylene) core unit as a bridge for electronic communication may be attributed to the cylindrical symmetry of acetylene unit which maintains the π-electron conjugation at any degree of rotation. A few prototype systems were fabricated by incorporating rigid rod molecules in semiconductor/metal hybrid systems. These include (i) single-molecule diodes by immobilizing them between both electrodes by sulfur–gold bonds,[35] (ii) nanocell electronic memories,[36] (iii) voltage-triggered conductance

switching[32,37,38] and (iv) photovoltaic systems by functionalization of redox/photo-active molecules on to semiconductor surfaces.[15-18, 39]

Recently Galoppini and coworkers[15-18,39] have investigated, in detail, the dynamics of the electron injection from excited Ru^{II}-polypyridine sensitizers to TiO_2 semiconductor through phenyleneethynylene bridging units. These studies suggest that the charge injection occurs over a long distance of 2.4 nm. The electronic coupling between Ru^{II}-polypyridine and phenyleneethynylene bridging unit is quite strong and thus assists in the fast electron injection into semiconductor nanoparticles.[15] Electrochemical studies have confirmed that phenyleneethynylene bridge structures promote strong coupling between gold electrode and ferrocene, thereby promoting rapid electron transport over long distances.[40]

Although a variety of phenylethynyl based molecular systems have been investigated, most of the photophysical reports are based on unsubstituted 1,4-bis(phenylethynyl)benzene (**1** in Chart 2.1).[41-44] The rotation of the central arene ring of this system revealed a very shallow potential of 0.5 kcal/mol between the fully planar and perpendicular structures.[41] It is also reported that **1** exists as a single species in the excited state and the photoexcitation do not bring about any significant changes in the bond order of acetylene group, ruling out a cumulenic/quinanoidal character in its singlet excited state (S_1).[44] Oligo(phenyleneethynylene)s, particularly their higher analogues possess poor solubility which is one of the major limiting factors in the design of organic molecular materials. To overcome the solubility problem, 2,5-dialkoxy

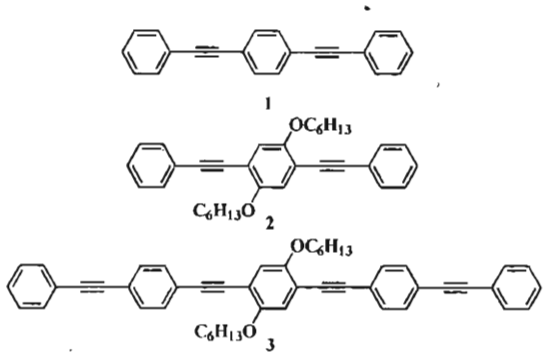

Chart 2.1. Phenylethynyl based molecular systems under investigation.

substituted derivatives of oligo(phenyleneethynylene)s have been synthesized and these molecular systems are widely used as building blocks for various functional molecular materials. However, the introduction of such groups with lone pair of electrons can influence the photophysical properties of phenylethynyl based systems and detailed experimental as well as theoretical understanding is essential for fine tuning their optoelectronic properties. With this objective, we have synthesized two model oligo(phenyleneethynylene)s possessing dialkoxy substitution, namely 1,4-bis(phenylethynyl)-2,5-bis(hexyloxy)benzene (**2**)[45] and 1,4-bis((4-phenylethynyl)phenylethynyl)-2,5-bis(hexyloxy)benzene (**3**) (Chart 2.1) and investigated their ground and excited state properties in detail.[46,47] Further, DFT (density functional theory) and TDDFT (time dependent density functional theory) levels of theoretical studies were carried out to understand the conformational, electronic and excited state properties of **2** and **3** in comparison with **1**.

2.3 Experimental Section

2.3.1. Materials and methods

The samples used for the study were purified by passing through recycling HPLC manufactured by Japan Analytical Industry Co., Ltd. All melting points are uncorrected and were determined on an Aldrich melting point apparatus. ^{1}H NMR and ^{13}C NMR spectra were recorded on a Bruker DPX-300MHz spectrometer. High Resolution Mass spectra were recorded on a JEOL JM AX 5505 mass spectrometer. The UV-Vis spectra were recorded on a Shimadzu 2401 or 3101PC spectrophotometer. The emission spectra were recorded on a Spex-Fluorolog, F112-X equipped with a 450W Xe lamp and a Hamamatsu R928 photomultiplier tube. The spectra recorded by keeping a 90° geometry and a slit width of 1 mm in the excitation and emission monochromators. Details of time correlated single photon counting fluorescence lifetime measurements were described earlier.[48]

2.3.2. General method of synthesis

The general strategy adopted for the synthesis of compounds **2** and **3** are shown in Scheme 2.1 (an alternate route for the synthesis of **2** is reported in reference 45). Compounds **4** and **5** were prepared following the procedure reported in the literature.[45] More recently the synthesis of **6** and **7** were reported by Xue et.al[49] by an alternate route. THF used was dried over sodium and diisopropylamine was dried over KOH. Solvents were deoxygenated by purging them with argon for 15 min before using in the reaction. The final

compounds were purified by passing through recycling preparative HPLC equipped with a UV as well as RI detector.

Preparation of 1,4-bis(phenylethynyl)-2,5-bis(hexyloxy)benzene (2). A mixture of TMS coupled monomer **5** (500 mg, 1.06 mmol), K_2CO_3 (882 mg, 6.36 mmol), PPh_3 (111 mg, 0.106 mmol), $Pd(PPh_3)_4$ (245 mg, 0.053 mmol), CuI (40 mg, 0.053 mmol) and C_6H_5I (284 μL, 2.54 mmol) was stirred in a solvent mixture of CH_3OH/THF (1:4) at room temperature for 15 h. After removal of the solvent under reduced pressure, the crude product was purified by column chromatography over silica gel (100-200 mesh) using ethylacetate/hexane (1:99) as eluent to yield 320 mg (63 %) of white colored product, mp. 114-116 °C. ^{1}H NMR(300 MHz, $CDCl_3$):δ 7.54-7.52 (m, 4H), 7.35-7.33 (m, 6H), 7.02 (s, 2H), 4.03 (t, 4H), 1.87-0.87 (m, 22H). ^{13}C NMR (75 MHz, $CDCl_3$): δ 153.67, 131.568, 128.21, 128.22, 123.49, 117.07, 114, 94.82, 85.96, 77.42, 69.68, 31.60, 30.88, 29.33, 25.73, 22.62, 14.0. Anal. Calcd for $C_{34}H_{38}O_2$: C, 85.31; H, 8.00. Found: C, 85.55; H, 8.18. Exact mass calculated for $C_{34}H_{38}O_2$ (M^+) is 478.2872, found 478.2887 (FAB high resolution mass spectrometry).

Preparation of 1,4-bis(4-bromo phenylethynyl)-2,5-bis(hexyloxy)benzene (6). A mixture of TMS coupled monomer **5** (500 mg, 1.06 mmol), K_2CO_3 (882 mg, 6.36 mmol), PPh_3 (111 mg, 0.106 mmol), $Pd(PPh_3)_4$ (245 mg, 0.053 mmol), CuI (40 mg, 0.053 mmol) and 1-bromo-4-iodo benzene (714 mg, 2.5 mmol) was stirred at room temperature in a solvent mixture of CH_3OH/THF (1:4)

Scheme 2.1. Synthetic route for the preparation of 2 and 3

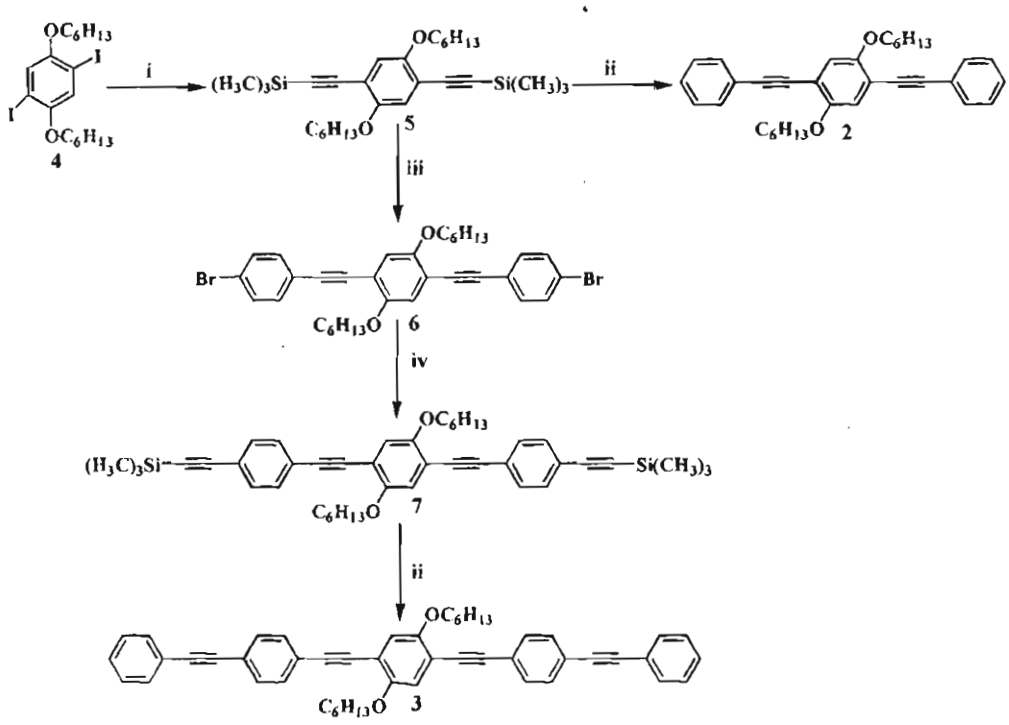

(i) (Trimethylsilyl)acetylene, $Pd(PPh_3)_2Cl_2$, CuI, $(i\text{-pr})_2NH$, 80 ^{0}C, 1 h; (ii) CH_3OH, K_2CO_3, THF, C_6H_5I, $Pd(PPh_3)_4$, CuI, PPh_3; (iii) CH_3OH, K_2CO_3, THF, BrC_6H_4I, $Pd(PPh_3)_4$, CuI, PPh_3; (iv) (Trimethylsilyl)acetylene, $Pd(PPh_3)_2Cl_2$, CuI, $(i\text{-pr})_2NH$, 80 ^{0}C, 3 h.

for 15 h. The crude product was purified by column chromatography over silica gel (100-200 mesh) using ethylacetate/hexane (1:19) as eluent to yield 460 mg (68 %) of yellow solid; mp 112-114 °C .^{1}H NMR (300 MHz, $CDCl_3$): δ 7.73-7.37 (m, 8H), 7.00 (s, 2H), 3.9 (t, 4H), 0.80-2.1 (m, 22H). ^{13}C NMR (75 MHz, $CDCl_3$): δ 153.63, 132.93, 131.59, 122.49, 122.38, 116.78, 113.82, 93.83, 87.08, 77.42, 77.00, 76.86, 76.58, 69.58, 31.56, 29.25, 25.715, 22.62, 14.01. m/z(FAB) 636.93, calcd. 636.46.

Preparation of 1,4-bis(hexyloxy)-2,5-bis((4-trimethylsilylethynyl)phenyl-ethynyl)benzene (7). To a stirring solution of aryl halide **6** (150 mg, 0.24

mmol), $Pd(PPh_3)_2Cl_2$ (16.50 mg, 0.024 mmol) and CuI (8.97 mg, 0.024 mmol) in 3 mL diisopropylamine, was added (trimethylsilyl)acetylene (75.5 μL, 0.29 mmol). The mixture was refluxed for 3 h under argon. After removal of the solvent, the crude product was crystallized using ethanol to give 64 mg (40%) of the product, mp. 124-126 °C. ^{1}H NMR (300MHz, $CDCl_3$):δ 7.37-6.9 (m, 10H), 4.02 (t, 4H), 1.9-0.9 (m, 22H), 0.2 (s, 9H). ^{13}C NMR(75 MHz, $CDCl_3$): δ 154.12, 131.85, 131.31, 116.84, 112.29, 77.42,77, 76.57, 69.6, 47.92, 29.27, 25.73, 22.62, 19.25, 14.01. m/z (FAB) 671.13, calcd. 671.07.

Preparation of 1,4-bis((4-phenylethynyl)phenylethynyl)-2,5-bis(hexyloxy) benzene (3). A mixture of 7 (300 mg, 0.45 mmol), K_2CO_3 (373.14 mg, 2.7 mmol), PPh_3 (47.16 mg, 0.18 mmol), $Pd(PPh_3)_4$ (104 mg, 0.09 mmol), CuI (17.10 mg, 0.09 mmol) and C_6H_5I (120.6 μL, 0.108 mmol) was stirred at room temperature in a solvent mixture of CH_3OH/THF (1:4) for 15 h. The crude product was purified by column chromatography over silica gel (100-200 mesh) using hexane/toluene (1:9) as eluent to yield 140 mg (46 %) of yellow colored solid; mp 173-175 °C. ^{1}H NMR (300 MHz, $CDCl_3$): δ 7.54-7.51 (m, 12H), 7.54-7.51 (m, 6H), 7.01(s, 2H), 4.04 (t, 4H), 1.88-0.90 (m, 22H). ^{13}CNMR (75 MHz, $CDCl_3$): δ 131.61, 131.5, 131.47, 128.45, 123.1, 116.87, 113.96, 69.64, 31.6, 31.2277, 29.3, 25.75, 22.64, 14.03. Anal. Calcd for $C_{50}H_{46}O_2$: C, 88.46; H, 6.83. Found: C, 88.43; H, 7.17. Exact mass calculated for $C_{50}H_{46}O_2$ (M^+) is 678.34979, found 678.34968 (FAB high resolution mass spectrometry).

2.3.3. Purification of compounds 2 and 3

In order to ensure high purity of the samples used in the photophysical studies, compounds **2** and **3** after conventional column chromatography, were further purified using recycling HPLC[50] with two columns connected in series. Typically 20-30 mg of phenyleneethynylenes, dissolved in chloroform (3 mL), was injected and eluted using the same solvent. Effective removal of even trace amounts of impurities could be achieved by recycling the samples for about 14-20 cycles. Figure 2.1 shows the chromatograms of phenyleneethynylenes obtained in the first cycle (peaks 'a' and 'b') and after recycling through HPLC. Peaks 'a_2' and 'b_2' in Figure 2.1 corresponds to compounds **2** and **3** which were further characterized by various analytical and spectroscopic techniques.

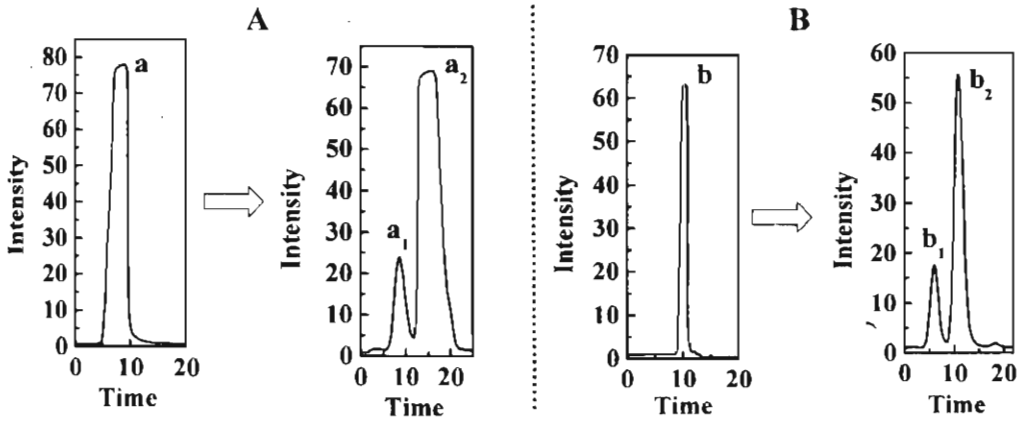

Figure 2.1. Chromatograms of phenyleneethynylenes obtained in the first cycle (peak 'a' and 'b') and after recycling (peaks 'a_1' and 'b_1' are impurity and 'a_2' and 'b_2' are purified products) through HPLC: **A)** compound **2** was recycled 17 times and **B)** compound **3** was recycled for 14 times.(**2** is monitored at 340 nm and **3** is monitored at 375nm).

2.4 Results and Discussion

2.4.1. Photophysical investigation

Absorption and emission properties. The absorption spectral features of **1**, shown in Figure 2.2 (trace 'a') was earlier reported by several groups as a broad band (partially resolved) in the spectral region of 250-350 nm.[42,51-53] In contrast, the absorption spectra of **2** and **3** recorded in different solvents (methylcyclohexane, toluene and dichloromethane) showed significantly different features with two well separated bands. For example, the spectrum of **2** in methylcyclohexane possess a shorter wavelength band between 275-325 nm, with partially resolved vibronic features and a long wavelength band with maximum around 367 nm of almost same intensity (trace 'b' in Figure 2.2).

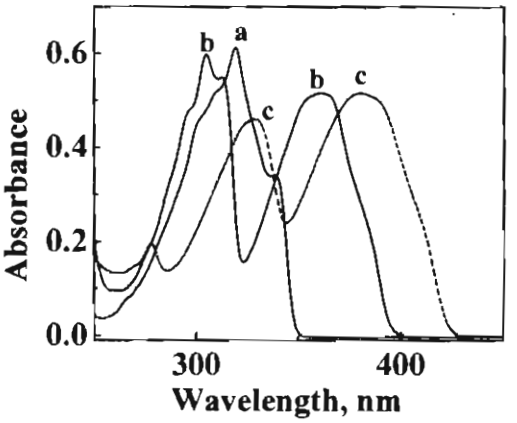

Figure 2.2. Absorption spectrum of phenyleneethynylenes in methyl-cyclohexane; (a) **1**; (b) **2**; (c) **3**.

In an earlier report, West and coworkers have reported the absorption spectra of **2** with similar spectral features.[45] In the case of **3**, both the absorption bands are red shifted by around 20 nm due to the increase in conjugation, however do not possess any distinct vibronic features. From these studies it is obvious that

the dialkoxy substitution has a significant effect on the photophysical properties of phenyleneethynylenes. The splitting of the absorption band observed for **2** and **3** compared to **1** are discussed in detail using theoretical studies (*vide infra*). The absorption spectral profile of **2** and **3** remains unaffected with increase in concentration (upto 15 μM) and were found to be independent of the nature of the solvent, ruling out the possibility of any ground state interactions such as aggregation. The singlet excited state energies of phenyleneethynylenes as determined from the cross over point between the normalized absorption and emission spectra were 3.16 eV for **2** and 2.96 eV for **3** (Figure 2.2 and Figure 2.3).

The fluorescence spectra of **2** and **3** were recorded by exciting at different wavelengths, ranging from 290 nm to 400 nm in three different solvents. A representative example (**2** and **3** in methylcyclohexane) is presented in Figure 2.3. In all the cases, the absorbance of the solution was kept as 0.1 at the excitation wavelength. The emission spectra of **2** and **3**, in methylcyclohexane, obtained by exciting at different wavelengths were normalized and presented in the inset of Figure 2.3. In contrast to the absorption spectra, the emission spectra of both the compounds possess well structured vibronic bands in methylcyclohexane, indicating that the excited state geometry of phenyleneethynylenes is more planar compared to ground state. These aspects were further confirmed by calculating the excited state energy barrier using theoretical methods (*vide infra*). The vibronic features of the normalized emission spectra were found to be identical on exciting at

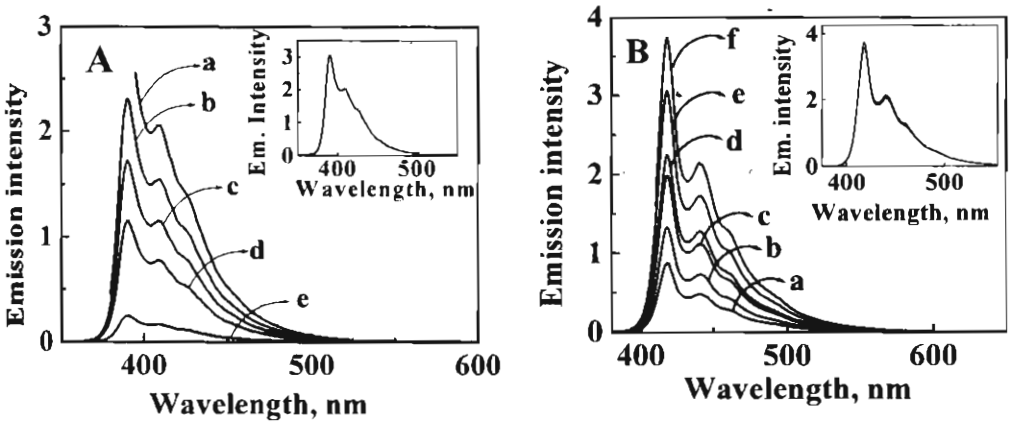

Figure 2.3. **A)** Fluorescence spectra of **2** in methylcyclohexane on exciting at (a) 320 (b) 340 (c) 350 (d) 370 (e) 385 and (f) 400 nm and **B)** fluorescence spectra of **3** in methylcyclohexane on exciting at (a) 310 (b) 320 (c) 340 (d) 350 (e) 375 and (f) 400 nm. The inset in Figure 2.3A and 2.3B shows the normalized emission spectrum of **2** and **3** at different exciting wavelengths.

different wavelengths (Figure 2.3) indicating the presence of a single emitting species. The emission spectra were further compared in methylcyclohexane, toluene and dichloromethane. Vibronic features in dichloromethane are less distinct compared to methylcyclohexane and no appreciable change in the spectral features was observed on varying the solvent polarity. The Stokes shift of phenyleneethynylenes **2** and **3** were calculated as ~2100 and ~2300 cm^{-1} respectively (Table 2.1). The Stokes loss reported for rigid aromatic molecules like fluorene is ~1430 cm^{-1} and that of biphenyls which undergo conformational change in the excited state leading to planarization is ~3310 cm^{-1}.[54] The intermediate values obtained for **2** and **3** suggest that these compounds undergo conformational changes in the excited state favoring a more stable planar conformation. Based on theoretical investigation it is confirmed that rotational energy barrier of the arene rings along the molecular

axis must be higher in the excited state and this limits the number of conformers leading to a structured emission (*vide infra*). Fluorescence excitation spectra of **2** and **3** were recorded by collecting the emission at three different wavelengths and resemble the UV-Vis absorption spectrum.

Table 2.1. Stokes shift and fluorescence lifetimes[b] (τ_f) of 2 and 3 in different solvents.

Solvent	Compound 2		Compound 3	
	$(\nu_{abs} - \nu_{em})^a$ (cm^{-1})	$\tau_f{}^b$ (ns)	$(\nu_{abs} - \nu_{em})^a$ (cm^{-1})	$\tau_f{}^b$ (ns)
Methylcyclohexane	2130	1.28	2500	0.88
Toluene	2130	1.37	2300	1.10
Dichloromethane	2000	1.50	2200	1.01

[a]($\nu_{abs} - \nu_{em}$), Stokes shift; [b]τ_f, fluorescence lifetime (error limit ± 5%)

Fluorescence lifetime measurements. To further confirm the presence of a single emitting species in the excited state, detailed fluorescence lifetime studies of **2** and **3** were carried out using single photon counting technique at different excitation wavelength and solvent polarity. Fluorescence lifetimes (τ_f) of **2** and **3** in different solvents are summarized in Table 2.1. The compounds were excited at 280, 375 and 394 nm and the emission was collected at different wavelengths. In a particular solvent system, fluorescence lifetime (τ_f) was found to be independent of the excitation wavelength and the wavelength at which the emission is collected. In all the cases, emission decay

exhibited monoexponential decay further confirming the presence of a single emitting species.

Fluorescence quantum yield. West and coworkers reported that phenyleneethynylenes (e.g. **2**) possess strong self-absorption/excimer formation and the measured quantum yield is highly dependent on their concentration and excitation wavelength.[45] In the present study, the fluorescence quantum yield was estimated, using dilute solutions of **2** and **3** and integrating the emission spectra. The experiments were repeated at four different concentrations by varying the absorbance at the excitation wavelength (355 nm). The absorbance at 355 nm was varied from 0.025 to 0.1, in each case, and matched with that of reference. A solution of diphenylanthracene in cyclohexane was used as the reference (Φ_f=0.9). The average quantum yield obtained from these measurements was 0.66 ±0.06 and 0.5 ±0.05 for **2** and **3**, respectively (Table 2.2).

Excited singlet state. The femtosecond laser flash photolysis was employed to investigate the absorption characteristics of excited singlet state of the phenyleneethynylenes **2** and **3**. The singlet state of both the compounds were generated by the direct excitation with 387 nm laser (pulse width 150 fs). The transient absorption spectra recorded at different time intervals, following the laser excitation of **2** and **3**, are shown in Figure 2.4. The difference absorption spectrum of **2** showed a band with maxima at 555 nm whereas higher homologue (**3**) exhibited two distinct bands (λ_{max} at 640 and 750 nm). A large bathochromic shift in the absorption maximum is observed for **3** compared to **2**

suggesting lower energy S_1-S_n transitions with increasing phenylethynyl units. The lifetimes measured from the absorption decay of S_1 matched well with the lifetimes measured from the fluorescence decay (Table 2.2).

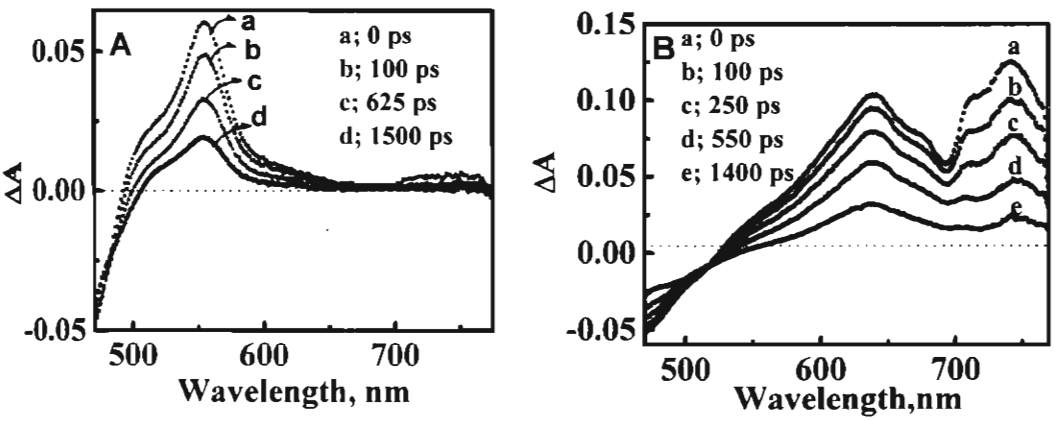

Figure 2.4. Time resolved transient absorption spectra of singlet excited states of **A) 2** and **B) 3** in toluene. The spectra were recorded at different intervals following the 387 nm laser pulse excitation.

Earlier reports have indicated that phenyleneethynylenes possess fluorescence quantum yields close to unity.[45] This observation implies that the radiative deactivation is the only pathway for the relaxation of the singlet excited state of phenyleneethynylenes. Schmieder et al. ruled out the possibility of the vibrational relaxation and intersystem crossing from the singlet excited state of an analogous molecule, 1,4-bis(9-ethynylanthracenyl)benzene.[55] The fluorescence quantum yield values estimated for **2** and **3** in the present experiments are much lower than unity (0.66 ±0.06 and 0.5 ±0.05 for **2** and **3** respectively). These observations indicate that one or more nonradiative pathways contribute to the deactivation of the singlet excited state. If this argument is true, we should be able to establish the deactivation pathways, for example, intersystem crossing, by monitoring the formation of long-lived

triplet excited state. The residual absorption seen at 1.5 ns in the femtosecond transient studies (Figure 2.4) is an indication of the presence of long-lived species. The obvious question is whether these long-lived transients correspond to the triplet excited state and these aspects were investigated using nanosecond laser flash photolysis studies.

Table 2.2. Singlet state properties of compounds 2 and 3.

Compound	λ_{So}[a] nm	ε[b] $M^{-1}cm^{-1}$	λ_f[c] nm	τ_f[d] ns	$S_{0\text{-}0}$[e] eV	ϕ_f[f] (λ_{exc}=355nm)	$\lambda_{So\text{-}Sn}$[g] nm
2	367	3.1×10^4	401	1.43	3.16	0.66 ±0.06	555
3	387	6.6×10^4	429	0.92	2.96	0.50 ±0.05	638, 740

[a]absorption maximum (λ_{So}), [b]molar extinction coefficient at absorption maximum (ε), [c]emission maximum (λ_f), [d]fluorescence lifetime (τ_f), [e]singlet excitation energy ($S_{0\text{-}0}$), [f]quantum yield of fluorescence (ϕ_f), [g]singlet excited state absorption ($\lambda_{So\text{-}Sn}$)

Triplet excited state. Both phenyleneethynylenes **2** and **3** possess strong absorption at around 355 nm which allows their direct excitation by the third harmonic of Nd:YAG laser (355-nm). The time resolved transient spectra, recorded by following 355-nm laser pulse excitation, of **2** and **3** at different time intervals are shown in Figure 2.5. The transient spectrum of **2**, recorded immediately after laser pulse showed depletion at 390 nm and absorption at 520 nm. Interestingly, in the case higher homologue phenyleneethynylene i.e. **(3)**, the absorption of the newly formed transient is red shifted to 660 nm. The transient absorption band observed for both **2** and **3** are prompt and assigned as triplet-triplet absorption based on the following observation: (i) the lifetime of the transient are readily quenched by oxygen (ii) the transients are quenched by

the addition of triplet energy acceptors such as oxazine. The triplet formation is complete within the pulse duration of 10 ns of the excitation pulse and the spectral characteristics of the triplet excited states are summarized in Table 2.3.

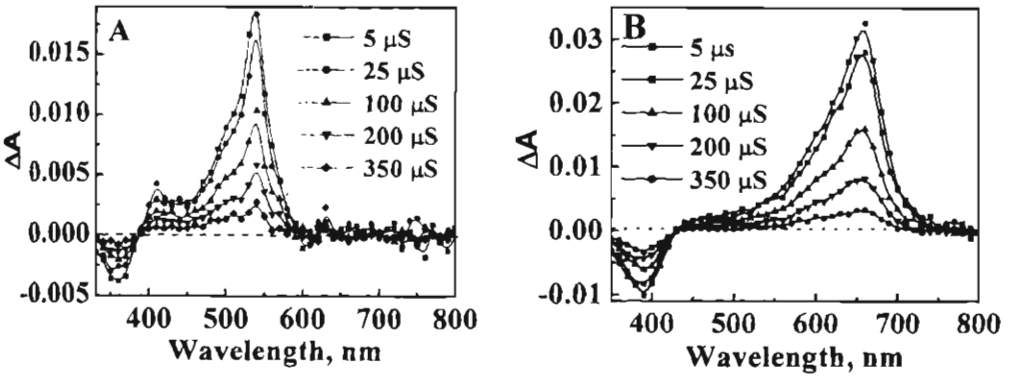

Figure 2.5. Transient absorption spectra of **A) 2** and **B) 3** recorded at (a) 5 (b) 25 (c) 100 (d) 200 (e) 350 ms following 355 nm laser excitation.

The triplet lifetimes of phenyleneethynylenes **2** and **3** were estimated as 140 μs and 218 μs (error limit of 5 %), respectively. The extinction coefficient of the triplet excited state of phenyleneethynylenes was determined by adopting total depletion method. The complete conversion of ground state molecules to the triplet excited state is achieved by increasing the intensity of the nanosecond laser (note that the absorbance at the excitation wavelength is kept as 0.02 for ensuring the total excitation). A high extinction coefficient values were estimated for **2** as 47,600 M^{-1} cm^{-1} and **3** as 31,000 $M^{-1}cm^{-1}$ (Table 2.3). The quantum yield of the triplet formation for **2** and **3** in toluene was determined by comparing it with 1-pyrenecarboxaldehyde (ϕ_T= 0.78) and the values obtained are 0.40 and 0.50 (error limit of 10 %) for **2** and **3** respectively. Further we have investigated the possible deactivation pathways for the triplet excited state

by monitoring the decay by increasing the laser energy and varying the ground state concentration.

Table 2.3. Triplet state properties 2 and 3 in toluene.

Compound	$\lambda_{T-T\,(max)}$ nm	$\varepsilon_{T\,(max)}$ $M^{-1}cm^{-1}$	ϕ_T	τ_T μs	k_{O2} $M^{-1}s^{-1}$	k_{sq} $M^{-1}s^{-1}$	$2k_{T-T}$ $M^{-1}s^{-1}$
2	520	47,000	0.40	140	1.6×10^9	6.0×10^7	2.0×10^9
3	660	31,000	0.50	218	1.5×10^9	6.0×10^7	1.6×10^9

[a]triplet absorption maximum, [b]triplet extinction coefficient, [c]triplet quantum yield, [d]triplet lifetime, [e]rate of triplet state quenching, [f]bimolecular rate constant for triplet-triplet annihilation.

Deactivation from triplet excited state. In order to investigate intermolecular interactions in the excited state, the effect of the triplet excited state at varying concentrations of **2** and **3** were investigated. Laser flash photolysis studies were carried out by recording the triplet lifetimes at different ground state concentrations of **2**, keeping the triplet excited state concentration constant. The concentration of the triplet excited state is maintained as low as 0.015 by varying the intensity of the exciting laser in each case, thus avoiding any triplet-triplet reaction. The bimolecular quenching constant for the triplet of **2** by its ground state was determined by measuring the pseudo first order rate constant at various concentrations. From the linear dependence of the pseudo first order rate constant on the ground state, the bimolecular quenching constant of **2** and **3** in toluene and acetonitrile was estimated as $\sim 2 \times 10^7\ M^{-1}s^{-1}$. The low values of the bimolecular quenching constant indicate that the decay of the triplet is not significantly influenced by the ground state concentration.

Interestingly, it was observed that the decay of the triplet excited state at 520 nm has a significant effect on the laser energy. At lower laser energies (< 0.5 mJ/pulse) the transient showed a first order kinetics, however deviation was observed on further increasing the laser energy. The rate law for the fast decaying process observed at higher energy is given by equation 2.1 as

$$d[^3\text{phenyleneethynylenes}]/dt = -k[^3\text{phenyleneethynylenes}]^2 \quad \text{----------(2.1)}$$

The second order-term becomes significant with increase in the energy which is attributed to an intermolecular triplet-triplet annihilation process. The bimolecular rate constant for **2** and **3** was calculated as 2×10^9 and 1.6×10^9 $M^{-1}s^{-1}$, respectively.

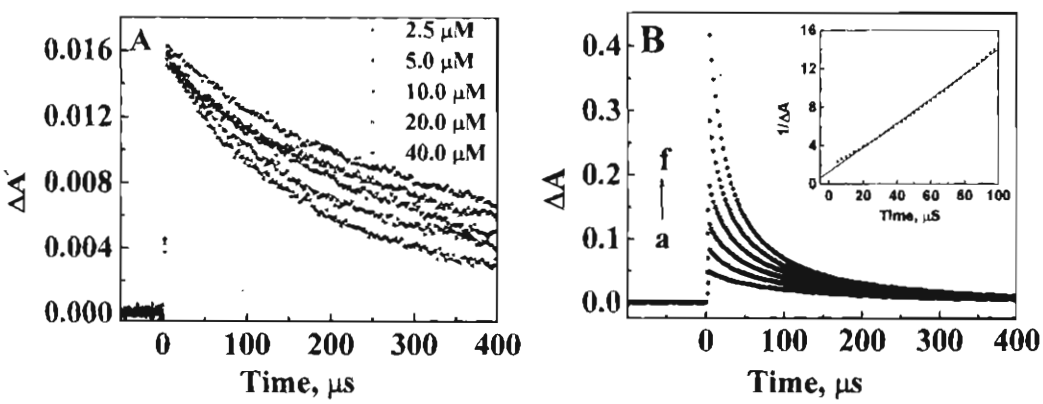

Figure 2.6. A) Ground state concentration dependence of **2** on the triplet decay at 520 nm in argon saturated toluene solution; Concentration of **2** varied as (a) 2.5 (b) 5 (c) 10 (d) 20 (e) 40 μM; **B)** Laser-power dependence on the absorption-time profiles of **3** (7.5 μM) at 520 nm obtained by 355-nm laser flash photolysis in argon saturated toluene. The power of the laser varied from (a) 0.2 (b) 1 (c) 3 (d) 5.0 (e) 7.5 (f) 10 mJ/pulse. Inset shows the fitting of the fast decaying process using the equation 2.1

Pulse radiolytic oxidation of phenyleneethynylenes. It has been shown earlier that radiolysis of chlorinated hydrocarbons such as methylenechloride produces highly oxidizing radical such as $RCl^{\cdot}$ which undergo diffusional

charge transfer with an added substrate. The transient absorption spectrum of the radical cation of phenyleneethynylenes recorded following the pulse radiolysis of a solution of **2** and **3** in O_2 saturated methylenechloride is shown in Figure 2.7. The transient difference absorption spectrum of $\mathbf{2}^{\cdot+}$ exhibits two bands one at 470 nm and the other around 510 nm (trace 'a'). The difference absorption bands are red shifted and appears around 520 and 570 nm in the case of $\mathbf{3}^{\cdot+}$ (trace 'b').

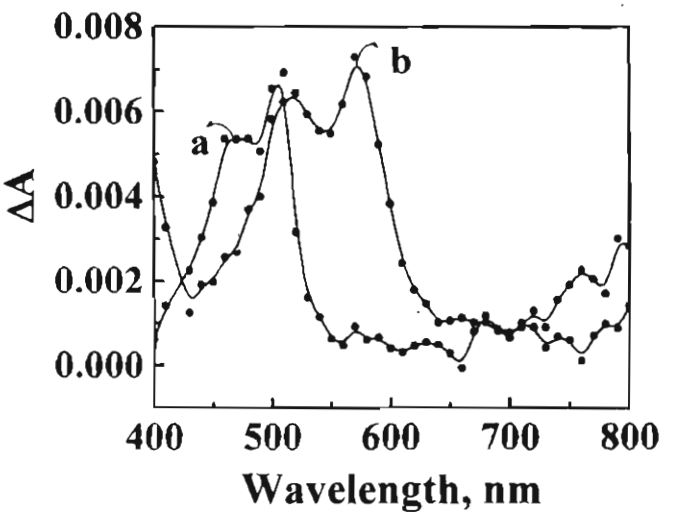

Figure 2.7. Transient absorption spectra of pulse radiolytically generated cations of (a) **2** and (b) **3** in methylenechloride. The spectra were recorded following the pulse radiolysis of O_2 saturated CH_2Cl_2 solution containing ~0.1 mM of phenyleneethynylenes.

Excited state interactions. We have investigated the possibility of electron transfer from the singlet as well as triplet excited state of phenyleneethynylenes by adding benzoquinone (BQ) and N,N-dimethylaniline (electron acceptor and electron donor respectively) in a polar solvent such as acetonitrile. On adding benzoquinone (BQ), the fluorescence of both **2** and **3** were quenched dramatically. The quencher molecule absorbs at shorter wavelength compared to the emission of **2** (or **3**), hence the possibility of the singlet energy transfer

can be ruled out. The quenching of the fluorescence of **2** at different concentration of BQ is shown in Figure 2.8A and the Stern-Volmer plot of I_0/I

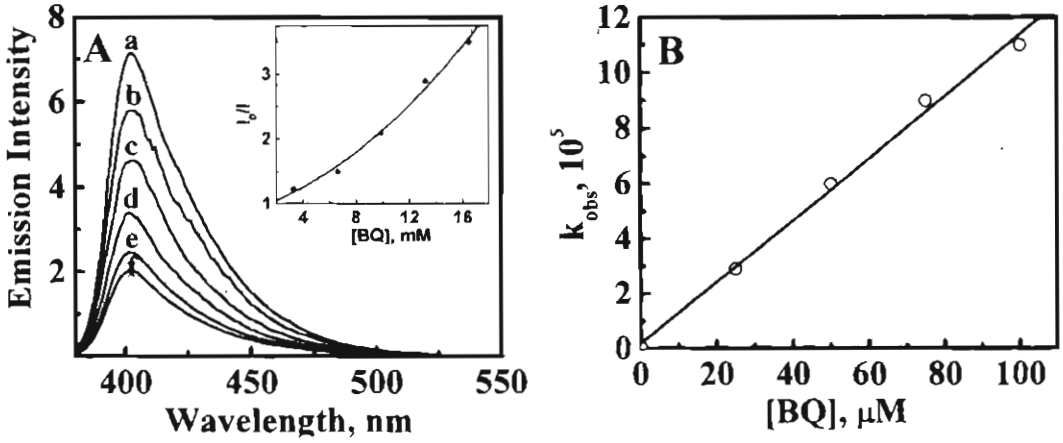

Figure 2.8. A) Fluorescence quenching of **2** by BQ at concentration levels of (a) 0 (b) 3.3 (c) 6.6 (d) 9.9 (e) 13.2 (f) 16.5 mM in acetonitrile. λ_{ex}=375 nm. (Optical Density at 375 nm kept as 0.1). Inset shows the Stern-Volmer fit using equation 2.3 **B)** Rate of triplet decay plotted against concentration of benzoquinone added.

against the quencher concentration showed a nonlinear curve. These results indicate the involvement of both static and dynamic quenching process as indicated below (Equation 2.2).

$$^1\mathbf{2}^* + BQ\ (or\ ^1(\mathbf{2}:::BQ)^*) \rightarrow \mathbf{2}^{\cdot+} + BQ^{\cdot-} \quad \ldots\ldots\ldots (2.2)$$

The nonlinear curve was further analyzed using a second order polynomial equation (equation 2.3),

$$I_0/I = 1 + (K + k_q\tau_f)[Q] + Kk_q\tau_f[Q]^2 \quad \ldots\ldots\ldots (2.3)$$

where 'I_0' is the fluorescence intensity in the absence of quencher and 'I' is the fluorescence intensity in presence of quencher, 'k_q' is the diffusional quenching constant, while 'K' represent the equilibrium constant of the complex formation between phenyleneethynylenes and benzoquinones (e.g. **2**:::BQ in

equation 2.2). The diffusional quenching constant for **2** and **3** was estimated as 5.3×10^{10} and 8.4×10^{10} $M^{-1}s^{-1}$ respectively. These results indicate that in the presence of BQ, intermolecular electron transfer process (equation 2.2) competes with intersystem crossing.

To investigate the possible reaction of the triplet excited state, the triplet decay was followed at their corresponding absorption maximum, at varying concentrations of BQ. The bimolecular quenching rate constant (k_q) was determined from the slope of the plots (Figure 2.8 B) on basis of the relationship

$$k_{obs} = 1/\tau_t + k_q[Q] \text{ ---------- (2.4)}$$

where k_{obs} is the observed rate constant in the presence of quencher, [Q] is the quencher concentration and τ_t is the lifetime of the triplet excited state in the absence of the quencher. The bimolecular quenching rate constants were estimated from the slope as 1.1×10^{10} $M^{-1}s^{-1}$ and 1.3×10^{10} $M^{-1}s^{-1}$ for **2** and **3**, respectively.

If the quenching process is based on the photoinduced electron transfer process, we should be able to characterize the electron transfer products namely the radical cation of **2** and the radical anion of BQ using nanosecond laser flash photolysis. The time-resolved absorption spectra following 355 nm laser excitation of **2** in deoxygenated solution of acetonitrile is shown in Figure 2.9.

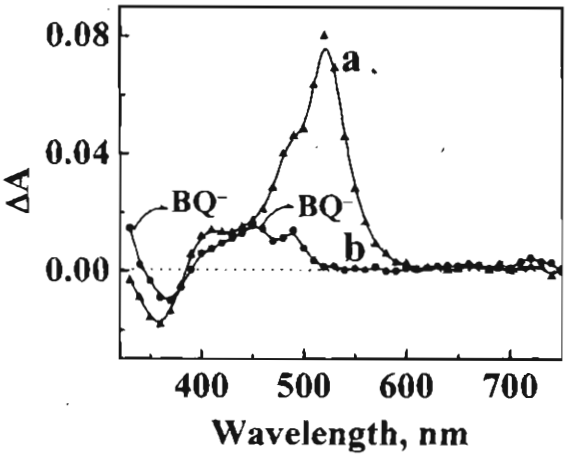

Figure 2.9. Time-resolved difference absorption spectra recorded after 20 μs following 355-nm laser pulse excitation of **2** in (a) absence and (b) presence of BQ (experiment was carried out using nanosecond laser flash photolysis set up).

The difference absorption spectra recorded 20 μs after the laser flash excitation exhibit two broad peaks, one around 450 nm and other around 490 nm. The decay of the transient at 450 nm corresponds to the absorption of BQ radical anion and the bleaching at 375 nm corresponds to the ground state recovery. The recovery at 375 nm consists of two terms: (a) the fast recovery of the ground state from the triplet of **2** and (b) the recombination of the long-lived radical cation of **2**. Both the radical anion of BQ and the radical cation of **2** possess absorption in the spectral region of 490 to 520 nm and hence difficult to resolve.

Excited state interaction with N,N-dimethylaniline. Fluorescence of both **2** and **3** are efficiently quenched by N,N-dimethylaniline (DMA). Figure 2.10 shows the quenching of fluorescence of **2** at different concentration of DMA and the quenching rate constant was estimated using Stern-Volmer equation (equation 2.5),

$$I_0/I = 1 + k_q\tau_f [Q] \ldots\ldots\ldots (2.5)$$

The high value of k_q (12.4×10^9 $M^{-1}s^{-1}$) suggest the possibility of the efficient interaction between DMA and the singlet excited state of **2**.

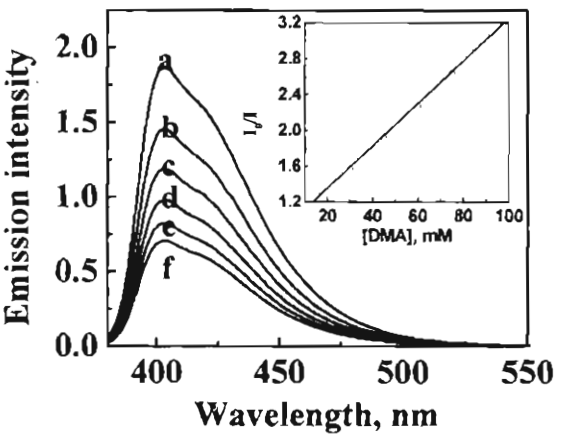

Figure 2.10. Fluorescence quenching of **2** by DMA at concentration levels of (a) 0 (b) 3.3 (c) 6.6 (d) 9.9 (e) 13.2 (f) 16.5 mM in acetonitrile. λ_{ex}=375 nm. (absorbance at 375 nm kept as 0.1). Inset shows the Stern-Volmer fit using equation 2.5.

The effect of DMA on the deactivation of the singlet excited state of **2** was further studied using the femtosecond laser flash photolysis. Spectrum recorded immediately after the laser excitation shows the absorption of the singlet excited state at 555 nm. Further, with increase in time the band at 555 nm is diminished and the absorption of triplet of **2** appeared at 520 nm (Figure 2.11).

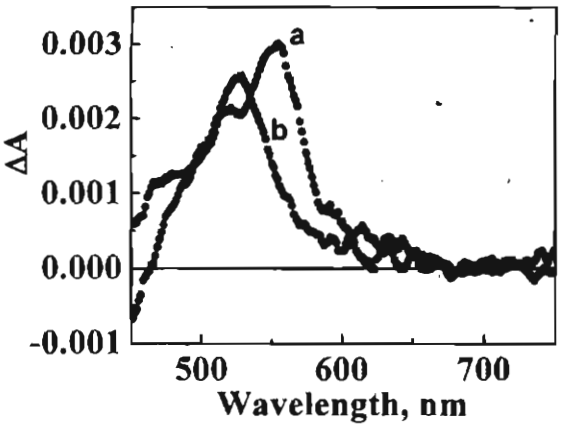

Figure 2.11. Time-resolved difference absorption spectra recorded after 1 ns following 387 nm laser pulse excitation of **2** in (a) absence and (b) presence of DMA (0.1 M) in a femtosecond laser flash photolysis apparatus.

To understand the reaction between the triplet of excited state of OPE with DMA, we recorded their decay in presence of different concentration of DMA using 355 nm nanosecond laser. Figure 2.12 shows the pseudo-first order decay of triplet and the low value of quenching rate (7.3×10^5 M^{-1} cm^{-1}) suggest that the electron transfer from the triplet to DMA is not significant. The transient absorption spectrum of **2** in presence of DMA shows the absorption of DMA radical cation at 375 nm.

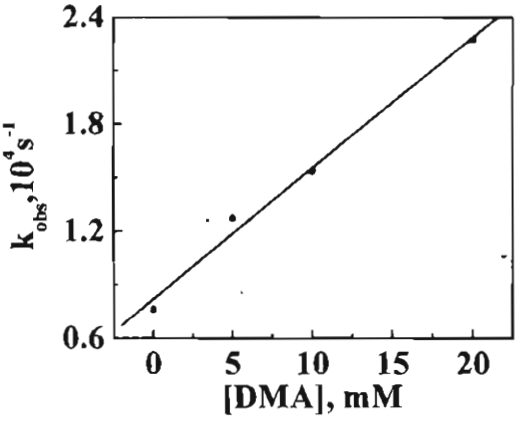

Figure 2.12. Dependence of pseudo-first-order rate constants for the triplet decay of **2** on the concentration of DMA. The triplet decay was monitored at 520 nm.

2. 4. 2. Theoretical investigations

Various conformations of phenyleneethynylene based rigid rod molecular systems (**2** and **3** in Chart 2.1) were optimized at AM1 level, a semiempirical method widely used for obtaining reliable geometries for organic systems. Highest and lowest energy conformations derived from AM1 level calculations were further optimized by B3LYP/6-31G* level density functional (DFT) method.[56,57] In DFT method, electron correlation effects were taken into account and this method is often used as a compromise for higher end calculation at a reasonable computational cost.[58,59] The basic photochemical properties of these systems were investigated by means of quantum chemical calculations employing mainly the time-dependent density functional theory (TDDFT) formalism[60-62] as well as Zerner's intermediate neglect of differential overlap (ZINDO/S) method.[63,64] TDDFT using B3LYP input has been proved to be more accurate for many molecular systems including poly(phenylenevinylyne) (PPV) type polymers.[65] For all the calculations, Gaussian03[66] suit of programs were used.

A detailed ground state conformational analysis of **2** and **3** were carried out using AM1 semiempirical quantum mechanical method. The stationary points thus obtained were confirmed as minima by performing normal coordinate analysis. The main focus of the present investigation is to understand the conformational, π-conjugation, and excited state properties of phenyleneethynylenes **2** and **3**, in comparison with the unsubstituted compound **1**. A completely planar geometry (**1a**) is the only minimum energy conformation

for **1** wherein one π-bond from each of the acetylene unit conjugate with 18 π-electrons from the three benzenoid rings resulting in an extended π-conjugation. In contrast, four different minimum energy conformations have been obtained for **2** and **3**. The conformations obtained for **2** are depicted in Figure 2.13 and conformations of **3** (namely **3a**, **3b**, **3c** and **3d**) also possess the same orientation of the alkoxy chain as in **2**. In the most stable conformation of **2** and **3** (i.e., **2a** in Figure 2.13), the alkoxy chain and the benzenoid rings occupy the same plane leading to maximum resonance interaction between the oxygen lone pairs and the arene ring π-electrons. In the next lower energy conformation (**2b** and **3b**), one alkoxy chain remains in the benzenoid plane and the other one is twisted out of the plane. Both the alkoxy groups are twisted out to opposite sides of the benzenoid plane in the third conformer, (**2c** and **3c**) while in the fourth conformer (**2d** and **3d**), both substituents are twisted out to the same side of the plane.

Starting from the most stable trans in plane conformation of compound **2** and **3** (**2a** in Figure 2.13), the rotation of the phenyl groups along the triple bond is modeled. In the case of conformation **2a**, the rotation of the central phenyl ring with respect to the terminal ones is modeled by constraining the angle between the planes of central and the terminal rings to the increments of 10°. The conformer with highest heat of formation corresponds to the one with central and terminal rings are orthogonal. This orthogonal conformation is found to 0.6 kcal/mol less stable than the fully planar structure **2a**. Further, by constraining the angle made by the terminal phenyl rings, one more conformation is

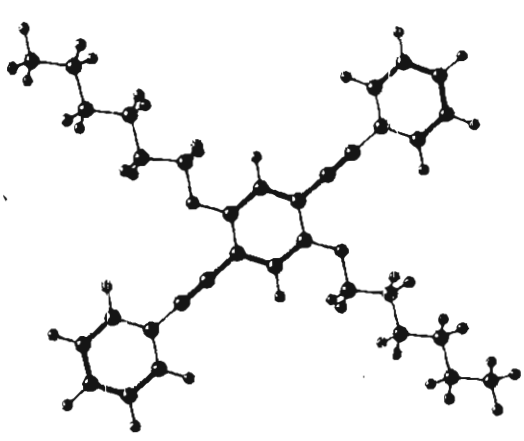

2a, E = 0.00 kcal/mole

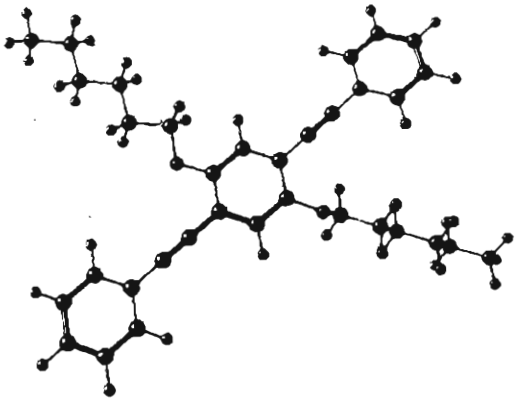

2b, E = 0.48 kcal/mol

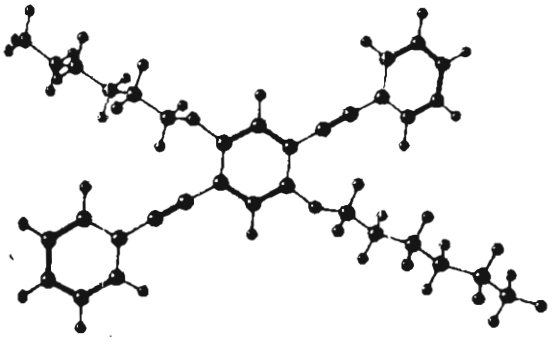

2c, E = 1.27 kcal/mol

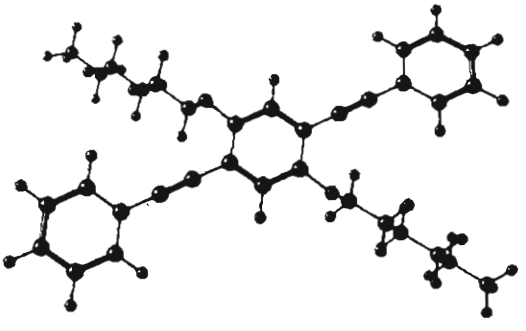

2d, E = 1.43 kcal/mol

Figure 2.13. Four different conformers of **2** obtained by AM1 semiempirical calculations and their relative heat of formation. Conformations of **3** namely **3a**, **3b**, **3c** and **3d** also follow the same order in orientation and energy.

obtained in which the terminal rings are orthogonal and the angle between the center and terminal ring planes is 45°. The energy required for such a twisting is only 0.3 kcal/mol. More intermediate twisted conformations are possible in the case of **3** due to the presence of five phenyl rings. A conformer in which all the adjacent phenyl rings are orthogonal to each other showed the highest heat of formation. Interestingly even this conformer was only 1 kcal/mol less stable than the planar conformer.

The most stable and the least stable structures at AM1 level were further optimized at B3LYP/6-31G* level of density functional theory. In order to reduce the computational cost, the hexyloxy substituents were replaced with ethyloxy substituents and the corresponding compounds were named as **2'** and **3'**. The structures optimized using AM1 and those obtained by DFT showed only little difference from the X-ray structure reported.[45] However, a more refined geometry in terms of dihedral angles and C-O bond distances were obtained by DFT level of optimization. For example, in the case of **2'** the $C(sp^2$, arene)-O-$C(sp^3$, alkyl) dihedral angle is calculated to be 107.4° by DFT which is only 0.28° higher than that in the X-ray structure while the AM1 calculations provided a lower value of 105.6°. Similarly in DFT level of optimization the $C(sp^2$, arene)-O bond distance showed a negligible difference of only 0.005 Å less than the X-ray structure. The most stable and the least stable optimized geometries of phenyleneethynylenes **1-3** and their relative energies are depicted in Figure 2.14.

It can be seen from Figure 2.14 that even at DFT level, there is only a difference of 4.8 kcal/mol between the most stable and the least stable structures. It indicates that the twisting of phenyl rings along the carbon-carbon triple bond is almost frictionless and one can expect planar as well as all sorts of twisted conformations for **1-3** at room temperature. The small barrier of rotation for the phenyl rings can be easily explained from the features of the π-electron conjugation in these molecules. The planar conformation possesses a completely extended conjugation of the phenyl π-electrons through

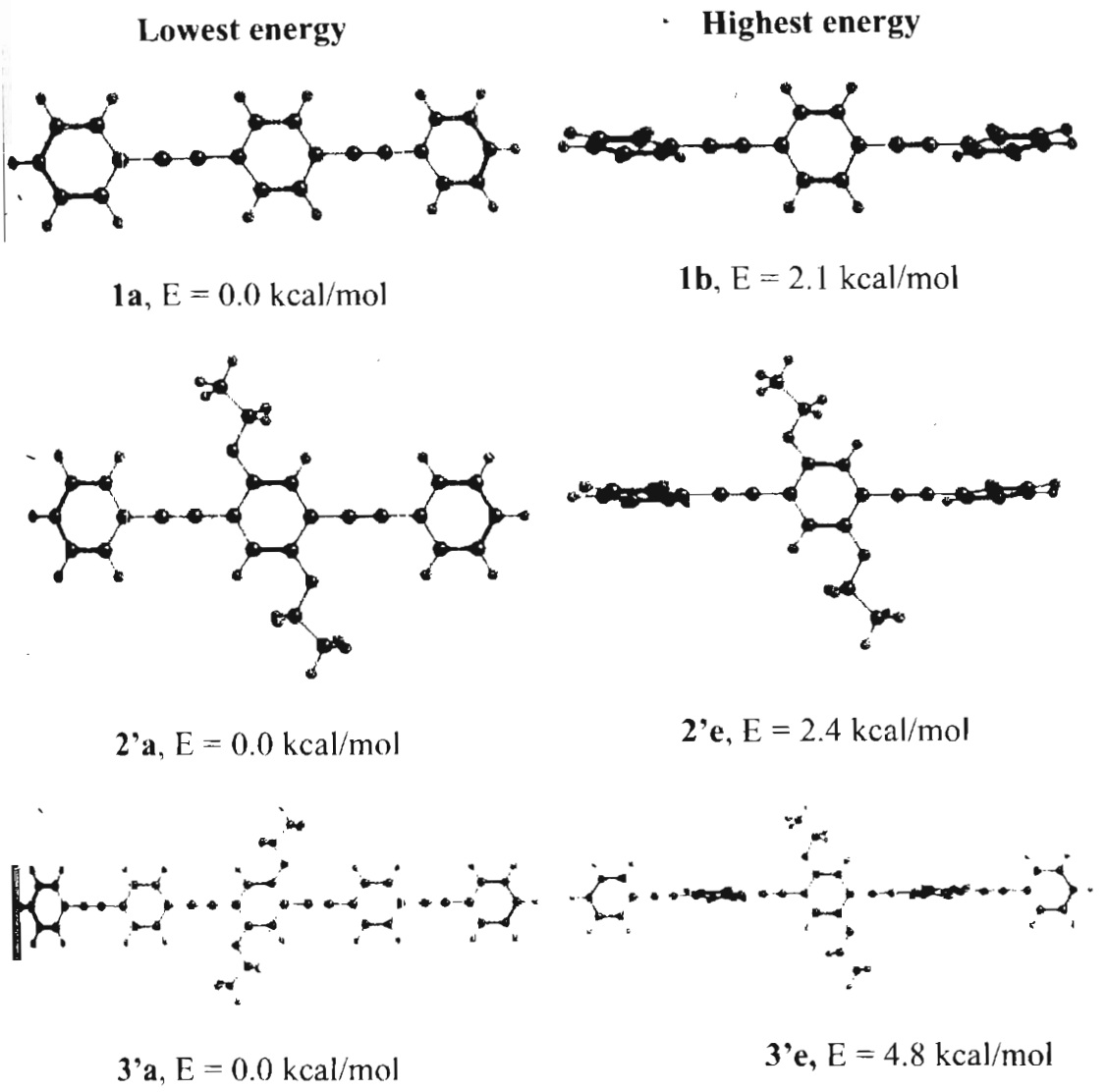

Figure 2.14. The most stable planar conformations and the least stable orthogonal conformations of **2** and **3** obtained by B3LYP/6-31G* method and their relative energies.

ne of the π bonds of each acetylenic bond. This smooth-conjugation is broken the orthogonal junctions in the perpendicular conformation and the system ses some energy. However, this loss of energy is partially compensated by e participation of the second π-bond of the acetylenic bond. This feature of e π-electron conjugation can be visualized through their molecular ctrostatic potential (MESP) distributions as well as the relevant molecular bitals as depicted in Figure 2.15.

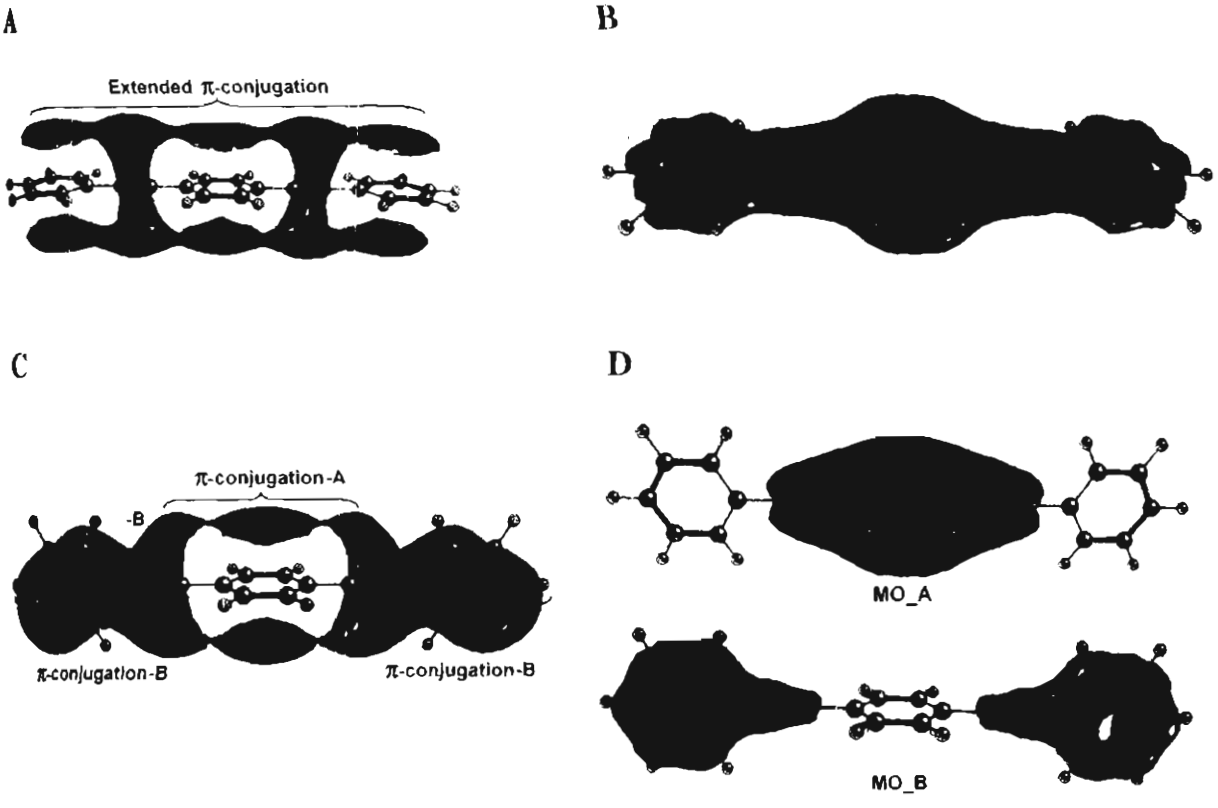

Figure 2.15. (**A**) and (**C**) shows the π-conjugation features visualized through the molecular electrostatic potential isosurfaces with value -9.4 kcal/mol for **1a** and **1b**. **B**) The molecular orbital showing the extended π-conjugation in **1a**. **D**) The molecular orbitals MO_A and MO_B supports the localized π-conjugations in **1b**.

Using the optimized planar geometries **1**, **2'a**, **3'a** at B3LYP/6-31G* level, the first 20 low lying excited states have been calculated at TDDFT and ZINDO/S levels. It is interesting to note that the unsubstituted phenylene-ethynylene **1** possesses only one singlet state with significant oscillator strength while **2'a**, and **3'a** showed two such states. These theoretical results are in good agreement with the number of absorption peaks observed for **1**- **3** (Figure 2.2). The absorption wavelengths and the corresponding MOs involved were obtained by TDDFT and ZINDO/S methods and compared with experimental results (Table 2.4). The singlet excited state of **1** corresponds to the electron

transition from HOMO to LUMO (cf. Figure 2.16 for the orbitals) and the calculated wavelength of 360 nm (TDDFT) and 365 nm (ZINDO/S) for this absorption is in reasonable agreement with the experimental value of 320 nm (Figure 2.2).

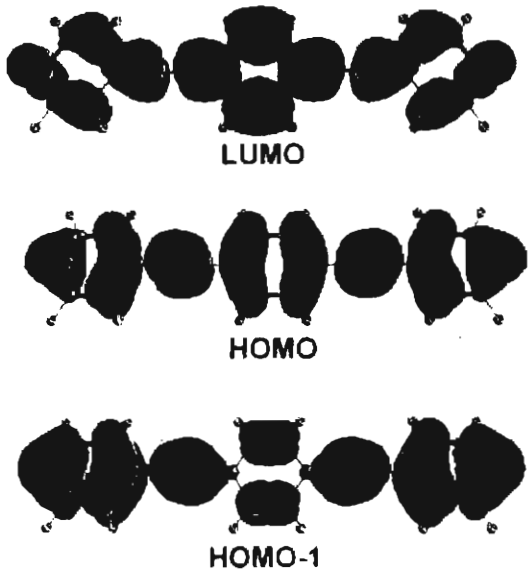

G28777

Figure 2.16. Frontier molecular orbitals of compound **1** obtained at B3LYP/6-31G* level. The singlet excited state corresponds to the electron transition from HOMO to LUMO.

The TDDFT level calculated spectra and the corresponding MO transitions for **2'a** is given in Figure 2.17. A comparison of the MOs of substituted system **1** in Figure 2.15 and **2'a** in Figure 2.17 suggest that the oxy substituent of **2'a** modifies its center arene ring π-orbitals through the resonance interaction with the oxygen lone pairs. This leads to the development of very similar orbital features for HOMO and HOMO-1 resulting in electronic transitions from both HOMO and HOMO-1 to LUMO for **2'a**. Similar orbital feature are observed in **3'a** as well. The calculated absorption maxima (λ_{cal}) are

also in good agreement with the experimental values (λ_{exp}) in all the three systems. In the case of **2'a** and **3'a**, the higher wavelength absorption corresponds to electronic transition mainly from HOMO to LUMO (Table 2.4). The lower wavelength absorption originates from HOMO-1 to LUMO and HOMO-2 to LUMO for **2'a** and **3'a**, respectively. The orbital features of HOMO-1 of **2'a** and HOMO-2 of **3'a** are found to be similar, which imply same type of electronic transition for lower wavelength absorptions.

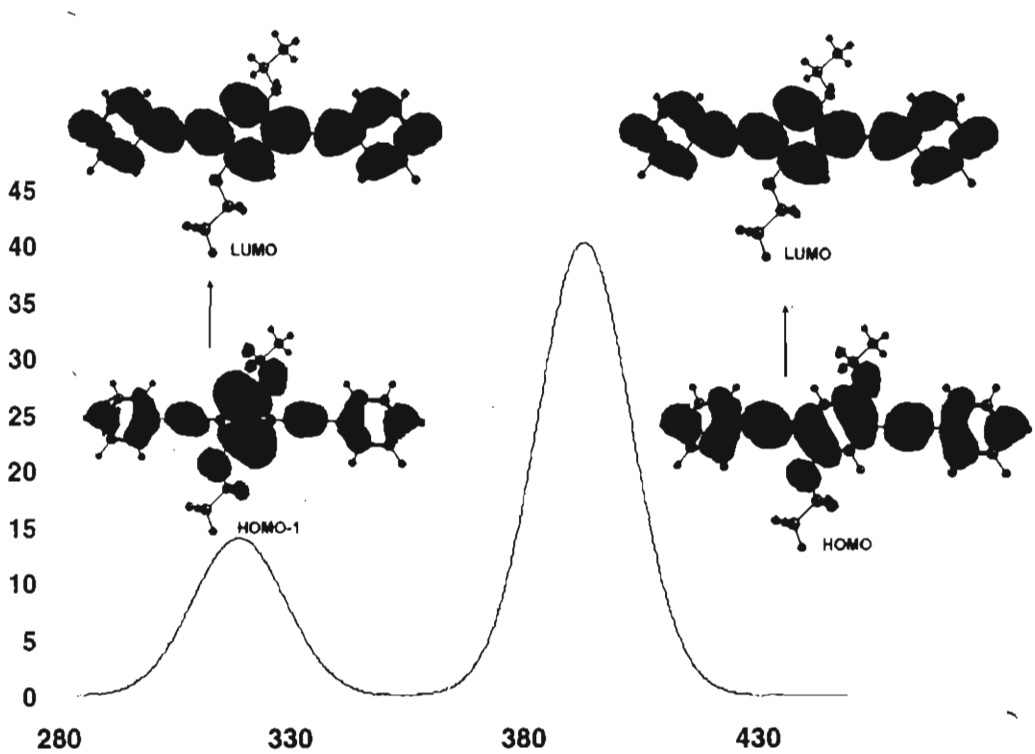

Figure 2.17. Absorption spectra calculated at TDDFT B3LYP/6-31G* level for **2'a**. The important MO transitions corresponding to the peaks at 320 and 394 nm are also depicted.

Further the absorption wavelengths calculated using TDDFT and ZINDO/S methods were compared. For **2'a**, ZINDO/S calculations performed on the DFT optimized structure provided a value of 379 nm (oscillator strength 1.199), closer to the experimental λ_{max} at 367 nm, whereas TDDFT gave the

absorption wavelength as 393 nm (oscillator strength 1.343). In contrast, the absorption wavelength obtained for the short wavelength band by TDDFT

Table 2.4. Experimental wavelengths (λ_{exp})[a], calculated absorption wavelengths (λ_{cal})[b] and oscillator strengths[b] for 1- 3.

Compound	Transition	λ_{exp} [a] (nm)	ZINDO/S		TDDFT	
			λ_{cal} [b] (nm)	Oscillator strength[c]	λ_{cal} [b] (nm)	Oscillator strength[c]
1	HOMO to LUMO	320	365	1.304	360	1.897
2'	HOMO to LUMO	367	379	1.199	393	1.343
	HOMO-1 to LUMO	307	268	0.247	319	0.467
3'	HOMO to LUMO	383	406	2.413	461	2.951
	HOMO-2 to LUMO	330	331	0.284	357	0.443

[a]Figure 2.2 A for **1**[52], **2** and **3**. [b]TDDFT and ZINDO/S level calculations using the B3LYP/6-31G* level optimized geometries of **1**, **2'**, and **3'**.

method (319 nm having an oscillator strength of 0.467) matched with the experimental λ_{max} (307 nm) while ZINDO/S delivered a much lower value of 268 nm with oscillator strength of 0.247. For the long wavelength band of **3'a**, TDDFT showed a large deviation of 58 nm higher than the observed wavelength at 383 nm, while the ZINDO/S gave comparable value of 406 nm. The short wavelength band of **3'a**, appeared at 330 nm and the theoretical absorption wavelength obtained by TDDFT and ZINDO/S are 357 and 331 nm respectively. The deviations observed between the theoretical and experimental absorption maximum may be due to the influence of the solvent. The solvent

molecules interacting at the acetylenic region can exert some steric effect, which would lead to some twisting of the arene rings and thereby reducing the degree of conjugation.

In order to understand the dependence of arene ring rotations of phenyleneethynylene on their electronic transition energies, computational experiment was carried out on **2'a**. In this experiment, several rotamers of **2'a** is optimized at B3LYP/6-31G* level by constraining the angle made by the central arene ring with the terminal ones at the increments of 15°. For each rotamer thus obtained, the S_0 to S_1 transition energy is calculated at TDDFT levels. The transition energies thus obtained are plotted against the dihedral angle and is presented in Figure 2.18. The orthogonal and the planar conformations show the highest and the lowest excitation energies, respectively. Based on Franck-Condon principle, the transition energy difference between these two extreme conformations is taken as a measure of the rotational barrier. This rotational barrier between the planar and orthogonal conformations of **2'a** in its excited state is turned out to be 15 kcal/mol at TDDFT level and 9.9 kcal/mol using ZINDO/S calculation. Phenylene-ethynylenes relax from the high energy orthogonal conformation to low lying planar conformation and the emission of the molecules is preferentially from the more planar structures resulting in structured emission spectrum. This type of relaxation phenomena has been well documented earlier in the case of oligo(phenylenevinylyne) (OPV) based systems.[67-69] The ground state structure of OPV is not planar, on excitation it undergoes a conformational change from

the twisted ground state geometry to planar conformation and the emission is from the more planar conformation.[67] The extent of planarization in OPV mainly depends on the substitution on the vinylic carbons and on phenyl ring.[68] Another feature of OPV is the alteration of bond order in the excited state resulting in partial delocalization of double bond throughout the system.[67, 69]

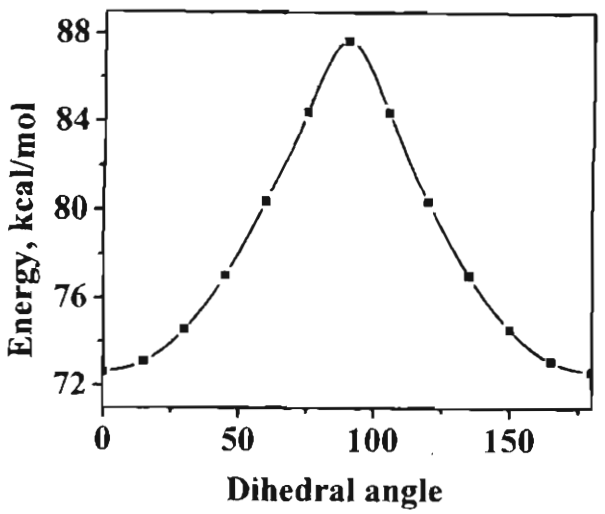

Figure 2.18. Transition energies for the first excited state of compound **2** obtained by TDDFT level of calculation at different dihedral angles.

2.5. Conclusions

We have synthesized two model phenyleneethynylene based rigid rod molecules which are widely used as building blocks in various functional molecular materials and investigated their photophysical, conformational, and electronic properties. Purification of this class of molecules is rather difficult and successfully carried out by recycling HPLC techniques. The photophysical and theoretical studies, suggest that phenyleneethynylenes exist in planar and several twisted conformations in its ground state due to the nearly free rotation of the arene rings along the molecular axis. On the other hand, their emission

spectra are highly structured as a consequence of the planarization of the molecules in the excited state. An idealized representation for the ground and excited states of a model phenyleneethynylene is shown in Scheme 2. 2.

Scheme 2.2. An Idealized representation of the ground and excited states of model phenyleneethynylenes.

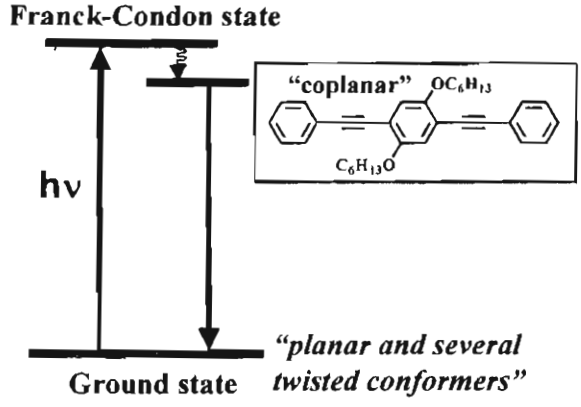

The emission properties and lifetimes of both the compounds were found to be independent of excitation wavelengths and solvent polarity, further confirming the existence of a single emitting species. The TDDFT results were found to be valuable for assigning the effect of alkoxy substituents on the absorption properties of **2** and **3**. The two distinct bands in the absorption spectra of **2** and **3** are due to the electronic transitions from nearly identical HOMO and HOMO-1/HOMO-2 to LUMO.

2.6. References

1. Bunz, U. H. F. *Chem. Rev.* **2000,** *100*, 1605.

2. Breen, C. A.; Rifai, S.; Bulovic, V.; Swager, T. M. *Nano Lett.* **2005**, *5* 1597.

3. Nesterov, E. E.; Zhu, Z.; Swager, T. M. *J. Am. Chem. Soc.* **2005,** *127*, 10083.

4. Englert, B. C.; Smith, M. D.; Hardcastle, K. I.; Bunz, U. H. F. *Macromolecules* **2004,** *37*, 8212.

5. Funston, A. M.; Silverman, E. E.; Miller, J. R.; Schanze, K. S. *J. Phys. Chem. B* **2004,** *108*, 1544.

6. Walters, K. A. *Chem. Commun.* **1998**, 1115.

7. Zhou, C.-Z.; Liu, T.; Xu, J.-M.; Chen, Z.-K. *Macromolecules* **2003,** *36*, 1457.

8. Glusac, K. D.; Jiang, S.; Schanze, K. S. *Chem. Commun.* **2002**, 2504.

9. Bangcuyo, C. G.; Ellsworth, J. M.; Evans, U.; Myrick, M. L.; Bunz, U. H. F. *Macromolecules* **2003,** *36*, 546.

10. Jegou, G.; Jenekhe, S. A. *Macromolecules* **2001,** *34*, 7926.

11. Hayashi, H.; Yamamoto, T. *Macromolecules,* **1998,** *31*, 6063.

12. Moroni, M.; Moigne, J. L. *Macromolecules* **1994,** *27*, 562.

13. Yamaguchi, Y.; Tanaka, T.; Kobayashi, S.; Wakamiya, T.; Matsubara, Y.; Yoshida, Z.-i. *J. Am. Chem. Soc.* **2005,** *127*, 9332.

14. Meier, H. *Angew. Chem. Int. Ed.* **2005,** *44*, 2482.

15. Piotrowiak, P.; Galoppini, E.; Wei, Q.; Meyer, G. J.; Wiewior, P. *J. Am. Chem. Soc.* **2003,** *125*, 5278.

16. Galoppini, E.; Guo, W.; Zhang, W.; Hoertz, P. G.; Qu, P.; Meyer, G. J. *J. Am. Chem. Soc.* **2002,** *124*, 7801.

17. Dong, W.; Schlegel, J. M.; Galoppini, E., *Tetrahedron* **2002,** *58*, 5027.

18. Hoertz, P. G.; Carlisle, R. A.; Meye, G. J.; Wang, D.; Piotrowiak, P.; Galoppini, E. *Nano Lett.* **2003**, *3*, 325.

19. Meier, H.; Mühling, B.; Kolshorn, H. *Eur. J. Org. Chem.* **2004**, 1033.

20. Wan, C.-W.; Burghart, A.; Chen, J.; Bergstrm, F.; Johansson, L. B.-ä.; Wolford, M. F.; GyumKim, T.; Topp, M. R.; Hochstrasser, R. M.; Burgess, K. *Chem.-Eur. J.* **2003,** *9*, 4430.

21. Koishi, K.; Ikeda, T.; Kondo, K.; Sakaguchi, T.; Kamada, K.; Tawa, K.; Ohta, K. *Macromol. Chem. Phys.* **2000,** *201*, 525.

22. Wosnick, J. H.; Mello, C. M.; Swager, T. M. *J. Am. Chem. Soc* **2005,** *127*, 3400.

23. Pinto, M. R.; Schanze, K. S. *Proc. Natl. Acad. Sci.* **2004,** *101*, 7505.

24. Disney, M. D.; Zheng, J.; Swager, T. M.; Seeberger, P. H. *J. Am. Chem. Soc.* **2004,** *126*, 13343.

25. Wilson, J. N.; Bunz, U. H. F. *J. Am. Chem. Soc.* **2005,** *127*, 4124.

26. Kim, I.-B.; Dunkhorst, A.; Gilbert, J.; Bunz, U. H. F. *Macromolecules* **2005,** *38*, 4560.

27. Ulrich, G.; Ziessel, R. *Synlett.* **2004**, 439.

28. Murphy, C. B.; Zhang, Y.; Troxler, T.; Ferry, V.; Martin, J. J.; Jones Jr., W. E. *J. Phys. Chem. B* **2004,** *108*, 1537.

29. Metivier, R.; Amengual, R.; Leray, I.; Michelet, V.; Genet, J.-P. *Org. Lett.* **2004,** *6*, 739.

30. Moon, J. H.; Deans, R.; Krueger, E.; Hancock, L. F. *Chem. Commun.* **2003**, 104.

31. Hacker, C. A.; Batteas, J. D.; Garno, J. C.; Marquez, M.; Richter, C. A.; Richter, L. J.; van Zee, R. D.; Zangmeister, C. D. *Langmuir* **2004,** *20*, 6195.

32. Stapleton, J. J.; Harder, P.; Daniel, T. A.; Reinard, M. D.; Yao, Y.; Price, D. W.; Tour, J. M.; Allara, D. L. *Langmuir* **2003,** *19*, 8245.

33. Cai, L.; Yao, Y.; Yang, J.; David W. Price, J.; Tour, J. M. *Chem. Mater.* **2002,** *14*, 2905.

34. Tour, J. M.; Jones, L.; Pearson, D. L.; Lamba, J. J. S.; Burgin, T. P.; Whitesides, G. M.; Allara, D. L.; Parikh, A. N.; Atre, S. V. *J. Am. Chem. Soc.* **1995,** *117*, 9529.

35. Elbing, M.; Ochs, R.; Koentopp, M.; Fischer, M.; von Hanisch, C.; Weigend, F.; Evers, F.; Weber, H. B.; Mayor, M. *Proc. Natl. Acad. Sci.* **2005,** *102*, 8815.

36. Tour, J. M.; Cheng, L.; Nackashi, D. P.; Yao, Y.; Flatt, A. K.; St.Angelo, S. K.; Mallouk, T. E.; Franzon, P. D. *J. Am. Chem. Soc.* **2003,** *125*, 13279.

37. Blum, A. S.; Kushmerick, J. G.; Long, D. P.; Patterson, C. H.; Yang, J. C.; Henderson, J. C.; Yao, Y. X.; Tour, J. M.; Shashidhar, R.; Ratna, B. R. *Nat. Mater.* **2005,** *4*, 167.

38. Donhauser, Z. J.; Mantooth, B. A.; Kelly, K. F.; Bumm, L. A.; Monnell, J. D.; Stapleton, J. J.; Price, D. W., Jr.; Rawlett, A. M.; Allara, D. L.; Tour, J. M.; Weiss, P. S. *Science* **2001,** *292*, 2303.

39. Galoppini, E.; Guo, W. *J. Am. Chem. Soc.* **2001,** *123*, 4342.

40. Creager, S.: Yu, C. J.; Bamdad, C.; O'Connor, S.; MacLean, T.; Lam, E.; Chong, Y.; Olsen, G. T.; Luo, J.; Gozin, M.; Kayyem, J. F. *J. Am. Chem. Soc.* **1999,** *121*, 1059.

41. Levitus, M.; Schmieder, K.; Ricks, H.; Shimizu, K. D.; Bunz, U. H. F.; Garcia-Garibay, M. A. *J. Am. Chem. Soc.* **2001,** *123*, 4259.

42. Li, H.; Powell, D. R.; Firman, T. K.; West, R. *Macromolecules* **1998,** *31*, 1093.

43. Beeby, A.; Findlay, K.; Low, P. J.; Marder, T. B. *J. Am. Chem. Soc.* **2002,** *124*, 8280.

44. Beeby, A.; Findlay, K. S.; Low, P. J.; Marder, T. B.; Matousek, P.; Parker, A. W.; Rutter, S. R.; Towrie, M. *Chem. Commun.* **2003**, 2406.

45. Li, H.; Powell, D. R.; Hayashi, R. K.; West, R. *Macromolecules* **1998,** *31*, 52.

46. James, P. V.; Sudeep, P. K.; Suresh, C. H.; Thomas, K. G. *J. Phys. Chem. A* **2006,** *110*, 4329.

47. Sudeep, P. K.; James, P. V.; Thomas, K. G.; Kamat, P. V. *J. Phys. Chem. A* **2006,** *110*, 5642.

48. Zeena, S.; Thomas, K. G. *J. Am. Chem. Soc.* **2001,** *123*, 7859.

49. Xue, C.; Luo, F.-T. *Tetrahedron* **2004,** *60*, 6285.

50. The recycling HPLC was manufactured by Japan Analytical Industry Co., Ltd. Two columns were employed to achieve effective separation of the impurities, first column with an exclusion limit of 5 x 10^3 and the other with a limit of 1 x 10^3. Polystyrene was used as packing material in both the columns. Retention period for compound **2** and **3** was found to be 48-53 min and 42-48 min, respectively.

51. Levitus, M.; Schmieder, K.; Ricks, H.; Shimizu, K. D.; Bunz, U. H. F.; Garcia-Garibay, M. A. *J. Am. Chem. Soc.* **2001,** *123*, 4259.

52. Beeby, A.; Findlay, K.; Low, P. J.; Marder, T. B. *J. Am. Chem. Soc.* **2002,** *124*, 8280.

53. Beeby, A.; Findlay, K. S.; Low, P. J.; Marder, T. B.; Matousek, P.; Parker, A. W.; Rutter, S. R.; Towrie, M. *Chem. Commun.* **2003**, 2406.

54. Berlman, I. B. *Handbook of fluorescence spectra of aromatic molecules, 2nd ed., Academic Press, London, New York* **1971**.

55. Schmieder, K.; Levitus, M.; Dang, H.; Garcia-Garibay, M. A. *J. Phys. Chem. A* **2002,** *106*, 1551.

56. Lee, C.; Yang, W.; Parr, R. G. *Phys. Rev. B* **1988,** *37*, 785.

57. Axel, D. B., *J. Chem. Phys.* **1993,** *98*, 5648.

58. Norton, J. E.; Houk, K. N. *J. Am. Chem. Soc.* **2005,** *127*, 4162.

59. Khuong, K. S.; Beaudry, C. M.; Trauner, D.; Houk, K. N. *J. Am. Chem. Soc.* **2005,** *127*, 3688.

60. Stratmann, R. E.; Gustavo, E. S.; Michael, J. F. *J. Chem. Phys.* **1998,** *109*, 8218.

Mark, E. C.; Christine, J.; Kim, C. C.; Dennis, R. S. *J. Chem. Phys* **1998,** *108*, 4439.

Bauernschmitt, R.; Ahlrichs, R. *Chem. Phys. Lett.* **1996,** *256*, 454.

Edwalds, W. D.; Zerner, M. C. *Theor. Chim. Acta* **1987,** *72*, 347.

Zerner, M. C.; Gilda H. Loew, R. F. K.; Mueller-Westerhoff, U. T. *J. Am. Chem. Soc.* **1980,** *102*, 589.

Yu, J. S. K.; Chen, W. C.; Yu, C. H. *J. Phys. Chem. A* **2003,** *107*, 4268.

Gaussian 03, V., Frisch, M. J.; Trucks, G. W.; Schlegel, H. B.; Scuseria, G. E.; Robb, M. A.; Cheeseman, J. R.; Montgomery, Jr. J. A.; Vreven, T.; Kudin, K. N.; Burant, J. C.; Millam, J. M.; Iyengar, S. S.; Tomasi, J.; Barone, V.; Mennucci, B.; Cossi, M.; Scalmani, G.; Rega, N.; Petersson, G. A.; Nakatsuji, H.; Hada, M.; Ehara, M.; Toyota, K.; Fukuda, R.; Hasegawa, J.; Ishida, M.; Nakajima, T.; Honda, Y.; Kitao, O.; Nakai, H.; Klene, M.; Li, X.; Knox, J. E.; Hratchian,H. P.; Cross,J. B.; Adamo, C.; Jaramillo, J.; Gomperts, R.; Stratmann, R. E.; Yazyev, O.; Austin, A. J.; Cammi, R.; Pomelli, C.; Ochterski, J. W.; Ayala, P. Y.; Morokuma, K.; Voth, G. A.; Salvador, P.; Dannenberg, J. J.; Zakrzewski,V. G.; Dapprich, S.; Daniels,. A. D.; Strain, M. C.; Farkas, O.; Malick, D. K.; Rabuck, A. D.; Raghavachari, K.; Foresman, J. B.; Ortiz, J. V.; Cui, Q.; Baboul, A. G.; Clifford, S.; Cioslowski, J.; Stefanov, B. B.; Liu, G.; Liashenko, A.; Piskorz, P.; Komaromi, I.; Martin, R. L.; Fox, D. J.; Keith, T.; Al-Laham, M. A.; Peng, C. Y.; Nanayakkara, A.; Challacombe, M.; Gill,

P. M. W.; Johnson, B.; Chen, W.; Wong, M. W.; Gonzalez, C.; Pople, J. A., Gaussian, Inc., Pittsburgh PA, **2003**.

67. Tretiak, S.; Saxena, A.; Martin, R. L.; Bishop, A. R. *Phys. Rev. Lett.* **2002,** *89*, 097402.

68. Oelkrug, D.; Tompert, A.; Gierschner, J.; Egelhaaf, H. J.; Hanack, M.; Hohloch, M.; Steinhuber, E. *J. Phys. Chem. B* **1998,** *102*, 1902.

69. dos Santos, D. A.; Beljonne, D.; Cornil, J.; Bredas, J. L. *Chem. Phys.* **1998,** *227*, 1.

CHAPTER 3

Effect of *meta* Substitution on the Electronic Properties of Donor-π-Acceptor Systems

3.1. Abstract

Phenyleneethynylene based donor-acceptor systems possessing N,N-dimethylaniline and pyridine in terminal positions were synthesized and varied their conjugation (**1** and **2**) and connectivity (*para* isomer **2** and *meta* isomer **3**) between the donor and acceptor groups. The absorption spectral features of the compounds **1-3** do not vary with solvent polarity. The *meta* connectivity prevents the effective interaction between the donor and acceptor which was confirmed by protonation studies. In nonpolar solvents, compounds **1-3** emit with high quantum yield in the short wavelength region. Interestingly, a large bathochromic shift in emission maxima was observed for all the compounds with increase in solvent polarity indicating that the bands originate from an intramolecular charge transfer state (ICT). These aspects were further investigated by (i) estimating the Full Width at Half Maximum (ii) Stokes shift (iii) emission yields. Based on these studies it is concluded that in the excited state of *meta* isomer, conjugation opens up leading to enhanced electronic coupling between the donor and acceptor. These aspects were further confirmed by theoretical studies.

2. Introduction to Donor-π-Acceptor Systems

Molecules containing donor-acceptor pair with appropriate linker groups ften undergo charge transfer, when excited with light of suitable frequency, sulting in an intramolecular charge transfer (ICT) state.[1] The geometric as well i the electronic structure of such molecular systems are considerably different in s ICT state compared to the ground state. In the case of push-pull chromophores, here the donor-acceptor pairs are linked through a π-conjugated system (D-π-A), e ground state of the molecule can exist in two extreme resonance structures: ectroneutral (N) and polar zwitterionic (Z) states as illustrated in Equation 3.1. alence Bond (VB) model describes the ground state S_0 and the first electronically cited singlet state S_1 of such compounds by a linear combination of zwitterionic d electroneutral resonance structures.

$$D^{+}\text{-}\pi\text{-}A^{-}\ \mathbf{(Z)} \leftrightarrow\ D\text{-}\pi\text{-}A\ \mathbf{(N)} \qquad (3.1)$$

$$\psi(S_0) = c\psi_Z - (1-c^2)^{1/2}\,\psi_N \qquad (3.2)$$

$$\psi(S_1) = (1-c^2)^{1/2}\,\psi_Z + c\psi_N \qquad (3.3)$$

Several approaches have been suggested for obtaining the contribution of e two limiting structures. For example, Wortmann and co-workers proposed a rameter 'c^2' which is related to the difference in the dipole moments ($\Delta\mu$) of the ectronically excited singlet state (S_1) and ground state (S_0) and this parameter n be experimentally obtained through electrooptical absorption measurements.[2-4] her important approaches are (i) mixed parameter 'MIX' by Barzoukas et al;[5]

(ii) paramater 'Bond Length Alteration' by Marder and coworkers[6-9] and (iii) parameter 'f' proposed by Lu, Chen and coworkers.[10] These aspects are summarized by Meier in a recent review.[11] Even though such parameters are proved to be successful for relatively short D-π-A systems with oligoene (OE) linkers, they are not adequate when linker consists of aromatic repeat units (for example, benzene unit). A Molecular Orbital (MO) model has been successfully adopted for discussing such systems.

According to the MO model, partial dipole moments are present on the donor and the acceptor sides of D-π-A chains. A representative example of D-π-A system with phenyleneethynylene linker is presented in Scheme 3.1.[11] Each partial moment is composed of an intrinsic part (μD, μA) and a part which is induced by the dipole on the other chain end (μDi, μAi). The induced part becomes smaller with increase in the distance between the donor and acceptor and the extent of the polarization from the ends of the chain towards the center rapidly decreases. This was also demonstrated by means of Bond Length Alteration (BLA) values and partial charges obtained by a DFT/B3LYP/6-31G* calculation.[12]

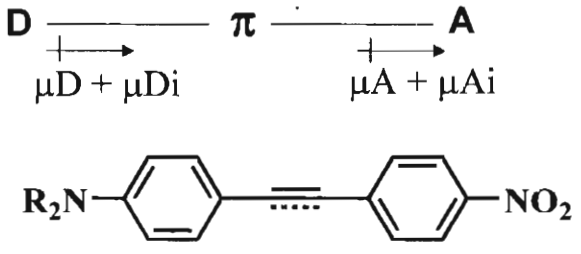

Scheme 3.1. MO model of D-π-A system with phenyleneethynylene linker.

The $S_0 \rightarrow S_1$ electronic transition of unsubstituted conjugated system such as n trans-stilbene and tolane is almost pure HOMO→LUMO transition. nterestingly, mixing of orbitals is observed even with one repeat unit (n=1) in the ase of D-OPV-A as well as D-OPE-A systems. With increase in repeat units (n), he energy of HOMO-1 approaches closer to the HOMO and the LUMO+1 closer o the LUMO. As a result, the overlap density of the HOMO and LUMO decreases nd various transitions such as HOMO-1→LUMO, HOMO→LUMO+1, and HOMO-1→LUMO+1 become important. AM1-INDO/S calculation was erformed for OPEs having dimethylamino and nitro groups at terminal positions Scheme 3.2) and the HOMO→LUMO transitions in these systems were haracterized by a strong intramolecular charge transfer (ICT) from the donor to he acceptor side. The long-wavelength absorption band of D-π-A systems is ssentially determined by the ICT and charge transfer plays a very minor role in ther transitions.

The effect of increasing the conjugation length and donor/acceptor strength n the charge transfer behaviour in oligo(1,4-phenyleneethynylene)s based D-π-A ystem has been studied, in detail, by Meier and co-workers.[13] Authors have repared a series of push-pull chromophores based on oligo(1,4-phenylene-thynylene)s (OPE) having didodecyl amino group as donor and varied their harge transfer property by (i) introducing cyano, formyl and nitro groups in the erminal position and (ii) extending the conjugation by increasing the repeat units

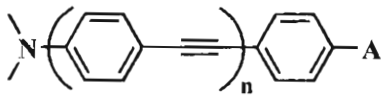

A= -H, -CN, -CHO, -NO_2
n = 1-4

Scheme 3.2. Push-pull chromophores based on oligo(1,4-phenylene-ethynylene)s *(adapted from reference 13).*

cheme 3.2). Conjugated oligomers of this type bearing donor-acceptor groups in eir terminal positions can be described either by VB or MO model. The VB odel can be explained based on the resonance between an electroneutral and a inoid type structure connected by cumulene units. In the present case all the mpounds exhibit values of δ (^{13}C-sp) between 86.9 and 94.8 ppm, which are se to the chemical shift of tolane (δ=89.4 ppm and any discernible contribution a cumulene structure can be excluded. Spectral properties of this class of olecule can be described by a MO model having partial dipole moments at the ains' ends. The polarization on the chain can be characterized by the olarization of the C-C triple bonds which decreases from both chain ends to the nter. For the donor-acceptor series presented in Scheme 3.2. The long avelength absorption band (S_0-S_1) shows different behaviour on extending the njugation from *n*=1 to n = 4: (i) a bathochromic shift for unsubstituted rivatives; (ii) virtually no effect for cyano derivatives and (iii) relatively large psochromic shifts for formyl and nitro derivatives. The energy of the electronic ansition lowers on extending the conjugation and generally a bathochromic shift observed. However, this effect is counteracted in the phenyleneethynylene based ush-pull systems by the effect of intramolecular charge transfer (ICT), which

creases with increase in the distance between the donor and acceptor groups. uthors suggest that in the case of the relatively weak acceptor group (-CN) both fects annihilate one another, whereas the reduction of the ICT predominates in e formyl and nitro series. Thus the OPE chain is somewhat more prone to overall psochromic effects than the related oligo(phenylenevinylene) systems. The ergy $E_{DA}(n)$ (equation 3.4) of an electron transition in D-π-A systems can be lit into two parts; the first part $E_S(n)$ accounts for the extension of conjugation in stems which posses either donor or acceptor moiety the second term ΔE_{DA} is a rrection term for the push-pull effect in series with terminal donor–acceptor bstitution.

$$E_{DA}(n) = E_S(n) - \Delta E_{DA}(n) \qquad (3.4)$$

A series of banana shaped oligo(aryleneethynylene)s containing pyridine ng as acceptor has been reported by Yamaguchi et al (Chart 3.1).[14] The emission fficiency markedly increases when the pyridine ring is present as the central unit ϕ_f = 0.48 for **ii**) where as substantially decreases when the pyridine groups are in e terminal position (ϕ_f = 0.03 for **iii**). Authors have also reported that the mitting efficiency can be further improved by introducing methoxy donor groups the terminal benzene rings (ϕ_f = 0.58 for **iv**).

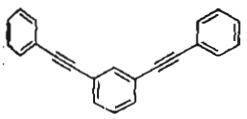

i ($\phi_f = 0.14$)

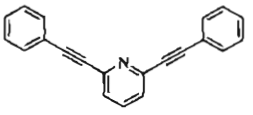

ii ($\phi_f = 0.48$)

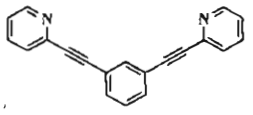

iii ($\phi_f = 0.03$)

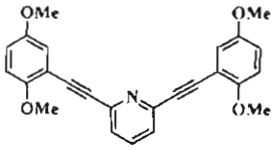

iv ($\phi_f = 0.58$)

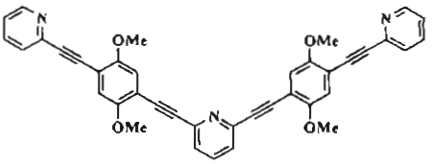

v ($\phi_f = 0.84$)

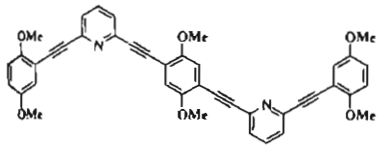

vi ($\phi_f = 0.91$)

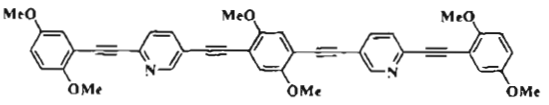

vii ($\phi_f = 0.76$)

Chart 3.1. Banana shaped oligo(aryleneethynylene)s containing pyridine ring as acceptor *(adapted from reference 14).*

Generally *meta* isomers are weak emitters compared to the *para* isomers, wever in the present case the *meta* substituted pyridine systems possess higher ission quantum yield than the corresponding *para* isomer. This anomalous aracter is explained by considering the movability of the dipolar structure **viii** r *meta* and *para* isomers in the excited state.[14]

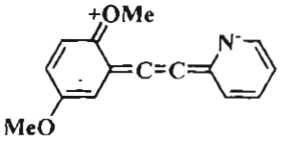

viii

n *meta* isomer **vi**, conjugation proceeds through two *ortho* positions with spect to the nitrogen atom, however, the conjugation interrupts at the *meta* sition in the case of *para* isomer. As a result, the number of equivalent dipolar

uctures is more for *meta* than the *para* isomer resulting in more quantum yield. ong the two *meta* conjugate systems (**v** and **vi**), the emission of **vi** is affected the solvent polarity. With increase in solvent polarity the fluorescence ximum of **vi** is shifted to longer wavelength with remarkable decrease in the antum yield. This disparity can be explained by the marked difference in the ound and excited state distribution of charges in **vi** compared to **v**. From these dies it is concluded that the *meta* as well as *para* isomers have different ground d excited state properties.[14]

It is true that the *meta* conjugation is not efficient as the *para* or *ortho* kage for electronic communication in the ground state. However, it is reported ently that the meta conjugate system communicates effectively in the excited te, and this enhanced coupling is termed as *'meta effect'*.[15-19] It was further monstrated that *meta* conjugated donor–acceptor system shows better charge paration in the excited state compared to the *para* isomer.[15] They employed bazole as donor and naphthalimide as acceptor using phenyleneethynylene kages. The absorption of this type of molecules is found to be independent of solvent while the emission spectra depends largely on the polarity indicating a arge separated excited state. Based on femtosecond transient absorption spectra d pump-probe techniques, the lifetime of the charge separated state of *meta* and *ra* isomers were estimated as 16.8 ns and 1.8 ns, respectively. The ratio of the te of the charge separation/charge recombination (k_{cs}/k_{cr}) was found to be 300

nd 3500 in the case of *para* and *meta* isomers respectively, indicating a ten fold fficiency in the case of meta isomer.[15] This behavjour may be attributed to the artial cumulenic type structure for the compound in the relaxed state. Recently, xcited state theoretical studies based on *meta* substituted diphenyl acetylene (DPA) ave further supported the possibility of a partial cumulenic character leading to an ncreased coupling between the donor and acceptor in the excited state.[20] Since *'meta ffect'* significantly increases the charge separated lifetimes, this approach provide reater potential for developing new molecular systems for applications in solar nergy cells. On the contrary, nonlinear optical properties which depends mainly on he ground state polarizabilities, decreases with the *meta* substitution.

Here we report the synthesis and photophysical properties of *meta* as well s *para* isomers of a new class of D-OPE-A system possessing N,N-imethylaniline and pyridine/pyridinium moieties at the terminal positions of henyleneethynylenes.

hart 3.2. Molecular systems under study

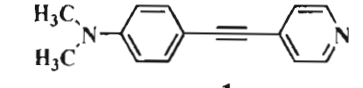

1

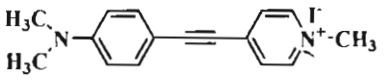

1Q

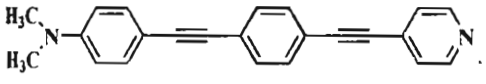

2

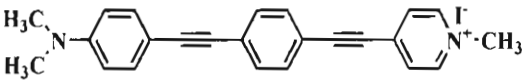

2Q

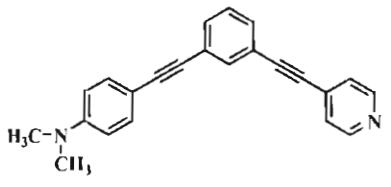

3

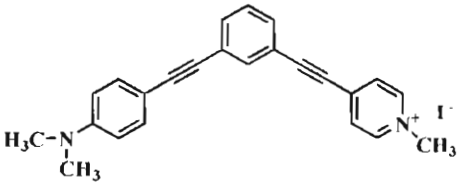

3Q

Experimental Section

3.1. Materials and methods

The samples used for the study were purified by passing through recycling PLC manufactured by Japan Analytical Industry Co., Ltd equipped with uv as well as RI detectors.. All melting points are uncorrected and were determined on Aldrich melting point apparatus. ^{1}H NMR and ^{13}C NMR spectra were recorded a Bruker DPX-300 MHz spectrometer. High Resolution Mass spectra were corded on a JEOL JM AX 5505 mass spectrometer. The UV-Vis spectra were corded on a Shimadzu 2401 or 3101PC spectrophotometer. The emission spectra ere recorded on a Spex-Fluorolog, F112-X equipped with a 450W Xe lamp and a amamatsu R928 photomultiplier tube. The spectra were recorded by keeping 90° eometry and a slit width of 1 mm in the excitation and emission onochromators.

3.2. General method of synthesis.

Diisopropylamine was dried over KOH. Solvents were deoxygenated by urging them with argon for 15 min, before using in the reaction. Elangovan and coworkers[21] have reported the synthesis of **1** and a modified procedure as entioned in Scheme 3.3A was adopted in the present case.

Scheme 3.3A. Synthesis of 1 and 1Q*

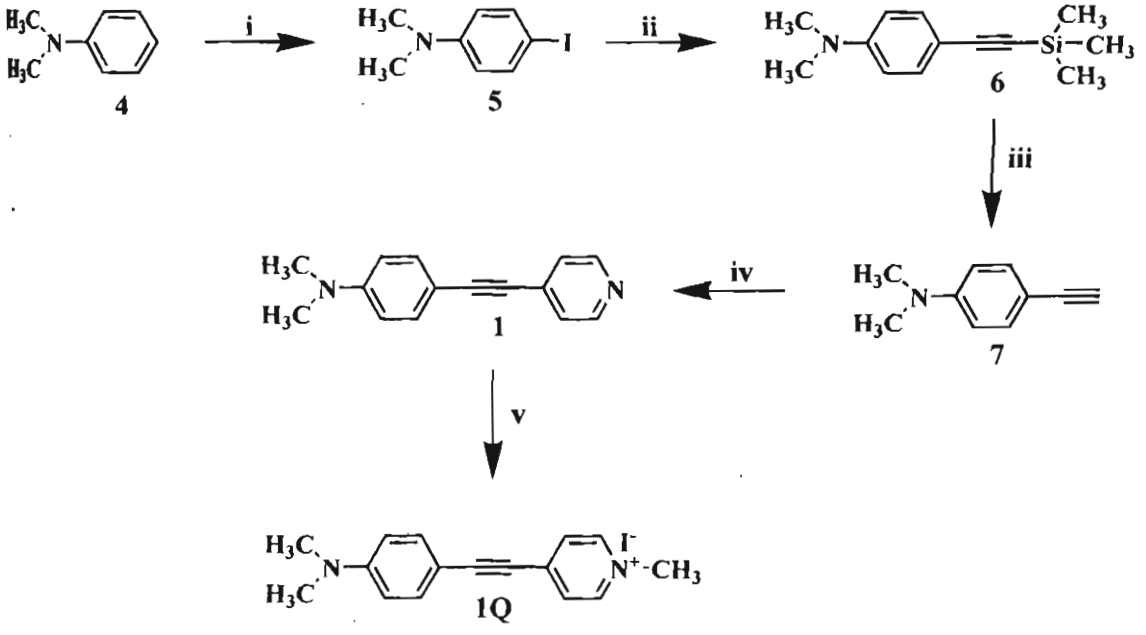

Scheme 3.3B. Synthesis of 2 and 2Q*

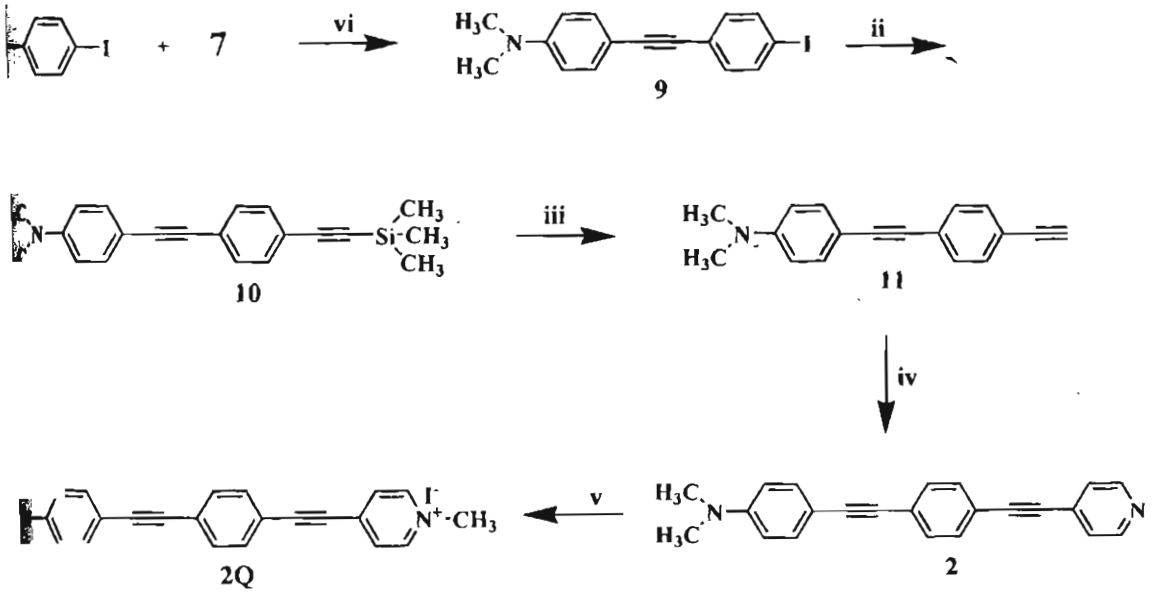

Reagents used are given at the end of the Scheme 3.3 in Page 75

eme 3.3C. Synthesis of 3 and 3Q

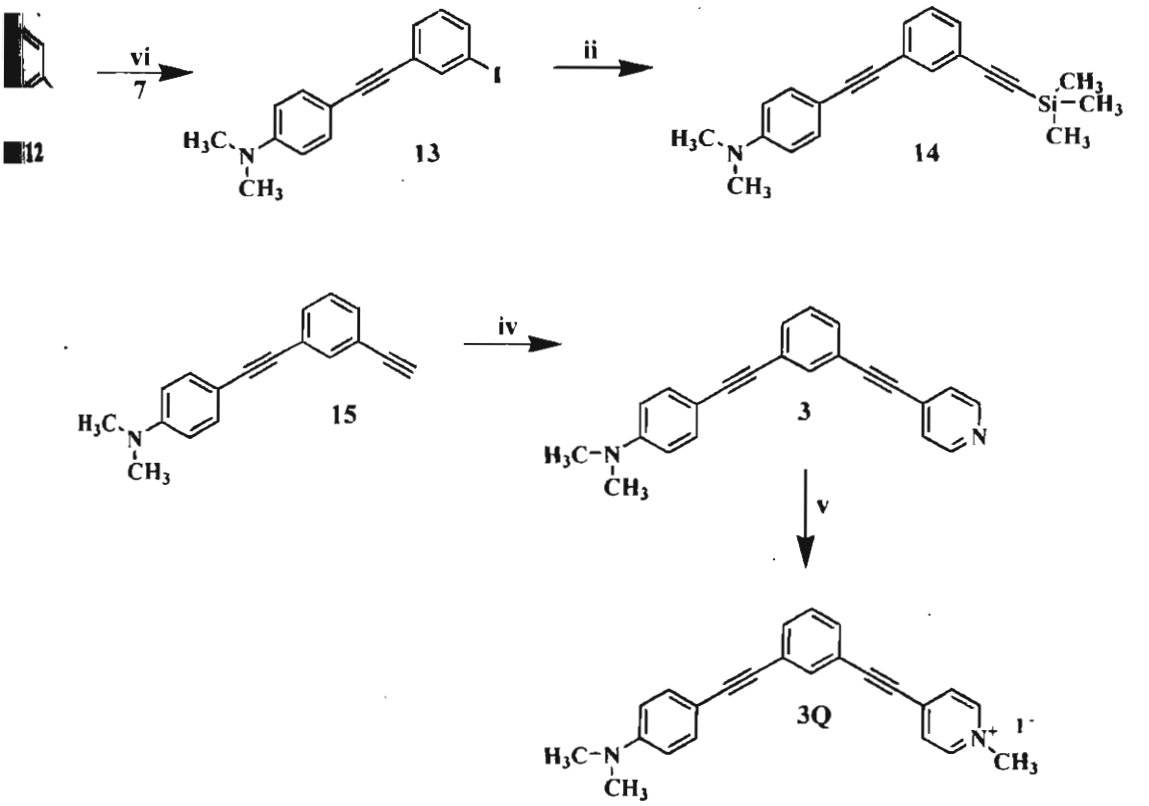

e 3.3. i) I_2, K_2CO_3, H_2O ii) (Trimethylsilyl)acetylene, $Pd(PPh_3)_2Cl_2$, CuI, (i-H iii) CH_3OH, THF, NaOH iv) IC_5H_4N, $Pd(PPh_3)_2Cl_2$, CuI, PPh_3, $(i\text{-}pr)_2NH$ v) vi) $Pd(PPh_3)_2Cl_2$, CuI, PPh_3, $(i\text{-}pr)_2NH$

paration of 4-iodopyridine. Synthesis of 4-iodopyridine was earlier ed by Coudret[22] and we have adopted a modified procedure. 4-pyridine (1.0 g, 10.6 mmol) was dissolved in 48 % aqueous HBF_4 (8.3 mL) ooled to -10 ^{0}C. To the resulting solution was added solid $NaNO_2$ (0.80 g, mol) in powdered form at such a rate that nitric oxide evolution is in a very ate. The solution was stirred for 30 min and KI (2.80 g, 17.0 mmol) ed in a mixture (40:60) of acetone:water (20 mL) was added. The excess

iodine was removed by adding an aqueous solution of $Na_2S_2O_3$, further neutralized with aqueous Na_2CO_3. The reaction mixture was extracted with ether, dried over anhydrous Na_2SO_4 and the solvent was evaporated to yield 4-iodopyridine as pale yellow solid (1.1 g, 50 %), mp. 101-103 °C. (mp. previously reported 100 °C; analytical and spectroscopic data are same as reported in reference [22])

Preparation of 6. To a mixture of **5** (2.0 g, 8 mmol), $Pd(PPh_3)_2Cl_2$ (284 mg, 0.40 mmol) and CuI (77 mg, 0.40 mmol) in diisopropylamine (20 mL) was added (trimethylsilyl)acetylene (1.24 mL, 8.0 mmol). The mixture was then heated to 70 °C for 1 h under argon atmosphere. The crude product was then purified by column chromatography over silica gel (100-200 mesh) using a mixture (1:50) of ethyl acetate and hexane as eluent to yield **6** (1.5 g, 85 %), mp. 87-89 °C; ^{1}H NMR (300 MHz, $CDCl_3$): δ 7.35 (d, 2H), 6.60 (d, 2H), 3.00 (s, 6H), 0.025 (s, 9H).; ^{13}C NMR (75 MHz, $CDCl_3$): δ 150.17, 133.08, 111.55, 109.85, 106.54, 91.13, 40.12, 0.2. m/z (FAB) found 217.36 Calc. 217.38.

Preparation of 7. To a solution of **6** (500 mg, 2 mmol) in a mixture of THF (7 mL) and methanol (11 mL), an aquoues solution of NaOH (0.7 mL, 5 N) was added and the mixture was stirred for 2 h. The reaction mixture was washed with water and extracted using chloroform. The organic layer was dried over anhydrous Na_2SO_4 and evaporated to yield **7** (276 mg, 83 %), mp.171-173 °C. ^{1}H NMR (300 MHz, $CDCl_3$): δ 7.34 (d, 2H), 6.60 (d, 2H), 2.97 (two singlets of –CH and –

$N(CH_3)_2$ merged together, 7H). ^{13}C NMR (75 MHz, $CDCl_3$): δ 150.32, 133.15, 111.62, 108.66, 84.82, 74.75, 40.12. m/z (FAB) found 145.10 Calc. 145.09.

Preparation of 1.[21] A mixture of **7** (50 mg, 0.2 mmol), $Pd(PPh_3)_2Cl_2$ (14 mg, 0.02 mmol), CuI (4 mg, 0.02 mmol), 4-iodopyridine (63 mg, 0.31 mmol) and PPh_3 (11 mg, 0.04 mmol) in diisopropylamine (2 mL) was stirred at room temperature for 24 h. The reaction mixture was filtered over celite using chloform as eluent and the solvent was evaporated. The crude product was then chromatographed over basic alumina using a mixture (2:3) of chloroform and hexane as eluent to yield **1** (28 mg, 42 %) as yellow colored solid, mp. 200 °C. ^1H NMR (300 MHz, $CDCl_3$): δ 8.5 (d, 2H), 7.4-7.3 (m, 4H), 6.67 (d, 2H), 3.0 (s, 6H). ^{13}C NMR (75 MHz, $CDCl_3$): δ 150.84, 149.78, 133.44, 132.7, 125.46, 111.15, 106.66, 96.40, 85.53, 40.40. Exact mass calculated for $C_{15}H_{14}N_2$ (M^{+}) is 222.1157, found 222.1144 (EI high resolution mass spectrometry).

Preparation of 1Q. A solution of **1** (50 mg, 0.22 mmol) in CH_3I (2 mL) was heated on a water bath at 50 °C for 2 h. The reaction mixture was cooled and the precipitate was filtered, dried to get **1Q** (mp. 210-212 °C) in quantitative yields. For spectroscopic studies the product was further purified by reprecipitation from methanol/hexane solvent mixture. ^1H NMR (300 MHz, $CDCl_3$): δ 8.6 (d, 2H), 7.8 (d, 2H), 7.4 (d, 2H), 6.7 (d, 2H), 4.21 (s, 3H), 3.0 (s, 6H). ^{13}C NMR (75 MHz, $CDCl_3$): δ 152.68, 145.91, 140.23, 135.18, 128.50, 112.81, 108.06, 105.81, 86.92, 48.22, 40.37.

Preparation of 9. A mixture of **7** (200 mg, 1.38 mmol), $Pd(PPh_3)_2Cl_2$ (97 mg, 0.12 mmol), CuI (23 mg, 0.12 mmol), p-diiodobenzene (454 mg, 1.38 mmol) and PPh_3 (72 mg, 0.24 mmol) in diisopropylamine (2 mL) was stirred at room temperature for 24 h. The reaction mixture was filtered over celite using chloform as eluent and the solvent was evaporated. The crude product was then chromatographed over alumina using hexane as eluent to get **9** (240 mg, 50 %) as white colored solid, mp.169-171 °C. ^{1}H NMR (300 MHz, $CDCl_3$): δ 7.65 (d, 2H), 7.4 (d, 2H), 7.22 (d, 2H), 6.67 (d, 2 H), 3.0 (s, 6H). ^{13}C NMR (75 MHz, $CDCl_3$): δ 150.22, 137.34, 132.78, 132.74 123.73, 111.78, 109.54, 92.9, 92.22, 86.53, 40.16. Exact mass calculated for $C_{16}H_{14}IN$ (M^+) is 347.0171, found 347.0168 (EI high resolution mass spectrometry).

Preparation of 10. To a mixture of **9** (100 mg, 0.28 mmol), $Pd(PPh_3)_2Cl_2$ (10 mg, 0.03 mmol) and CuI (5 mg, 0.03 mmol) in diisopropylamine (2 mL), was added (trimethylsilyl)acetylene (50 μL, 0.31 mmol) and heated at 70 °C for 1 h under argon atmosphere. The crude product was then purified by column chromatography over silica gel (100-200 mesh) using a mixture (1:50) of ethyl acetate and hexane as eluent to yield **10** (65 mg, 71 %), mp. 119-121 °C. ^{1}H NMR (300 MHz, $CDCl_3$): δ 7.43-7.26 (m, 6H), 6.63 (d, 2H), 3.0 (s, 6H), 0.22 (s, 9H). ^{13}C NMR (75 MHz, $CDCl_3$): δ 150.4, 132.97, 132.17, 132.01, 124.54, 122.07, 112.17, 109.81, 105.14, 95.89, 93.05, 87.39, 40.36, 0.16. m/z (FAB) found 317.50 Calc. 317.16.

Preparation of 11. To a solution of **10** (165 mg, 0.53 mmol) in a mixture of THF (1.7 mL) and methanol (2.6 mL), an aqueous solution of NaOH (0.2 mL, 5 N) was added, stirred at room temperature for 2 h. The reaction mixture was washed with water and extracted using chloroform. The organic layer was dried over Na_2SO_4 and evaporated to yield **11** (117 mg, 92 %), mp.180-182 °C. ^{1}H NMR (300 MHz, $CDCl_3$): δ 7.69-7.06 (m, 6H), 6.64 (d, 2H), 3.21 (s, 1H), 3.00 (s, 6H). ^{13}C NMR (75 MHz, $CDCl_3$): δ 150.24, 132.78, 131.95, 131.05, 124.75, 120.84, 111.78, 109.56, 92.91, 87.01, 83.52, 78.42, 40.14. Exact mass calculated for $C_{18}H_{15}N$ (M^{+}) is 245.1204, found 245.1249 (EI high resolution mass spectrometry).

Preparation of 2. Compound **11** was reacted with reagents in step (iv) in Scheme 3.3B (note that the same procedure was adopted for the preparation of **1** in Scheme 3.3A and the details are provided in page 77) and the crude product was purified by column chromatography over basic alumina using a mixture (2:3) of chloroform and hexane as eluent to yield **2** (28 mg, 43 %) as a yellow colored solid, mp. 280 °C. ^{1}H NMR (300 MHz, $CDCl_3$): δ 8.6 (d, 2H), 7.50-7.37 (m, 8H), 6.68 (d, 2H), 3.00 (s, 6H). ^{13}C NMR (75 MHz, $CDCl_3$): δ 150.32, 132.84, 131.7, 131.24, 125.22, 113.15, 104.78, 93.48, 87.12, 76.58, 40.16. Exact mass calculated for $C_{23}H_{18}N_2$ (M^{+}) is 322.1470 found 322.1452 (EI high resolution mass spectrometry).

Preparation of 2Q. Compound **2** was reacted with CH_3I as mentioned in step (v) in Scheme 3.3B (note that the same procedure was adopted for the preparation of **1Q** in Scheme 3.3A and the details are provided in page 77). Product **2Q** was obtained in almost quantitative yield, mp. > 300 °C (decompose). ^{1}H NMR (300 MHz, $CDCl_3$): δ 8.86 (d, 2H), 8.13 (d, 2H), 7.67 (d, 2H), 7.55 (d, 2H), 7.39 (d, 2H), 6.78 (d, 2H), 4.37 (s, 3H), 3.00 (s, 6H). ^{13}C NMR (75 MHz, DMSO): δ 151.41, 146.52, 139.07, 133.65, 133.59, 132.27, 129.83, 126.99, 119.62, 112.79, 108.51, 102.56, 95.98, 87.94, 87.85, 48.70, 40.87.

Preparation of 13. A mixture of **4** (50 mg, 0.345 mmol), 1,3-diiodobenzene (113 mg, 0.34 mmol), $Pd(PPh_3)_4$ (24 mg, 0.035 mmol), CuI (7 mg, 0.04 mmol) and PPh_3 (18 mg, 0.07 mmol) in diispropylamine (2 mL) was stirred for 15 h at room temperature. The reaction mixture was filtered over celite using chloform as eluent and the solvent was evaporated. The crude product was then chromatographed over alumina using hexane as eluent to get **13** (40 mg, 33 %) as a white solid, mp. 93 °C. ^{1}H NMR (300 MHz, $CDCl_3$): δ 7.85 (s, 1H), 7.61 (d, 1H), 7.45 (d, 1H), 7.40 (d, 2H), 7.06-7.01 (m, 1H), 6.67 (d, 2H), 3.00 (s, 6H). ^{13}C NMR (75 MHz, $CDCl_3$): δ 150.24, 139.84, 136.32, 132.15, 130.32, 129.71, 126.43, 111.82, 109.81, 96.19, 93.74, 92.28, 40.23. m/z (FAB) found 347.03 Calc. 347.02.

Preparation of 14. To a solution of **5** (50 mg, 0.14 mmol), CuI (2.73 mg, 0.014 mmol), $Pd(PPh_3)_2Cl_2$ (10 mg, 0.014 mmol) in diispropylamine (2 mL) was added

(trimethylsilyl)acetylene (0.02 mL, 0.159 mmol) and heated at 70 ^{0}C for 1 h under argon atmosphere. The reaction mixture was filtered over celite using chloform as eluent and the solvent was evaporated. The crude product was then chromatographed over alumina using hexane as eluent to yield **14** (35 mg, 76 %), mp. 93 °C. ^{1}H NMR ($CDCl_3$, 300 MHz) δ 7.6 (s, 1H), 7.3-7.4 (m, 4H), 7.2 (m, 1H), 6.6 (d, 2H), 2.9 (s, 6H), 0.2(s, 9H). ^{13}C NMR (75 MHz, $CDCl_3$): δ 150.39, 135.03, 133.02, 130.95, 131.41, 130.95, 128.39, 124.74, 123.58, 112.10, 110.20, 104.85, 96.43, 94.72, 91.61, 86.88, 40.49, 0.28. m/z (FAB) found 317.10 Calc. 317.16.

Preparation of 15. To a solution of **14** (45 mg, 0.141 mmol) in a mixture of THF (0.46 mL) and methanol (0.72 mL), an aqueous solution of NaOH (0.05 mL, 5 N) was added and the mixture was stirred for 2 h at room temperature. The reaction mixture was washed with water and extracted using chloroform. The organic layer was dried over Na_2SO_4 and evaporated to yield **15** (33 mg, 94 %) as a pale yellow solid, mp. 91°C. ^{1}H NMR ($CDCl_3$, 300 MHz): δ 7.92 (s, 1H), 7.90 (d, 1H), 7.60-7.2 (m, 4H), 6.87 (d, 2H), 3.04 (s, 1H), 3.0 (s, 6H). ^{13}C NMR (75 MHz, $CDCl_3$): δ 150.20, 134.85, 132.82, 131.53, 130.95, 128.28, 124.66, 122.28, 111.86, 109.85, 96.20, 91.55, 86.52, 83.12, 40.26. m/z (FAB) found 245.09 Calc. 245.12.

Preparation of 3. A mixture of 7 (33 mg, 0.134 mmol), 4-iodopyridine (41.4 mg, 0.20 mmol), $Pd(PPh_3)_2Cl_2$ (9.43 mg, 0.013 mmol), CuI (2.57 mg, 0.013 mmol)

and PPh_3 (7.06 mg, 0.027 mmol) was added to a degassed solution of diispropylamine (2 mL) and the mixture was stirred for 15 h at room temperature. The reaction mixture was filtered over celite using chloform as eluent and the solvent was evaporated. The crude product was then chromatographed over neutral alumina, using a mixture (1:10) of chloroform and hexane as eluent to yield **3** (15 mg, 34 %) as a brown solid, mp. 181-183 °C. ^{1}H NMR ($CDCl_3$, 300 MHz): δ 8.62-8.60 (d, 2H), 7.69 (s, 1H), 7.51-7.30 (m, 7H), 6.68-6.65 (d, 2H), 3.00 (s, 6H). ^{13}C NMR (75 MHz, $CDCl_3$): δ 150.23, 149.73, 134.57, 132.82, 132.19, 131.39, 130.58, 128.48, 125.56, 124.90, 122.27, 111.83, 96.17, 93.49, 91.86, 86.92, 86.38, 40.23. Exact mass calculated for $C_{23}H_{18}N_2$ ($M^{\cdot+}$) is 322.1470, found 322.1427 (EI high resolution mass spectrometry).

Preparation of 3Q. Compound **3** was reacted with CH_3I as mentioned in step (v) in Scheme 3.3C (note that the same procedure was adopted for the preparation of **1Q** in Scheme 3.3A and the details are provided in page 76). Product **3Q** was obtained in almost quantitative yield, m. p. 197-202 °C. ^{1}H NMR ($CDCl_3$, 300 MHz) 8.87 (d, 2H), 8.15 (d, 2H), 7.76 (s, 1H), 7.62-7.59 (m, 2H), 7.49-7.44 (m, 1H), 7.37 (d, 2H), 6.73 (d, 2H), 4.37 (s, 3H), 2.98 (s, 6H).

3.4. Results and discussion

3.4.1. Photophysical investigation

Absorption, emission and excitation spectra and fluorescence decay profile of compounds **1-3** are presented in Figures 3.1-3.3. The main objective of this

:hapter is to understand the effect of (i) conjugation on the photophysical properties of D-OPE-A system possessing N,N-dimethylaniline and pyridine moieties at the terminal positions of phenyleneethynylenes (by comparing **1** and **2**) and (ii) *meta/para* connectivity in D-OPE-A system (by comparing **2** and **3**). The absorption spectral features of **1-3** are significantly different (trace 'a' in Figures 3.1A-3.3A): compound **1** possesses a single absorption band whereas two transitions are observed for **2** and absorption spectrum is more structured in the case of **3**. These aspects were examined theoretically and results are summarized in Section 3.5. The sharp absorption band observed in the case of **1** is due to the HOMO-LUMO transition, whereas compound **2** possesses two well-separated bands originating from HOMO/HOMO-1 energy levels. The absorption maximum of the low energy band of compounds **1-3** remain unaffected in solvents of varying polarity implying that the ground state and Franck-Condon state possess more or less same polarity. The molar extinction coefficient of **1**, **2** and **3** in toluene at their respective absorption maximum were estimated to be 2.67 x 10^4 cm^{-1} (352 nm), 3.80 x 10^4 cm^{-1} (367 nm) and 2.84 x 10^4 cm^{-1} (331 nm). On comparing the S_0-S_1 energy gap of the *para* substituted compounds **1** and **2**, a bathochromic shift of 15 nm along with a large increase in molar exctinction coefficient, was observed on increasing the conjugation. Interestingly the absorption maximum of the *meta* isomer **3** underwent blue shift (λ_{max} = 331 nm) as compared to the corresponding *para* isomer **2**, indicating a lower degree of

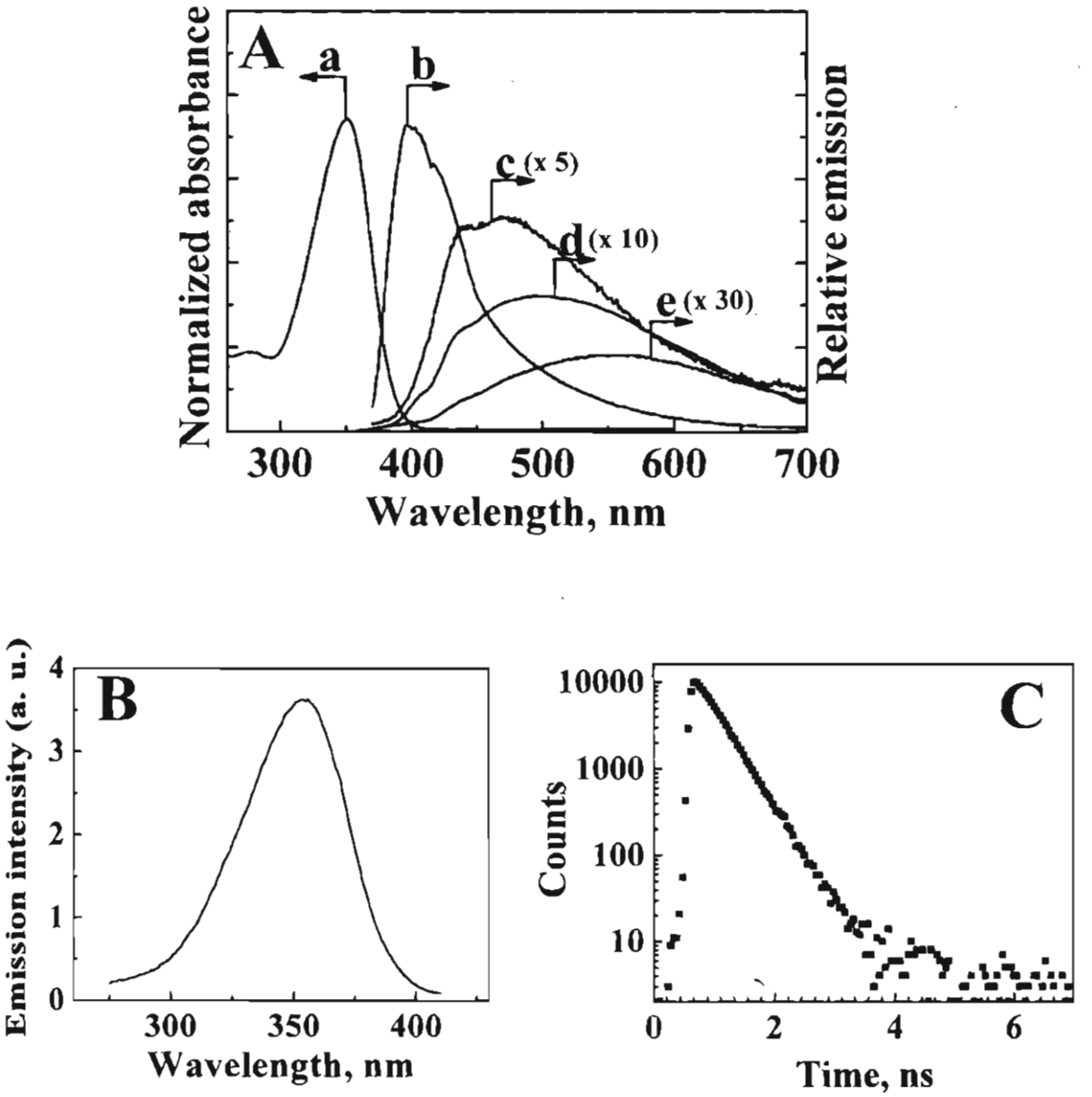

Figure 3.1. **A)** The normalized absorption spectra (a) of **1** in acetonitrile and normalized emission spectra of **1** in (b) toluene, (c) dichloromethane, (d) acetone and (e) acetonitrile. **B)** Excitation spectra of the compound **1** in acetonitrile (emission collected at 550 nm **C)** Fluorescence lifetime profile of the compound **1** in acetonitrile.

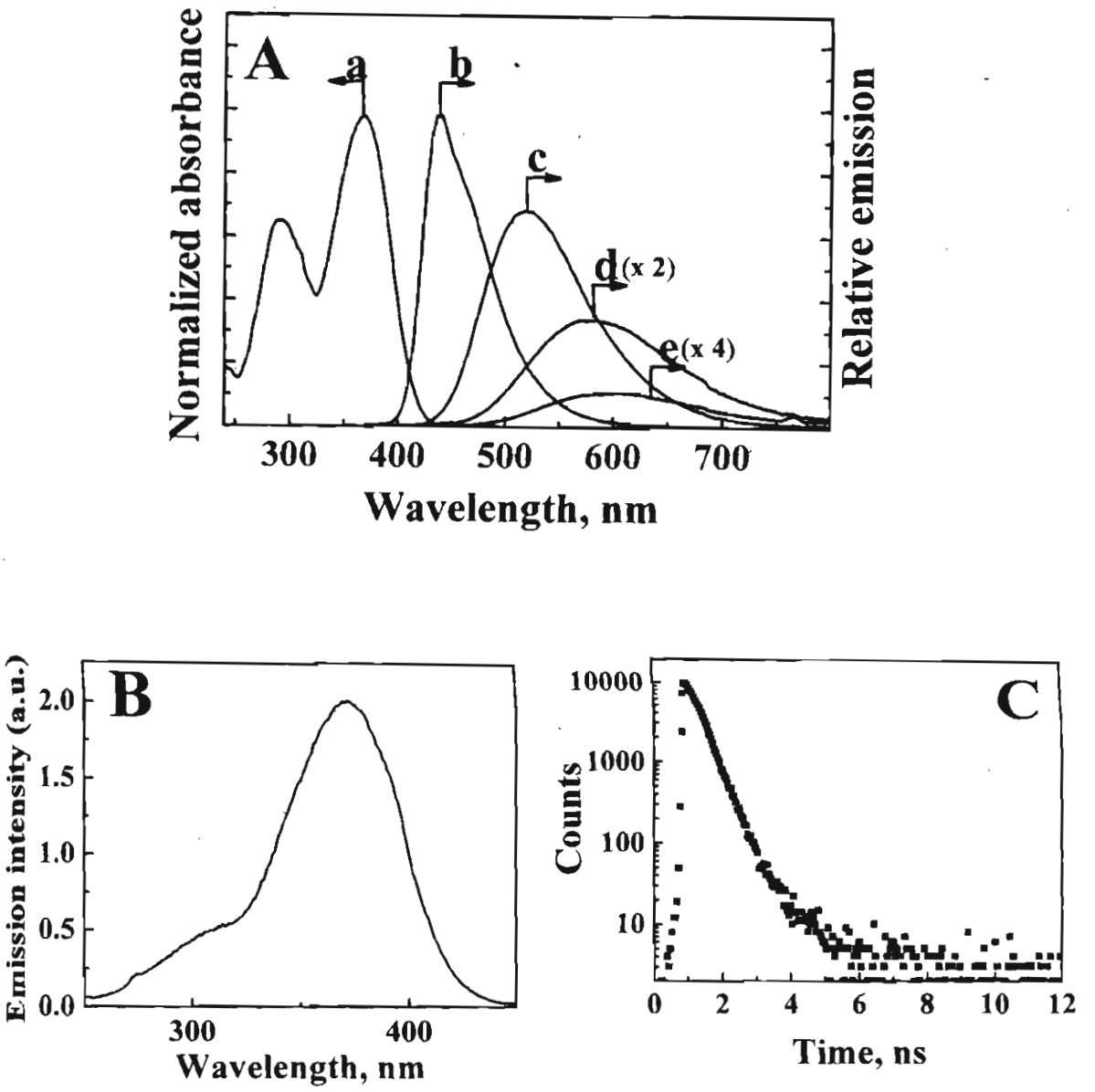

Figure 3.2. A) The normalized absorption spectra (a) of **2** in acetonitrile and normalized emission spectra of **2** in (b) toluene, (c) dichloromethane, (d) acetone and (e) acetonitrile. **B)** Excitation spectra of the compound **2** in acetonitrile (emission collected at 600 nm) **C)** Fluorescence lifetime profile of the compound **2** in acetonitrile.

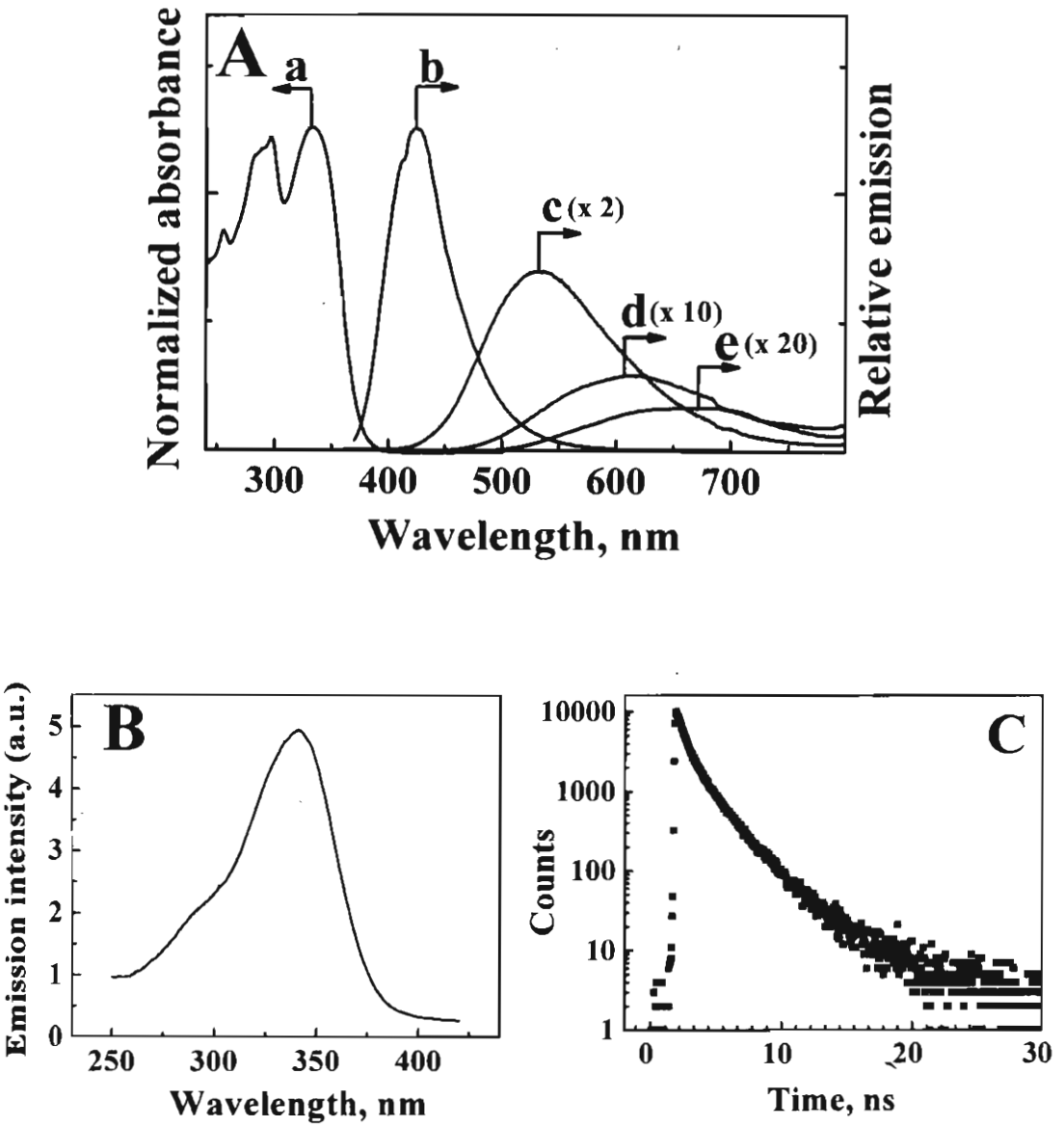

Figure 3.3. A) The normalized absorption spectra (a) of **3** in acetonitrile and normalized emission spectra of **3** in (b) toluene, (c) dichloromethane, (d) acetone and (e) acetonitrile. **B)** Excitation spectra of the compound **3** in acetonitrile (emission collected at 650 nm) **C)** Fluorescence lifetime profile of the compound **3** in acetonitrile

conjugation in the ground state. In effect, the *meta* connectivity prevents the effective interaction between the donor and acceptor, which was further confirmed by protonation studies. Compounds **1-3** emits in the short wavelength region in nonpolar solvents, for example, the emission maximum of the compounds **1-3** in toluene are 399, 439 and 425 nm respectively (trace 'b' in Figures 3.1A-3.3A). A large bathochromic shift in emission maxima was observed for all the compounds with increase in solvent polarity (trace 'c-e' in Figures 3.1A-3.3A) indicating that the bands originate from an intramolecular charge transfer state (ICT). These aspects were further investigated by (i) estimating the Full Width at Half Maximum (Table 3.1) (ii) Stokes shift (Table 3.2) (iii) emission yields (Table 3.3).

With increase in solvent polarity, the Full Width at Half Maximum (FWHM) gradually increases for compounds **1-3** (Table 3.1). In toluene the emission spectrum is found to be narrow for all the three compounds and the FWHM is estimated to be in the range of 3200-3600 cm^{-1}. On increasing the solvent polarity, the emission spectrum shifts to longer wavelengths with a considerable degree of broadening (the FWHM for **1** in dichloromethane and acetone are 5848 and 7214 cm^{-1}, respectively). Such broad bands in the red region usually originate from a charge transfer state.

A substantial increase in Stokes shift was observed for all the three compounds in polar solvents confirming the presence of a stabilized charge transfer state (Table 3.2). In a particular solvent system, the Stokes shift value (ν_{st})

Table 3.1. FWHM[a] of the emission spectrum of compounds 1-3 in different solvents.

Compound	*FWHM(cm^{-1})[a]*			
	Toluene	*Dichloromethane*	*Acetone*	*Acetonitrile*
1	3451	5848	7214	6586
2	3233	3974	4580	4446
3	3595	4651	4728	-

[a]Full Width at Half Maximum

is more or less in the same range for *p*-substituted compounds (**1** and **2**). For example, in toluene, ν_{st} is in the range of 3300-4300 cm^{-1} whereas in acetonitrile the Stokes shift is much larger (10200-10700 cm^{-1}). One of the interesting observations is that the *meta* isomer (**3**) possesses a higher ν_{st} value compared to the *para* isomer (**2**) suggesting that the excited state charge transfer is more efficient in the former one.

Table 3.2. Stokes shift values of 1-3 in toluene and acetonitrile

Compound	*λ_{abs} (nm)[a]*		*λ_{fl}(nm)[b]*		*ν_{st} (cm^{-1})[c]*	
	TOL[d]	*ACN[e]*	*TOL[d]*	*ACN[e]*	*TOL[d]*	*ACN[e]*
1	352	351	399	550	3306	10267
2	367	370	439	604	4248	10692
3	331	330	425	650	6682	14918

[a]absorption maximum(λ_{abs}), [b]emission maximum(λ_{fl}), [c]Stokes Shift(ν_{st}), [d]tolune, [e]acetonitrlie.

A red shift in emission band accompanied by substantial broadening, on increasing the polarity, is indicative of a polar excited state resulting from a stabilized charge transfer state. Excited state dipole moment is an important parameter generally used to understand the nature of excited state of molecules. According to Lippert-Mataga equation (Equation 3.5), the solvatochromic shift of the emission spectra can be used for estimating the excited state dipole moment

$$\nu_{st} = 2(\mu_e-\mu_g)^2\Delta f/hca^3 + \text{constant} \qquad (3.5)$$

where,

$$\Delta f = [(\varepsilon - 1)/(2\varepsilon + 1)] - [(n^2 - 1)/(2n^2 + 1)] \qquad (3.6)$$

'ν_{st}' is the Stokes shift, 'μ_e' is the excited state dipole moment, 'μ_g' is the ground state dipole moment, 'c' is the velocity of light, 'a' is the Onsager radius, 'Δf' is the solvent polarity parameter and 'ε'and 'n' are the dielectric constant and refractive index, respectively. The excited state dipole moment values can be obtained from the plot of Stokes shift (ν_{st}) against Δf (Figure 3.4). Slope of the *meta* substituted compound **3** is larger (compared to **1** and **2**) indicating a large change in dipole moment on photoexcitation. Estimation of the excited state dipole moment of **2** and **3** are difficult due to their large molecular geometries: compound **2** possess a rod like molecular geometry whereas **3** possess a V-shaped geometry and the estimation of the exact Onsager radius 'a' for such geometrical shapes is difficult.

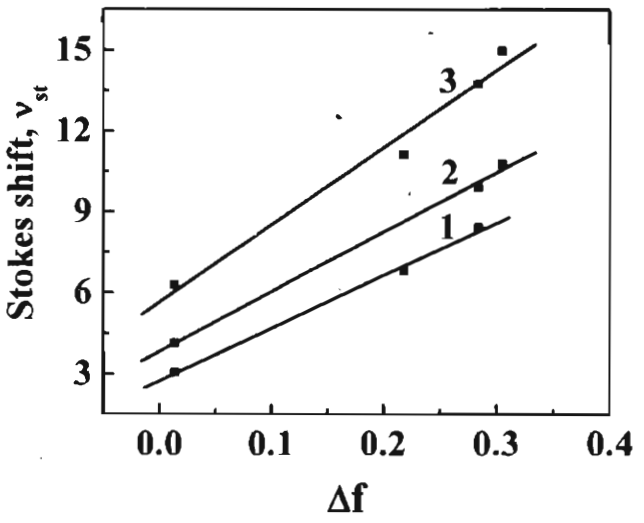

Figure 3.4. Lippert – Mataga plot for **1 – 3**

Compounds **1-3** emits with relatively high quantum yield (ϕ_f) in nonpolar solvents, for example quantum yield of fluorescence in toluene is 0.11 for **1**, 0.61 for **2** and 0.28 for **3**. A dramatic decrease in fluorescence quantum yield was observed for all the three compounds, with increase in the solvent polarity and it is reasonable to believe that the emission of **1-3** originates from a charge separated state. The charge transfer state is stabilized with increase in polarity and the decay through nonradiative channel predominates as evident from the decrease in ϕ_f. Further we have quantified the radiative (k_r) and the total nonradiative rate constants (k_{nr}^{tot}) from the excited singlet state, using equations 3.7 and 3.8.

$$k_r = \frac{\phi_f}{\tau_f} \qquad (3.7)$$

$$k_d = \frac{(1-\phi_f)}{\tau_f} \qquad (3.8)$$

The quantum yield (ϕ_f), fluorescence lifetime (τ_{fl}), radiative rate constant (k_r), nonradiative rate constant (k_d) of **1-3** in toluene and acetonitrile are summarized in Table 3.3. It was observed that the rate constant of singlet-state deactivation through nonradiative channels increases with solvent polarity.

Table 3.3. Photophysical properties[a-e] of 1-3 in toluene and acetonitrile.

	ϕ_f^a		τ_{fl}(ns [b]		$k_r(10^7)^c$		$k_{d(}10^8)^d$		*Emissive rate=$(k_r/k_d)^e$*	
	TOL[f]	*ACN[g]*	*TOL[f]*	*ACN[g]*	*TOL[f]*	*ACN[g]*	*TOL[f]*	*ACN[g]*	*TOL[f]*	*ACN[g]*
1	0.11	0.001	2.5	0.39	4.4	0.25	3.56	25.6	0.12	0.001
2	0.61	0.017	1.22	0.45	50.0	3.8	3.2	21.8	1.56	0.017
3	0.28	-	4.8	0.55, 2.63	5.8	-	1.5	-.	0.38	-

[a]quantum yield (ϕ_f), [b]fluorescence lifetime (τ_{fl}), [c]radiative rate constant (k_r), [d]nonradiative rate constant (k_d), [e]emissive rate, [f]toluene and [g]acetonitrile.

The increased charge transfer character in the excited state of phenylene-ethynylenes is a subject of intense interest. Theoretical calculations has shown that the excited state of the *meta* substituted bis(phenylethynyl) benzene possess cumulenic character which allows charge transfer in the excited state.[18] For a series of dimethylamino substituted stilbenes, it was reported that the *meta* derivatives possess higher excited state dipole moments compared to *ortho* and *para* isomers[16] which is rationalized by involving a twisted intramolecular charge transfer (TICT)[1] process. It was proposed that the twisting is more in the case of *meta* isomer than the *para* and *ortho* isomer and the charge is effectively localized

on the donor-acceptor side. In the present case the *meta* substituted compound **3** possess higher lifetime in toluene indicating stabilization in the excited state. The excitation spectra of the compounds are also presented in the Figures 3.1B-3.3B. The excitation spectral features remained more or less the same irrespective of the polarity of the solvents. The excitation spectra of compounds **2** and **3** contain two bands similar to that in the absorption spectra although the intensities are different.

Effect of protonation of the pyridine ring. Effective interaction between the donor and acceptor moieties through phenyleneethynylene bridging units in compounds **1-3** were further investigated by protonation studies. Addition of varying amounts of TFA to an acetonitrile solution of *para* isomers (**1** and **2**) led to a decrease in the S_0-S_1absorption bands, accompanied by the formation of an intense red-shifted absorption band (Figure 3.5A and 3.6A). The new band observed in the case of *para* isomers was attributed to a charge transfer transition from the dimethylamino moiety to the pyridinium moiety through phenylene-ethynylene bridging units. The charge transfer interaction is more effective in the case of **1** possessing one phenylethynyl unit compared to **2** having two repeat units. Interestingly in the case of *meta* isomer (**3**), no new charge transfer band was observed (Figure 3.7A) on addition of TFA indicating that there is no electronic communication between the donor-acceptor pair in its ground state (a slight variation in the intensity of the bands were observed). For better comparison, the absorption spectra of **1-3** in acetonitrile in its unprotonated (trace

'a'), protonated (trace 'b') and quaternized forms (trace 'c') are presented in Figures 3.5B-3.7B.

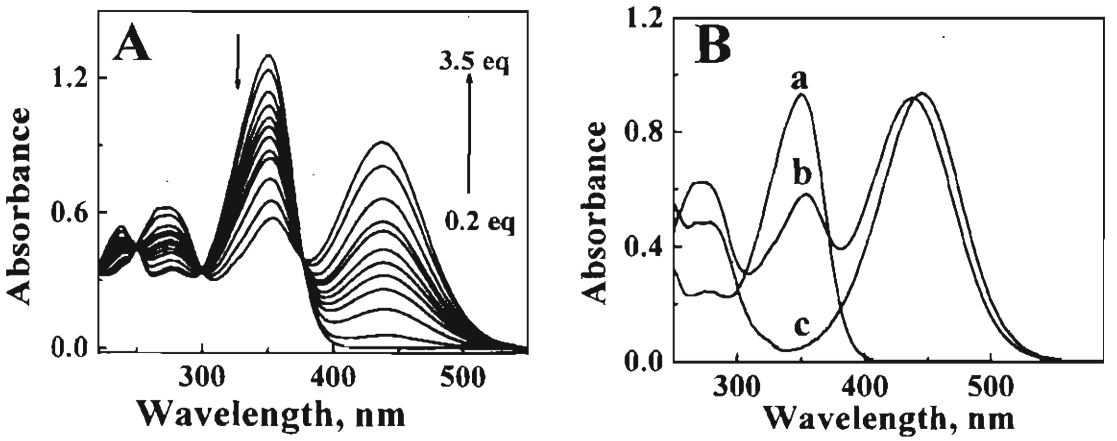

Figure 3.5. **A)** Changes in the absorption spectra of **1** in acetonitrile on addition of TFA. **B)** Absorption spectra of **1** in acetonitrile in its (a) unprotonated form, (b) protonated form and (c) quaternized form (**1Q**).

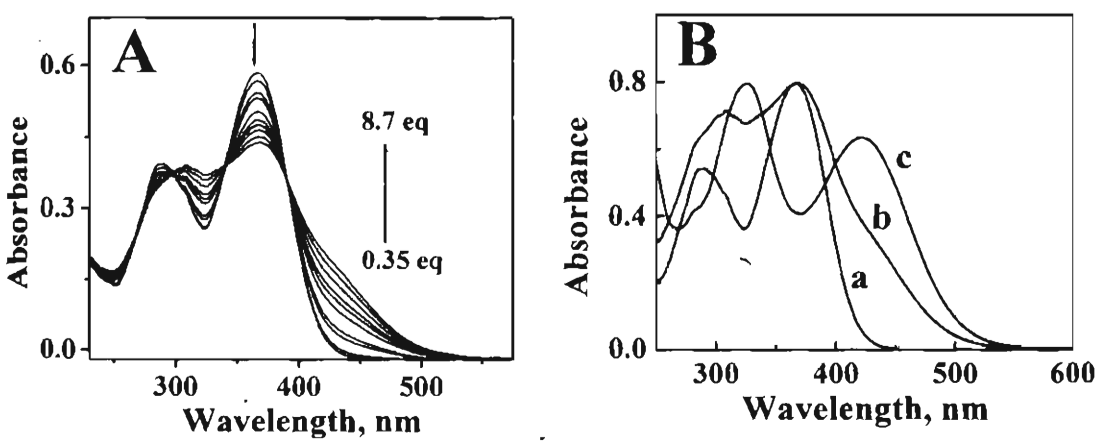

Figure 3.6. **A)** Changes in the absorption spectra of **2** in acetonitrile with the addition of TFA. **B)** Absorption spectra of **2** in acetonitrile in its (a) unprotonated form, (b) protonated form and (c) quaternized form (**2Q**).

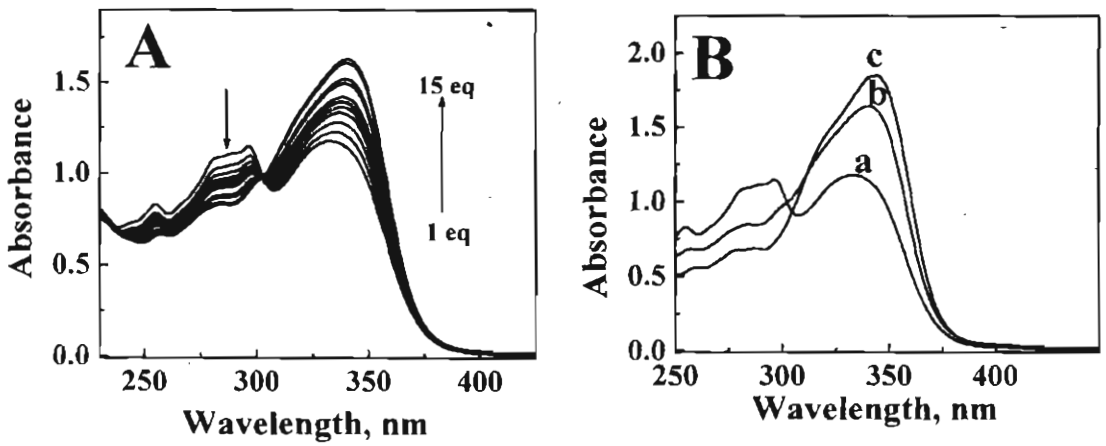

Figure 3.7. A) Changes in the absorption spectra of **3** in acetonitrile with the addition of TFA. **B)** Absorption spectra of **3** in acetonitrile in its (a) unprotonated form, (b) protonated form and (c) quaternized form (**3Q**).

3.4.2. Theoretical investigation

Phenyleneethynylene based rigid rod molecular systems were optimized at AM1 semiempirical and B3LYP/6-31G* level density functional theory (DFT) methods.[23,24] The basic photochemical properties of these systems were investigated by means of quantum chemical calculations employing mainly the time-dependent density functional theory (TDDFT)[25-27] as well as Zerner's intermediate neglect of differential overlap (ZINDO/S) method.[28,29] For all the calculations, Gaussian03[30] suit of programs were used.

The molecular systems **1-3** and their protonated forms were optimized at the B3LYP/6-31G* level of theory by applying a dielectric constant equal to the solvent polarity of acetonitrile. Figures 3.8-3.10 shows the comparison of the native form and protonated forms of the compounds with the relevant bond lengths.

Conjugation features of **1-3** in its ground state can be examined by comparing the bond lengths in their optimized structures. On addition of TFA pyridine ring get protonated and the lone pair is pulled more effectively from the nitrogen atom of dimethylamino group in the case of **1**. This is reflected in the N-C bond length between the dimethylamino group and the adjacent phenyl group where the distance decreases from 1.374 to 1.367 Å on protonation (Figure 3.8). Correspondingly, we could observe an increase in the triple bond length from 1.220 to 1.224 Å and a decrease in the single bond length on both sides of triple bonds.

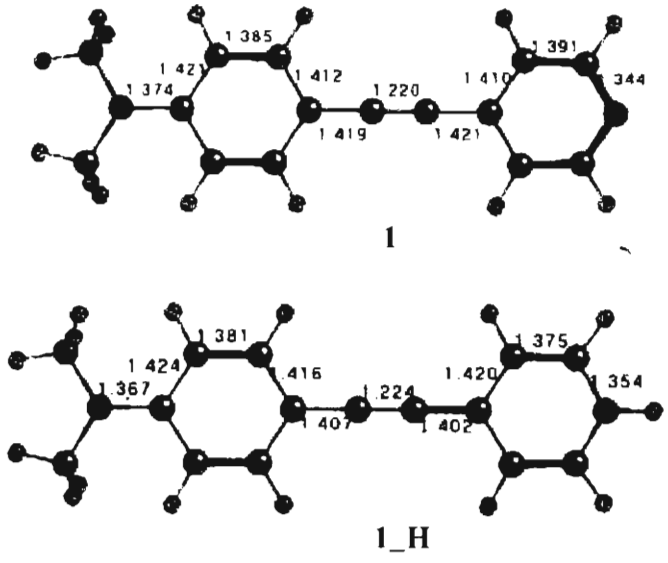

Figure 3.8. Optimized geometries of **1** and protonated form **1_H** using B3LYP/6-31G* level of theory.

On comparing the *para*, and *meta* isomers (**2** and **3**), latter one possess shorter triple bonds and longer single bonds compared to the *para* isomer (Figure 3.9 and Figure 3.10). These results again confirm that the extent of delocalization

is lesser in the case of *meta* isomer **3** compared to *para* isomer **2**. Protonation of *para* isomer **2** also brings about significant bond length changes; the extent of variation decreases with the distance from the pyridinium moiety (Figure 3.9).

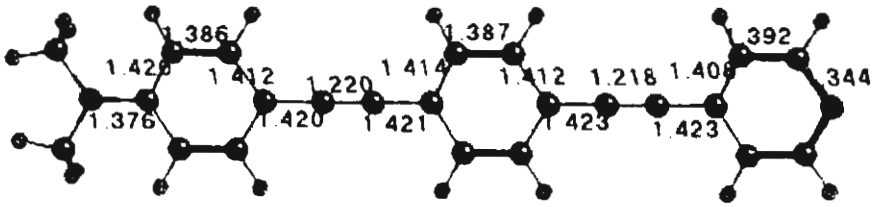

2

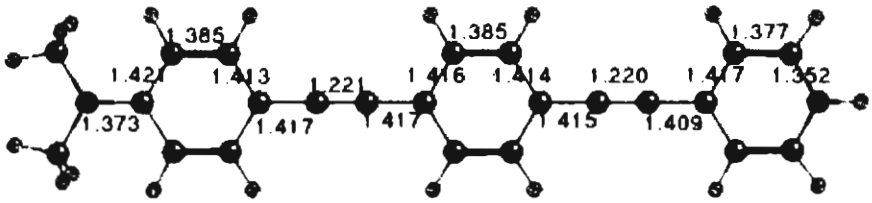

2_H

Figure 3.9. Optimized geometries of **2** and protonated form **2_H** using B3LYP/6-31G* level of theory

However in the case of the protonated form of *meta* isomer (**3_H**) it is interesting to note that the structural rearrangement is pronounced only in the one half where in pyridinium is attached and the other half possessing the donor group remains unaltered (Figure 3.10). Thus it is clear that the *meta* junction of the central phenyl ring prevents the electronic communication between the two halves in the ground state.

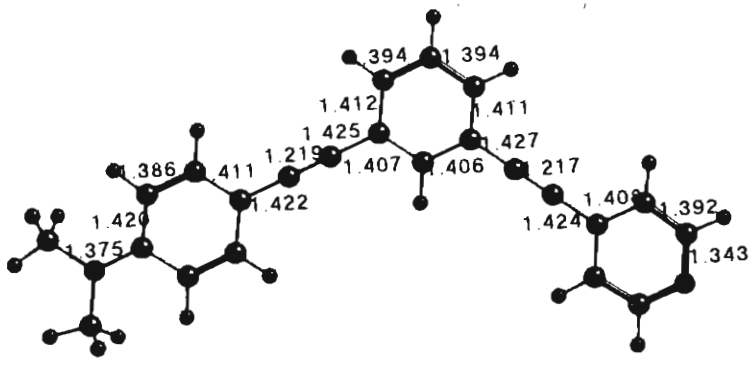

3

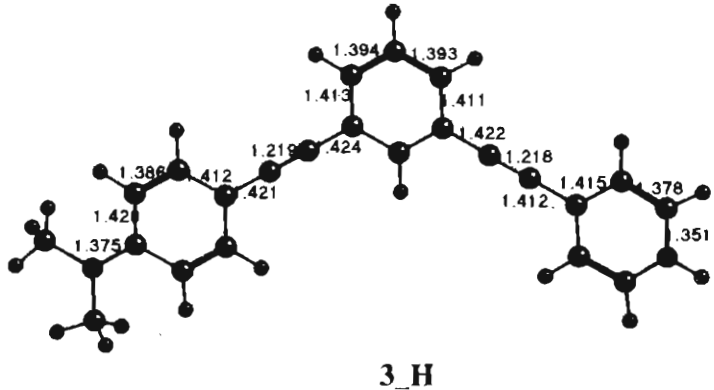

3_H

Figure 3.10. Optimized geometries of **3** and protonaed form **3_H** using B3LYP/6-31G* level of theory.

TDDFT calculations

Using the optimized planar geometries of the compounds **1-3** and their protonated forms at B3LYP/6-31G* level, the first 20 low lying excited states have been calculated at TDDFT and ZINDO/S levels and the results obtained are presented on Table 3.4. It is interesting to note that **1** possesses only one singlet state with significant oscillator strength while the *para* isomer **2** and the *meta* isomer **3** showed two such states. These theoretical results are in good agreement with the number of absorption peaks observed for **1-3** (Figure 3.1-3.3A). The wavelength of excitation and the corresponding MO transitions obtained by

TDDFT and ZINDO/S studies and the absorption maximum obtained by experimental studies are presented in Table 3.4. Although for the neutral molecules, the values obtained closely agree with the experimental spectra, the protonated forms of these molecules showed considerable deviation from the experimental value.

Table 3.4. Experimental wavelengths (λ_{exp})[a], calculated absorption wavelengths (λ_{cal})[b] and oscillator strengths[b] for 1- 3.

Compound	Transition	Experimental wavelength[a] λ_{exp}, (nm)	ZINDO		TDDFT	
			λcal, nm	Oscillator strength	λcal, nm	Oscillator strength
1	HOMO to LUMO	351	350	0.8037	344	1.0161
2	HOMO to LUMO	370	377	1.4598	419	1.4023
	HOMO-1 to LUMO+1	286	273	0.1149	319	0.8273
3	HOMO to LUMO+1	330	349	0.9254	339	1.4294
	HOMO-1 to LUMO	297	328	0.5116	298	0.5919

[a]Figure 3.1 A, 3.2 A and 3.3 A for **1**, **2** and **3**. TDDFT and ZINDO/S level calculations using the B3LYP/6-31G* level optimized geometries of **1**, **2**, and **3**.

The singlet excited state of **1** corresponds to the electron transition from HOMO to LUMO (Figure 3.11 for the orbitals) and the calculated wavelength of 344 nm (TDDFT) and 350 nm (ZINDO/S) for this absorption is in agreement with the experimental value of 351 nm. By comparing the orbital features we can see

that the electron density clearly shifts from N,N-dimethylaniline to the pyridine moiety which acts as the acceptor.

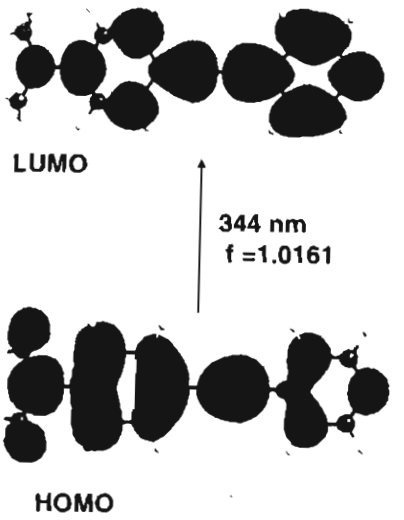

Figure 3.11. HOMO-LUMO transition of compound **1**. (Calculated wavelengths and oscillator strengths indicated are obtained by TDDFT method).

In the case of *para* isomer **2,** the long wavelength absorption corresponds to transition from HOMO to LUMO while the high energy absorption is due to the transition from HOMO-1 to LUMO (Figure 3.12). The calculated wavelengths of absorption for the transitions obtained by ZINDO method (377 and 273 nm) are in good agreement with the experimental values (370 and 286 nm). The orbital features clearly indicates that for HOMO/ HOMO-1 the charge density is more localized on the donor part while for LUMO the charge density is localized on the acceptor part i.e. around pyridine. Clearly both the electronic transition involves a shift in the charge density from the donor side to the acceptor side.

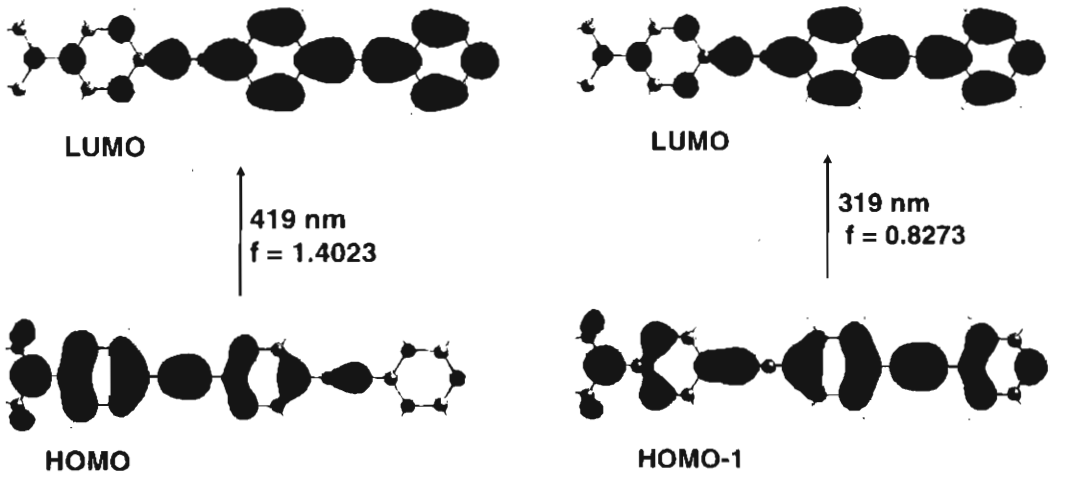

Figure 3.12. MOs involved in the transition of **2** (Calculated wavelengths and oscillator strengths indicated are obtained by TDDFT method).

For the *meta* isomer **3,** theoretical calculations showed that the two bands in the absorption spectra can be attributed to the transition from HOMO to LUMO+1 as well as from HOMO-1 to LUMO (Figure 3.13). TDDFT level of theory gave comparatively agreeable values (339 nm and 298 nm) with the experimental spectrum (333 nm and 297 nm). It is interesting to note that for the *meta* isomer **3**, on excitation, the charge density is not transferred from the donor to the acceptor moiety. The transitions are localized either on the donor or on acceptor side (Figure 3.13) where the *meta* conjugated phenyl ring acts as a junction. The long wavelength transition mainly involves the charge shift from the donor side to the central phenyl ring and the short wavelength transition involves mainly the transition from the central phenyl ring to the acceptor side.

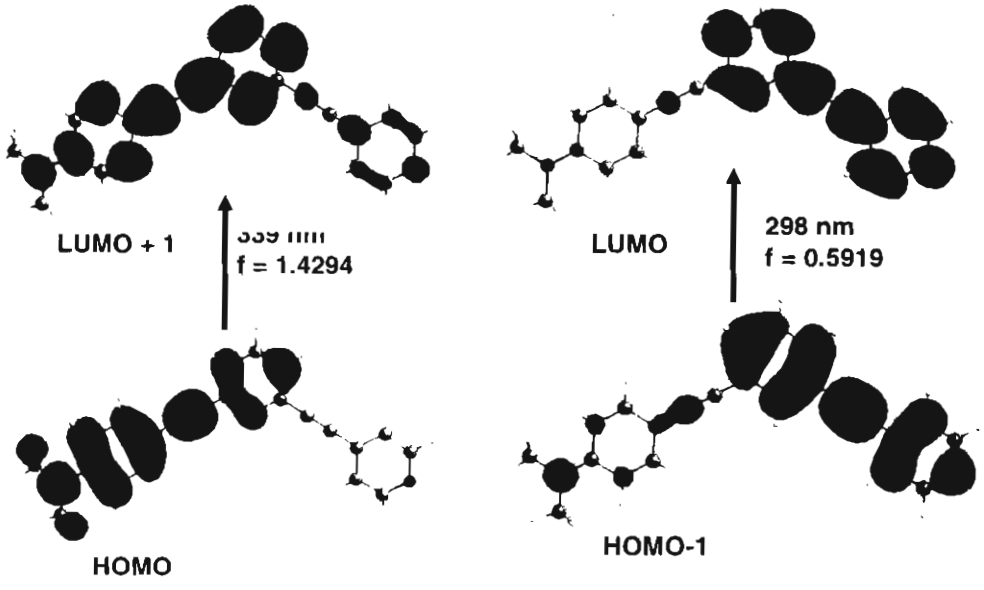

Figure 3.13. MOs involved in the transition of **3**. (Calculated wavelengths and oscillator strengths indicated are obtained by TDDFT method).

With the addition of protons, pyridinium ions are formed which possess higher acceptor strength. This results in the alteration of bond lengths and charge distribution in the molecule and indicated by the formation of a new charge transfer band in the UV-Vis absorption spectrum (Figures 3.5 & 3.6). However in the case of *meta* isomer, the *meta* connectivity between the donor and acceptor prevents the effective communication and no new charge transfer band was observed (Figure 3.7). The orbitals involved in the transition of protonated forms of **1-3** (**1_H** to **3_H**) remained the same compared to unprotonated forms of **1-3**. However the orbital feature of **1_H-3_H** showed a more charge transfer character. In the case of protonated form of **3** (**3_H**) the effective electron transfer from the donor side to the acceptor side is prevented at the *meta* junction (Figure 3.14).

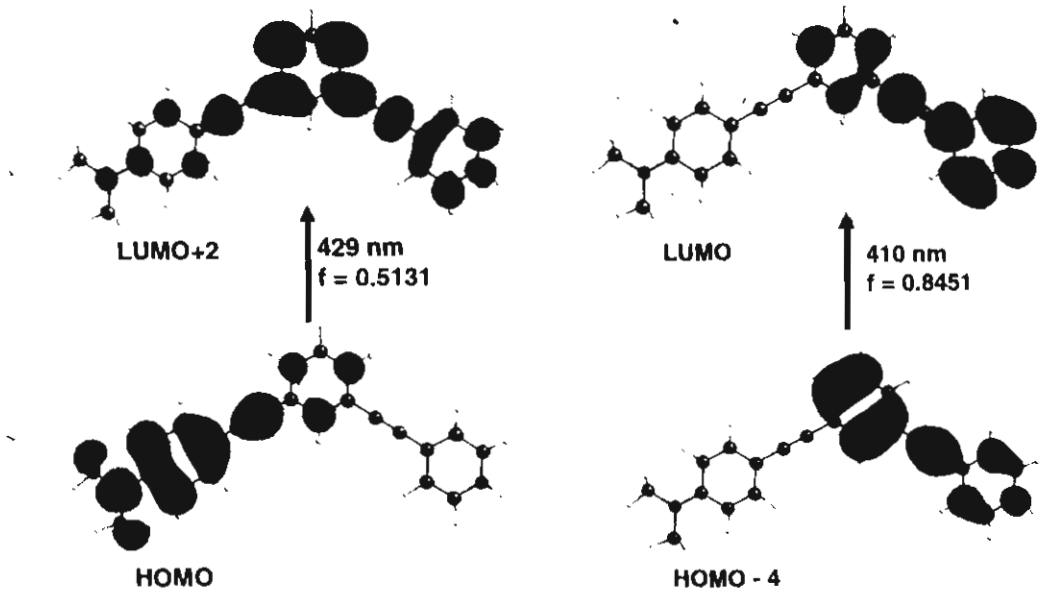

Figure 3.14. MOs involved in the transition of **3_H** (Calculated wavelengths and oscillator strengths indicated are obtained by TDDFT method).

For the protonated compounds **1-3**, the calculated wavelengths of absorption obtained by TDDFT and ZINDO levels of theory are much higher than the experimental values. The large difference in the calculated values may be due to the counter ion effect which is not be properly accounted in theoretical methods. As we know the counter ions have significant effect on the overall electronic structure of the material which will result in changes in the electronic distribution. Agreeable values were obtained by modeling a neutral system wherein a counter ion is placed at a particular distance from the +vely charged acceptor moiety. For example; the protonated form of **2**, shows the charge transfer band at 443 nm in acetonitrile while the TDDFT and ZINDO levels of theory gave the results as 760

nm and 560 nm respectively. But by placing the counter ion at a distance of 4 Å, much closer value of 467 nm is obtained (Figure 3.15).

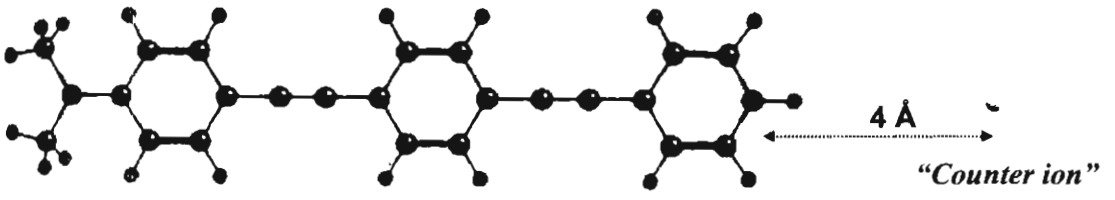

Figure 3.15. Model system for charged species.

A comparison of the theoretical values obtained for the positively charged systems and neutral systems in comparison with the experimental values is given in Table 3.5.

Table 3.4. Experimental wavelengths (λ_{exp})[a], calculated absorption wavelengths (λ_{cal})[b] and oscillator strengths[c] for 1- 3.

Compound	ZINDO				Experimental Wavelength[a] λexp, nm
	+vely charged system		With counter ion		
	Transition	λcal(nm)[b],f[c]	Transition	λcal(nm)[b],f[c]	
1_H	HOMO to LUMO	488 f = 1.1837	HOMO-3 to LUMO	424 f = 0.9831	436
	HOMO-4 to LUMO	265 f = 0.188	HOMO-3 to LUMO+2	283 f = 0.0504	353
2_H	HOMO to LUMO	560 f =1.2536	HOMO to LUMO	441 f =1.4966	443
	HOMO-2 to LUMO	386 f = 0.2961	HOMO to LUMO+2	346 f = 0.0691	367
3_H	HOMO-4 to LUMO	414 f = 1.0561	HOMO to LUMO	387 f = 0.4165	341
	HOMO to LUMO + 3	360 f = 0.6918	HOMO-5 to LUMO	366 f = 0.9250	281

[a]Figure 3.5 A, 3.6 A and 3.7 A for **1**, **2** and **3**. ZINDO/S level calculations using the B3LYP/6-31G* level optimized geometries of **1_H**, **2_H**, and **3_H**.

3.5. Conclusions

Donor-acceptor systems based on phenyleneethynylene with varying conjugation and connectivity (*para* and *meta* isomers) have been synthesized and their photophysical properties were studied using various spectroscopic and theoretical techniques. In the ground state, the *meta* connectivity prevents the effective communication between the donor and acceptor groups while in the excited state the channels open up and the interaction between the donor and acceptor is possible. The absorption maximum of the low energy band of compounds **1-3** remain unaffected in solvents of varying polarity implying that the ground state and Franck-Condon state possess more or less same polarity. A large bathochromic shift in emission maximum was observed for all the compounds with increase in solvent polarity indicating that the bands originate from an intramolecular charge transfer state (ICT). The extent of charge transfer was further compared by estimating the (i) Full Width at Half Maximum (ii) quantum yield (iii) Stokes shift. The coupling between the donor and the acceptor in the excited state was found to be maximum for *meta* isomer than the *para* isomers **1** and **2**. For compounds **1** and **2** on adding TFA, the intensity of the band corresponding to S_0–S_1 transition decreases accompanied by the formation of a new charge transfer band in the absorption spectra. However in the case of compound **3**, *meta* connectivity prevents the effective conjugation between the

donor and acceptor and charge transfer band was not observed. The orbitals involved in the transition and the orbital features of **1-3** and their protonated forms were analysed using theoretical studies.

3.6. References

1. Grabowski, Z. R.; Rotkiewicz, K.; Rettig, W. *Chem. Rev.* **2003,** *103*, 3899.
2. Rudiger, W.; Constantina, P.; Robert, J. T.; Christian, G.; Christopher, R. M.; Paul, M. L.; Ralph, G. D.; Patricia, M. C.; Hans, H.; Julia, E. R.; Donald, M. B. *J. Chem. Phys.* **1996,** *105*, 10637.
3. Würthner, F.; Thalacker, C.; Matschiner, R.; Lukaszuk, K.; Wortmann, R. *Chem. Commun.* **1998,** 1739.
4. Beckmann, S.; Etzbach, K.-H; Krämer, P.; Lukaszuk, K.; Matschiner, R.; Schmidt, A. J.; Schuhmacher, P.; Sens, R.; Seybold, G.; Wortmann, R.; Würthner, F. *Adv. Mater.* **1999,** *11*, 536.
5. Barzoukas, M.; Runser, C.; Fort, A.; Blanchard-Desce, M. *Chem. Phys. Lett.* **1996,** *257*, 531.
6. Marder, S. R.; Gorman, C. B.; Tiemann, B. G.; Perry, J. W.; Bourhill, G.; Mansour, K., *Science* **1993,** *261*, 186.
7. Marder, S. R.; Cheng, L.-T.; Tiemann, B. G.; Friedli, A. C.; Blanchard-Desce, M.; Perry, J. W.; Skindhoj, J. *Science* **1994,** *263*, 511.
8. Marder, S. R.; Gorman, C. B.; Meyers, F.; Perry, J. W.; Bourhill, G.; Bredas, J.-L.; Pierce, B. M. *Science* **1994,** *265*, 632.

9. Gorman, C. B.; Marder, S. R. *Chem. Mater.* **1995,** *7*, 215.

10. Lu, D.; Chen, G.; Perry, J. W.; III, W. A. G. *J. Am. Chem. Soc.* **1994,** *116*, 10679.

11. Herbert, M. *Angew. Chem. Int. Ed.* **2005,** *44*, 2482.

12. Delgado, M. C. R.; Hernández, V.; Casado, J.; Navarrete, J. T. L.; Raimundo, J.-M.; Blanchard, P.; Roncali, J. *Chem.-Eur. J.* **2003,** *9*, 3670.

13. Meier, H.; Mühling, B.; Kolshorn, H. *Eur. J. Org. Chem.* **2004,** 1033.

14. Yamaguchi, Y.; Kobayashi, S.; Wakamiya, T.; Matsubara, Y.; Yoshida, Z.-i. *Angew. Chem. Int. Ed.* **2005,** *44*, 7040.

15. Thompson, A. L.; Ahn, T. S.; Thomas, K. R. J.; Thayumanavan, S.; Martinez, T. J.; Bardeen, C. J. *J. Am. Chem. Soc.* **2005,** *127*, 16348.

16. Lewis, F. D.; Yang, J. S. *J. Am. Chem. Soc.* **1997,** *119*, 3834.

17. Lewis, F. D.; Weigel, W.; Zuo, X. *J. Phys. Chem. A* **2001,** *105*, 4691.

18. Thompson, A. L.; Gaab, K. M.; Xu, J.; Bardeen, C. J.; Martinez, T. J. *J. Phys. Chem. A* **2004,** *108*, 671.

19. Lewis, F. D.; Weigel, W. *J. Phys. Chem. A* **2000,** *104*, 8146.

20. Gaab, K. M.; Thompson, A. L.; Xu, J.; Martinez, T. J.; Bardeen, C. J. *J. Am. Chem. Soc.* **2003,** *125*, 9288.

21. Elangovan, A.; Wang, Y. H.; Ho, T. I. *Org. Lett.* **2003,** *5*, 1841.

22. Coudret, C. *Synth. Commun.* **1996,** *26*, 3543.

23. Lee, C.; Yang, W.; Parr, R. G. *Phys. Rev. B* **1988,** *37*, 785.

24. Axel, D. B. *J. Chem. Phys.* **1993,** *98*, 5648.

25. Stratmann, R. E.; Gustavo, E. S.; Michael, J. F. *J. Chem. Phys.* **1998,** *109*, 8218.

26. Bauernschmitt, R.; Ahlrichs, R. *Chem. Phys. Lett.* **1996,** *256*, 454.

27. Mark, E. C.; Christine, J.; Kim, C. C.; Dennis, R. S. *J. Chem. Phys.* **1998,** *108*, 4439.

28. Zerner, M. C.; Gilda H. Loew, R. F. K.; Mueller-Westerhoff, U. T. *J. Am. Chem. Soc.* **1980,** *102*, 589.

29. Edwalds, W. D.; Zerner, M. C. *Theor. Chim. Acta* **1987,** *72*, 347.

30. Gaussian 03, V., Frisch, M. J.; Trucks, G. W.; Schlegel, H. B.; Scuseria, G. E.; Robb, M. A.; Cheeseman, J. R.; Montgomery, Jr. J. A.; Vreven, T.; Kudin, K. N.; Burant, J. C.; Millam, J. M.; Iyengar, S. S.; Tomasi, J.; Barone, V.; Mennucci, B.; Cossi, M.; Scalmani, G.; Rega, N.; Petersson, G. A.; Nakatsuji, H.; Hada, M.; Ehara, M.; Toyota, K.; Fukuda, R.; Hasegawa, J.; Ishida, M.; Nakajima, T.; Honda, Y.; Kitao, O.; Nakai, H.; Klene, M.; Li, X.; Knox, J. E.; Hratchian,H. P.; Cross,J. B.; Adamo, C.; Jaramillo, J.; Gomperts, R.; Stratmann, R. E.; Yazyev, O.; Austin, A. J.; Cammi, R.; Pomelli, C.; Ochterski, J. W.; Ayala, P. Y.; Morokuma, K.; Voth, G. A.; Salvador, P.; Dannenberg, J. J.; Zakrzewski,V. G.; Dapprich, S.; Daniels, A. D.; Strain, M. C.; Farkas, O.; Malick, D. K.; Rabuck, A. D.; Raghavachari, K.; Foresman, J. B.; Ortiz, J. V.; Cui, Q.; Baboul, A.

G.; Clifford, S.; Cioslowski, J.; Stefanov, B. B.; Liu, G.; Liashenko, A.; Piskorz, P.; Komaromi, I.; Martin, R. L.; Fox, D. J.; Keith, T.; Al-Laham, M. A.; Peng, C. Y.; Nanayakkara, A.; Challacombe, M.; Gill, P. M. W.; Johnson, B.; Chen, W.; Wong, M. W.; Gonzalez, C.; Pople, J. A., Gaussian, Inc., Pittsburgh PA, 2003.

CHAPTER 4

Synthesis and Photophysical Studies of Phenyleneethynylene Based Bipyridine Ligands and an Iridium Complex

4.1. Abstract

Two bipyridine derivatives possessing unsubstituted and methoxy substituted phenyleneethynylenes (**1** and **2**) and an iridium complex ($Ir(Phbpy)_2Cl_2$) were synthesized. The photophysical properties of these systems were investigated using various spectroscopic and theoretical techniques. Compounds **1** and **2** exist in its *trans* conformation and the absorption in these systems originate from a π-π^* transition. The methoxy substituted compound (**2**) possess higher quantum yield of emission ($\phi_f = 0.12$) compared to unsubstituted compound **1** ($\phi_f = 2.4 \times 10^{-3}$) and this is explained on the basis of highly emissive charge transfer state for **2**. Both the compounds exhibit monoexponential decay in acetonitrile with lifetimes of 1.5 ns for **1** and 2.3 ns for **2**. The triplet excited state properties of both the ligands were characterized using nanosecond laser flash photolysis studies and the lifetimes were found to be 22 μs (for **1**) and 10 μs (for **2**). On addition of H^+/Zn^{2+} ions to these compounds, the intensity of π-π^* transition decreases along with the formation of a red shifted band through a clear

isobestic point. The newly formed band at the longer wavelength region may be attributed to the polarization due to the complexation as well as conformational changes. Emission yield of the monoprotonated as well as Zn^{2+} complexed forms of **1** is much higher than the non-protonated form. The monoprotonated form of the molecule exists in a locked *cis* conformation through N-H^+--N bonding and the high emission yield of the *cis* conformation is attributed to its rigid structure which prevents the deactivation through non-radiative channels. The newly synthesized iridium complex possesses excellent luminescent properties; the quantum yield of luminescence of $Ir(Phbpy)_2Cl_2$ complex ($\phi_L = 0.30$) is found to be 4-fold higher compared to the corresponding iridium complex with 2,2'-bipyridine (ϕ_L of $Ir(bpy)_2Cl_2 = 0.075$) and the luminescence lifetime is found to be 0.9 μs.

4.2. Introduction

Design of molecular materials for various optoelectronic applications such as in organic light emitting devices (OLEDs) is an active area of research in this decade.[1-3] However, fine tuning the optical properties of such materials for various applications still remains a challenge. Molecular systems based on 2,2'-bipyridines and phenanthrolines[4] are ideal building blocks for the construction of such molecular materials due to their ability to (i) tune the photophysical properties by structural modification and (ii) complex with a wide range of metal cations.[5-7] The complexes based on 2,2'-bipyridines have been extensively used in

solar energy harvesting systems, photonic[8] and luminescent devices[9, 10] as well as in chiral molecular recognition.[11, 12]

4.2.1. Photophysical properties of bipyridines

Bipyridines are weakly fluorescent in nonaqueous solvents and an enhanced fluorescence is observed in water as well as in presence of protons and zinc ions.[13-15] The photophysics of bipyridines are complex in nature due to the (i) presence of very close lying $n\pi^*$ and $\pi\pi^*$ transitions, (ii) possibility of free rotation along the single bond connecting the two pyridine units and (iii) formation of aggregates at a concentration above 10^{-4} M.[16]

There are several conflicting reports in the literature regarding the photophysics of bipyridines.[13-15] For example, Harriman and coworkers reported a blue shift in the absorption spectra from ~340 nm in nonaqueous solvents to 325 nm in water with a substantial increase in quantum yield.[17] The change in fluorescence was attributed to the interplay of $n\pi^*$ and $\pi\pi^*$ orbitals, due to the variation in polarity. The authors have concluded that the enhanced emission of bipyridines in polar solvents originates from the $\pi\pi^*$ transition.

In another attempt to understand the enhanced emission in aqueous solution, Hoffman et al. proposed the formation of a covalent hydrate.[14, 15] The hydrated species can be deprotonated by adding a base which is accompanied by a decrease in fluorescence. Authors could not observe any fluorescence corresponding to di-protonated form in the nonaqueous solution which they

attribute to the rapid deprotonation in the excited state. Authors have concluded that the fluorescence of bipyridines in nonaqueous solvents as well as in acidic solutions originate from the $\pi-\pi^*$ transition and the low fluorescence quantum yield of bipyridine is attributed to the intersystem crossing or internal conversion.[14]

The photophysical properties of bipyridines were reinvestigated by Castellucci et al. and proposed that the fluorescence observed in aqueous medium may be due to the impurities present in water. They calculated the energy of the singlet and triplet states by theoretical methods and suggested that the fast intersystem crossing between the singlet and triplet states is responsible for the low fluorescence emission in these systems.[16] This was experimentally proved by sub-picosecond transient absorption studies of bipyridines; a decrease in the intensity of S_1-S_n transition with a concomitant increases in the intensity of the triplet-triplet absorption was observed with time.[18] Authors have also calculated the quantum yield of triplet state as 0.8 and the lifetime of the S_1 state as 64 ps in acetonitrile.

The geometric, electronic, vibrational and conformational analysis of 2,2'-bipyridine and its protonated forms have been examined using various theoretical and experimental methods.[19-22] 2,2'-bipyridine possesses a planar *trans*-configuration in the solid state and the dipole moment measurements have shown that they exist in a nearly planar arrangement with a dihedral angle of 20° in

solution.[23] The monoprotonated form of 2,2'-bipyridine possess *cis*-configuration and a weak hydrogen bond exists between the cationic hydrogen and other pyridine ring. The N-H^+--N bonding is strong enough to overcome the repulsion of the *ortho* hydrogens in the *cis*-conformation[20] and bond angle is calculated to be 108.5°. On complexation with metal ions, 2,2'-bipyridine adopts a planar *cis*-conformation and Wasielewski and coworkers have exploited the *cis-trans* conformational change for developing new sensory materials.[24]

Photophysical properties of bipyridines can be fine tuned by extending their conjugation and this chapter mainly describes our attempts to design luminescent bipyridine derivatives possessing phenyleneethynylenes and their iridium complex. A brief introduction on the photophysical properties of iridium complexes is presented below.

4.2.2. Introduction to iridium complexes

When potential is applied across the emissive layer of an organic light emitting diode (OLED), excitons are generated which recombines to emit light.[1] The excitons generated are of two kinds: singlet excitons and triplet excitons, of which the singlet excitons are only emissive. This in principle reduces the efficiency of the OLED to 25 % since the singlet to triplet ratio of exciton generation is 1:3. By doping transition metal complexes into the emissive layer, the triplet and singlet excitons can be mixed by spin–orbit coupling. Thus the triplet states become emissive thereby improving the efficiency of the layer by

several times. The efficiency of a metal centre to promote the mixing is indicated by its spin-orbit coupling constant.

Transition metal complexes, particularly iridium complexes, are gaining increased attention in recent years due to their high spin-orbit coupling constant. For example spin-orbit coupling constant value for iridium is 3909 cm^{-1} while that of ruthenium is 1402 cm^{-1} [25] Also, iridium complexes possess high luminescence quantum yield and excellent colour tuning ability. Colour tuning of the iridium complexes from orange-red to saturated red was achieved recently by varying the substituents on quinoline derivatives.[26]

It was demonstrated that the iridium complexes are promising candidates for labelling biomolecules (for example, luminescent bioconjugates of oligonucleotides or human serum albumin).[27, 28] Luminescence of mononuclear as well as dinuclear iridium complexes, immobilized on the polymer matrix are efficiently quenched by the presence of oxygen and are proposed as oxygen sensors.[29]

Although iridium complexes are considered as versatile candidates for various optoelectronic applications, there are only few reports on the synthesis and photophysical properties of iridium complexes with bipyridine based ligands.[30-33] It may be noted that most of the reports on iridium complexes are based on 2-phenylpyridine derivatives (cyclometalated iridium complexes).[34-37] The preparation of the complex of the type IrL_2Cl_2 with 2,2'-bipyridine ligands

have been first reported in 1969 by De Simone et al.[30] The electrochemistry of this iridium bipyridine complex has been reported by DeArmond.[31] A modified procedure of the preparation of $Ir(bpy)_2Cl_2$ by refluxing 2,2'-bipyridine with $IrCl_3.H_2O$ has been reported by Brewer et.al.[32] Recently luminescent properties of a series of iridium complexes with varying substituents have been reported.[33] A high quantum yield of 0.94 has been reported for an iridium complex with dimethyl bipyridine as ligand.[33] The synthesis of $Ir(bpy)_3^{3+}$ was first described by Martin et al. in 1958 by fusing K_3IrCl_6 and 2,2'-bipyridine for 20 min.[38] In 1974, Demas et al. prepared $Ir(bpy)_3^{3+}$ in 50 % yield by a different method.[39] A modified procedure which involves the substitution of the *cis*-$[Ir(bpy)_2(OSO_2CF_3)]^{2+}$ with 2,2'-bipyridine to yield $Ir(bpy)_3^{3+}$ in 85 % was reported by Meyer et al. in 1984.[40]

In this chapter we report the synthesis of two bipyridine derivatives possessing unsubstituted and methoxy substituted phenyleneethynylenes. The emission properties of these ligands are distinctly different and these aspects are described in detail. Complexation properties of these ligands are further exploited by synthesizing an iridium complex of the type IrL_2Cl_2 and their luminescent properties are reported.

4.3. Experimental Section

4.3.1. Materials and methods

The samples used for the study were purified by passing through recycling HPLC manufactured by Japan Analytical Industry Co., Ltd. All melting points are

uncorrected and were determined on an Aldrich melting point apparatus. ^{1}H NMR and ^{13}C NMR spectra were recorded on a Bruker DPX-300MHz spectrometer. High Resolution Mass spectra were recorded on a JEOL JM AX 5505 mass spectrometer. The UV-Vis spectra were recorded on a Shimadzu 2401 or 3101PC spectrophotometer. The emission spectra were recorded on a Spex-Fluorolog, F112-X equipped with a 450W Xe lamp and a Hamamatsu R928 photomultiplier tube. The spectra were recorded by keeping a 90° geometry and a band pass of 1 nm in the excitation and emission monochromators. Details of time correlated single photon counting fluorescence lifetime measurements were described in Section 2.3.1.

THF used was dried over sodium and diisopropylamine was dried over KOH. Solvents were deoxygenated by purging them with argon for 15 min, before using in the reaction. The final compounds were purified by passing through recycling preparative HPLC equipped with a UV as well as RI detector.

4.3.2. General method of synthesis

General scheme adopted for the synthesis of the ligands **1** and **2** are shown in Scheme 4.1. Synthesis of the ligand **1** has been reported by two different groups[41] and we have adopted a different procedure as shown in Scheme 4.1. Compounds **4**, **5** and **6** were prepared by following the reported procedure.[42]

Preparation of 4,4'-bis[(trimethylsilyl)ethynyl]-2,2'-bipyridine (7). To a solution of dibromo derivative **6** (300 mg, 1.0 mmol), $Pd(PPh_3)_2Cl_2$ (67.0 mg, 0.01

mmol) and CuI (18.1 mg, 0.02 mmol) in 6 mL triethylamine under stirring, was added (trimethylsilyl)acetylene (0.8 mL, 5.73 mmol). The mixture was refluxed for 6 h under argon. After removal of the solvent, the crude product was purified

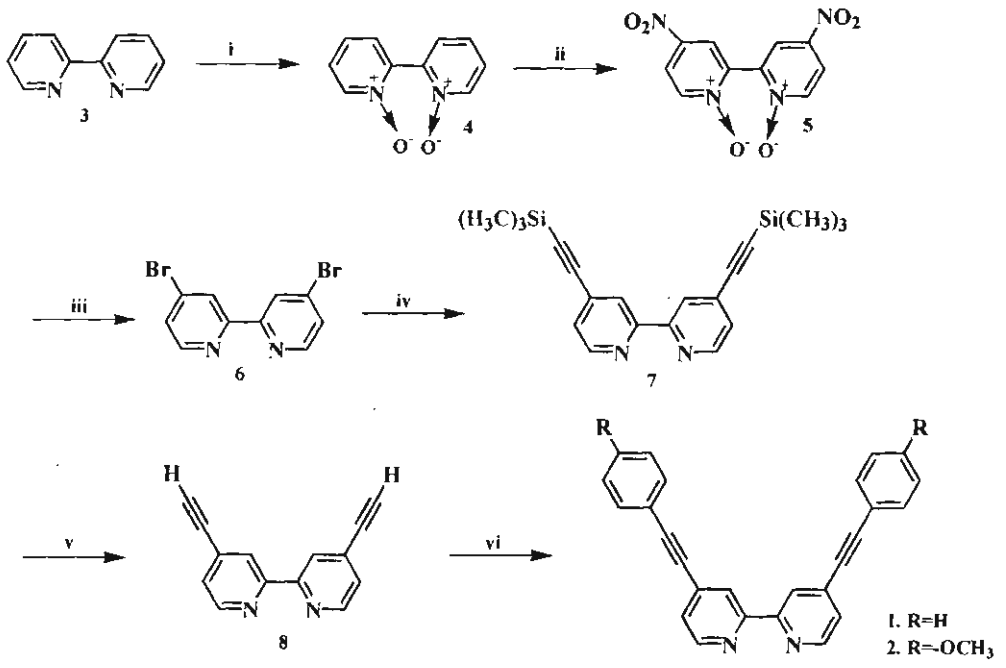

Scheme 4.1. (i) H_2O_2/AcOH; (ii) HNO_3/H_2SO_4; (iii) PBr_3,CH_3COBr; (iv) TMSA, CuI, $Pd(PPh_3)_2Cl_2$, Et_3N; v) NaOH, THF, CH_3OH; (vi) RC_6H_4I, CuI, $Pd(PPh_3)_2Cl_2$, $(i\text{-}pr)_2NH$, PPh_3

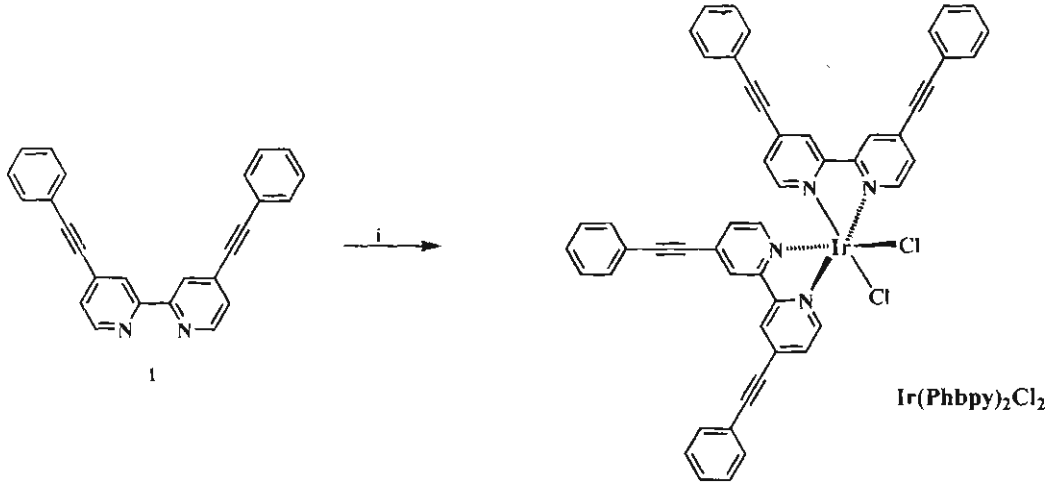

Scheme 4.2. (i) $IrCl_3$, ethylene glycol, 180 °C.

by column chromatography over basic alumina using toluene as eluent to yield 211 mg (63 %) of **7** as brown solid, mp. 119–121 °C. ^{1}H NMR (300MHz, $CDCl_3$): δ 8.60 (d, 2H), 8.43 (s, 2H), 7.30 (d, 2H), 0.23 (s, 9H). ^{13}C NMR (75 MHz, $CDCl_3$): δ 155.57, 149.07, 132.26, 125.72, 123.63, 102.37, 99.87, 96.18, 0.20. m/z (FAB) found 348.9 Calc. 348.6.

Preparation of 4,4'-bis(ethynyl)-2,2'-bipyridine (8). Silylated derivative **7** (280 mg, 0.08 mmol) was first dissolved in a mixture of THF (2.7 mL) and methanol (4.0 mL) and sodium hydroxide solution (0.3 mL of 5N) was added. The solution was stirred for 2 h, evaporated the solvent and extracted with chloroform. After drying over anhydrous Na_2SO_4 the solvent was removed to give **8** (150 mg, 91%), mp. 190 °C. m/z (FAB) found 205.52 (MH^+) Calc. 204.2. Compound **8** was directly used for the synthesis of **1** and **2** without purification).

Preparation of 4,4'-bis(phenylethynyl)-2,2'-bipyridine (1). A mixture of acetylene terminated monomer **8** (150 mg, 0.73 mmol), PPh_3 (38 mg, 0.14 mmol), $Pd(PPh_3)_2Cl_2$ (50 mg, 0.07 mmol), CuI (40 mg, 0.07 mmol) and C_6H_5I (167 μL, 1.6 mmol) was stirred at room temperature in 3 mL of diisopropylamine for 15 h. After removal of the solvent under reduced pressure, the crude product was purified by column chromatography over basic alumina using a mixture (1:19) of ethyl acetate and hexane to yield 136 mg (52 %) of **1** as white solid, mp. 202–204 °C. ^{1}H NMR (300 MHz, $CDCl_3$): δ 8.70 (d, 2H), 8.5 (s, 2H), 7.6-7.4 (m, 12H); ^{13}C NMR (75 MHz, $CDCl_3$): δ 149.02, 131.91, 131.96, 129.24, 128.50, 125.66,

23.45, 122.13, 94.46, 86.89. Exact mass calculated for $C_{26}H_{16}N_2$ (M^+) is 56.1313, found 356.0613 (EI high resolution mass spectrometry).

Preparation of 4,4'-bis[(4-methoxy)phenylethynyl]-2,2'-bipyridine (2). A ixture of acetylene terminated monomer **8** (60 mg, 0.29 mmol), PPh_3 (15 mg,)6 mmol), $Pd(PPh_3)_2Cl_2$ (20 mg, 0.03 mmol), CuI (6 mg, 0.03 mmol) and $_6H_4OMe$ (151 mg, 0.6 mmol) was stirred at room temperature in 3 mL of isopropylamine for 15 h. After removal of the solvent under reduced pressure, e crude product was purified by column chromatography over basic alumina ing a mixture (1:19) of ethyl acetate and hexane to yield 55 mg (45 %) of **2** as ite solid, mp. 209–211 °C. ^{1}H NMR (300 MHz, $CDCl_3$): δ 8.63 (d, 2H), 8.51 (s, I), 7.48 (d, 4H), 7.36 (d, 2H), 6.91 (d, 2H), 3.85 (s, 6H). ^{13}C NMR (75 MHz, DCl_3): δ 148.95, 133.56, 133.26, 125.42, 123.26, 114.17, 85.95, 55.35. Exact ass calculated for $C_{28}H_{20}N_2O_2$ (M^+) is 416.1525, found 416.1548 (EI high solution mass spectrometry).

Synthesis of Ir[(Phbpy)$_2$]Cl$_2$. A mixture of $IrCl_3.3H_2O$ (25 mg, 0.084 mmol) d **1** (90 mg, 0.25 mmol) was added to 4 mL of degassed ethylene glycol. The ixture was stirred at 180 °C under argon atmosphere in the absence of light for h. After cooling, the mixture was poured into an aqueous solution saturated with PF_6. The precipitate was allowed to settle overnight, filtered, washed with water d redissolved in chloroform. After drying over anhydrous Na_2SO_4, the solvent s evaporated to get the crude product. It was then purified by column

chromatography over neutral alumina using a mixture (1:3) of acetonitrile and toluene to yield **Ir[(Phbpy)$_2$]Cl$_2$** as yellow solid, the mass spectrum showed fragmentation peaks at m/z 975.1271 and 977.1004 (MALDI mass spectroscopy).

4.4. Results and Discussion

4.4.1. Photophysical investigation

Absorption and emission properties. The absorption spectra of both the ligands were recorded in solvents of varying polarity and remain more or less unchanged. Absorption spectrum of **1** and **2** recorded in acetonitrile is shown in Figure 4.1A. The absorption spectrum of **1** possesses well structured vibronic bands in acetonitrile with maximum around 300 nm. A bathochromic shift of 24 nm is observed for **2** (λ_{max}=324 nm), which may be due to the electron donating ability of methoxy group. The molar extinction coefficient of **1** and **2** at their corresponding absorption maxima were found to be 4.83 x 10^4 $M^{-1}cm^{-1}$ and 5.32 x 10^4 $M^{-1}cm^{-1}$, respectively.

The normalised emission spectra of the compounds **1** and **2** are presented in Figure 4.1B. Both the compounds showed structureless emission spectra with maximum at 360 and 423 nm, respectively. The Stokes shift for **1** and **2** in acetonitrile were calculated as 5821 cm^{-1} and 6883 cm^{-1}, respectively. The large Stokes shifts observed in these systems indicate that the change in geometry associated with the excitation of the molecules is considerable. Fluorescence excitation spectra of **1** and **2** collected at their respective emission maxima are

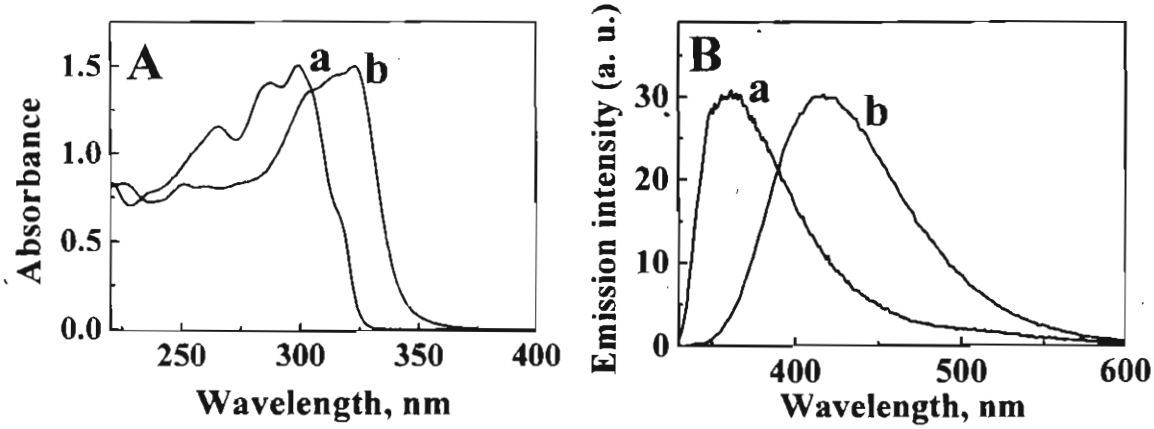

Figure 4.1 A) Absorption spectra of **1** (a) and **2** (b) and **B)** Emission spectra of **1** (a) and **2** (b) in acetonitrile.

shown in the Figure 4.2 and matches well with the peak positions in the corresponding absorption spectra. It is reported that the bipyridine compounds possess low emission in nonaqueous solvents.[15-17] Fluorescence quantum yield of both the compounds were determined in acetonitrile by the relative method using optically dilute solutions (absorbance at the exciting wavelength is 0.2) in comparison with quinine sulfate (ϕ_f=0.546). The quantum yields of **1** and **2** were

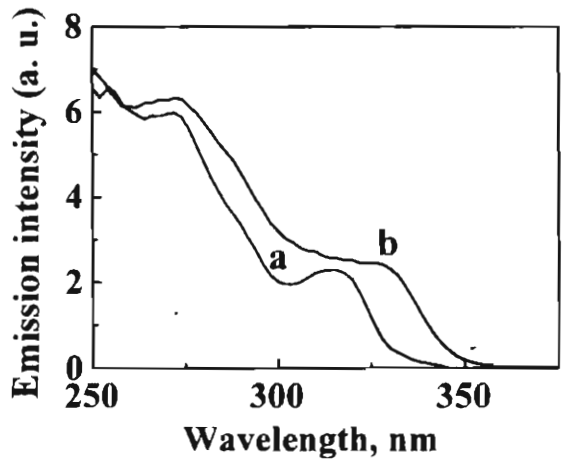

Figure 4.2. Excitation spectra of 1 (a) and 2 (b) in acetonitrile collected at 360 nm and 423 nm respectively.

Fluorescence lifetime measurements of **1** and **2** were carried out using single photon counting technique. Compounds were excited at 355 nm and the emission decays were followed at their respective emission maxima. Both the compounds exhibits monoexponential decay in acetonitrile with lifetimes of 1.5 ns for **1** and 2.3 ns for **2**.

Transient absorption spectra. The triplet excited properties of **1** and **2** were characterized using nanosecond laser flash photolysis experiments. The difference absorption spectra, recorded immediately after the laser pulse excitation, possess well defined band at 420 nm for **1** and 500 nm for **2** (Figure 4.3). These bands were readily quenched in oxygenated solution and attributed to the triplet-triplet absorption of the compounds. Lifetimes of the triplet excited states were estimated in deaerated acetonitrile by fitting the absorption-time decay curves to first-order kinetics. The triplet lifetimes of **1** and **2** were found to be 22 μs and 10 μs, respectively.

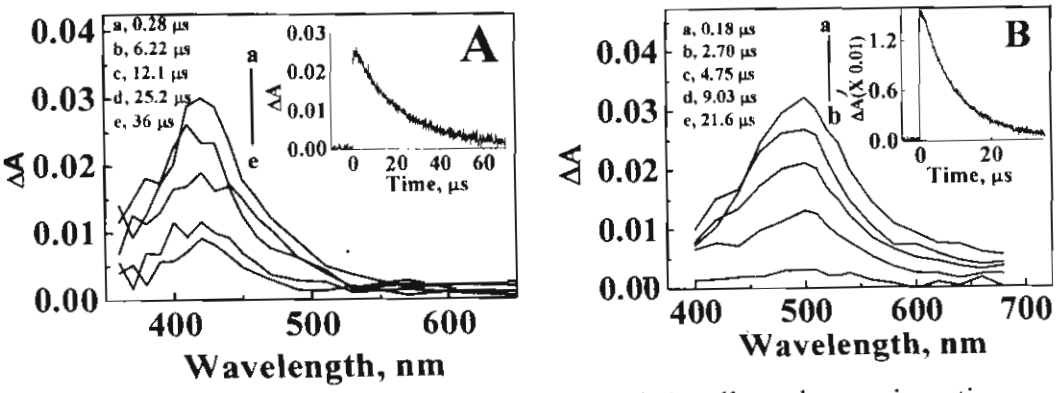

Figure 4.3. Transient absorption spectra of **A) 1** collected at various time intervals from 0.28 to 36 μs **B) 2** from 0.18 to 21 μs following 268 nm laser excitation (pulse width 5 ns). Inset of Figure 4.3A and 4.3B shows the absorption-time decay curves monitored at 450 and 550 nm, respectively.

Fluorescence and phosphorescence at low temperature. Emission spectra of **1** and **2** in acetonitrile were recorded at low temperature (77 K) where the molecular motions are more or less suppressed (Figure 4.4). Interestingly a large bathochromic shift was observed for both the compounds at 77 K. By decreasing the temperature, the emission maximum got shifted from 360 nm (298 K) to 410 nm (77 K) for **1** and from 423 nm (298 K) to 450 nm (77 K) for **2**. The large bathochromic shift observed in these compounds at low temperature may be due to the interchange of the energy levels involved in the transition. The emission from a lower energy state may become predominant by decreasing the temperature.

Phosphorescence spectra of the compounds were measured in a SPEX phosphorimeter equipped with a flash lamp. The signals from the sample, falling on the photomultiplier, are collected by a control module for a preset length of time. Solutions were thoroughly degassed before all measurements. The phosphorescence of **1** in methylcyclohexane showed a vibronically structured band with a maximum at 456 nm (Figure 4.4A) and that of **2** in acetonitrile appeared around 492 nm (Figure 4.4B). The phosphorescence intensity decay exponentially with first order kinetics with time t, obeying the equation (4.1),

$$\mathbf{I_t = I_0 \exp(-t/\tau)} \qquad \textbf{(4.1)}$$

where I_0 and I_t are the phosphorescence intensities at 'zero' time and time 't', respectively. The phosphorescence lifetime (τ) of both the compounds were estimated to be 0.8 ms.

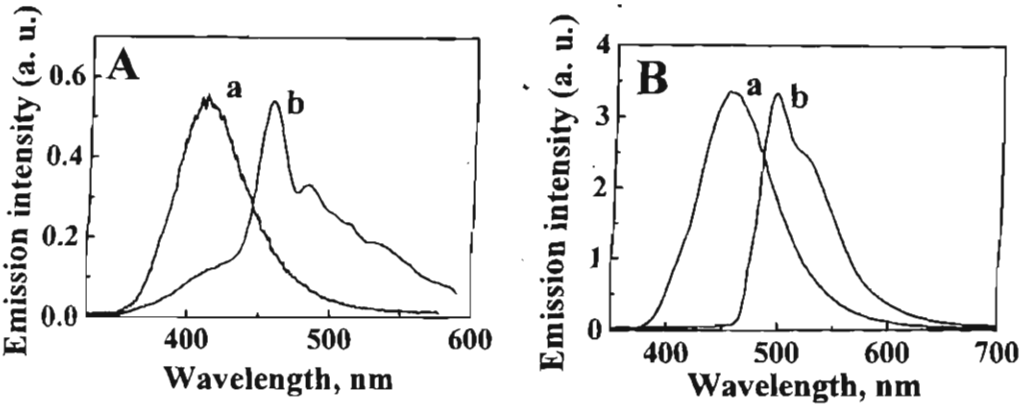

Figure 4.4. A) Fluorescence spectrum (a) of **1** recorded in acetonitrile and phosphorescence spectrum (b) of **1** recorded at 77 K in methylcyclohexane glass **B)** Fluorescence (a) and phosphorescence (b) spectra of **2** recorded at 77 K in acetonitrile.

4.4.2. Effect of complexation with H^+ and Zn^{2+} ions

Several conformers are possible for 2,2'-bipyridine in solution due to the free rotation of pyridine molecules along the carbon-carbon single bond and its complexation with protons and a variety of metal cations have been reported.[5-7] Complexation of **1** and **2** with Zn^{2+}/H^+ ions in acetonitrile brings about significantly different effects on their photophysical properties and these aspects are presented in this section.

It has been observed that the absorption as well as emission of **1** and **2** are highly sensitive to H^+ ions. In the present study, trifluoroacetic acid (TFA) was used for protonating the pyridyl nitrogens (Figure 4.5) and acetonitrile was used as the solvent. In the case of unsubstituted compound **1**, the absorption spectral features remain more or less unaffected at lower concentrations of TFA (< 2 equivalents). Interestingly, a decrease in absorbance of the vibronically structured band in the spectral region of 280-300 nm, accompanied by the formation of a

long wavelength band was observed with increase in the concentration of TFA (Figure 4.5A). These changes were marked by the presence of a clear isobestic point at 315 nm. The corresponding emission spectral changes are presented in Figure 4.5B. As mentioned earlier, compound **1** possesses an emission maximum at 360 nm with a very low quantum yield of 2.4×10^{-3}. Addition of TFA results in the lowering of emission intensity accompanied by the formation of an intense band at 512 nm through a clear isobestic point at 400 nm (Figure 4.5B). Interestingly, a dramatic increase in the quantum yield of fluorescence was observed in presence of TFA. For example, ϕ_f of **1** in presence of 100 equivalents of TFA is estimated to be 0.13; a 50 fold enhancement in the quantum yield.

Similar absorption spectral changes were observed on addition of TFA to methoxy substituted compound **2**. A decrease in the intensity of the absorption band centered around 321 nm and the formation of a new band with maximum at 380 nm was observed with a clear isobestic point at 336 nm (Figure 4.5C). Methoxy substituted compound **2** possesses an emission maximum at 423 nm with high emission quantum yield (ϕ_f =0.12) compared to **1** (Table 4.1). In contrast to the results obtained for unsubstituted compound **1**, a substantial decrease in emission quantum yield was observed for **2** on addition of TFA (Figure 4.5D). The quantum yield of **2** on addition of 100 equivalents of TFA was estimated as 2.8×10^{-3}.

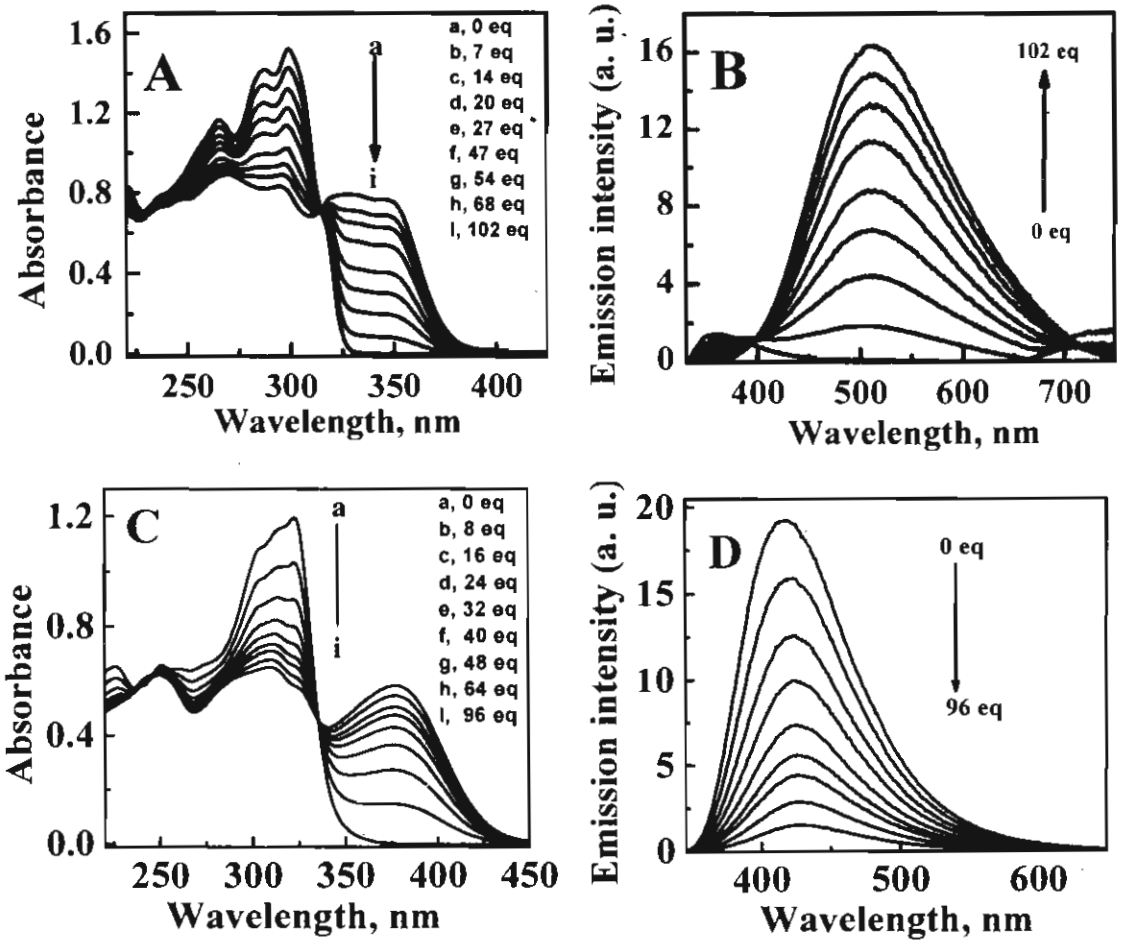

Figure 4.5. Absorption/emission spectral changes upon addition of TFA to a solution **1** and **2** in acetonitrile: **A)** absorption spectra of **1** on addition of TFA and **B)** the corresponding emission spectral changes; **C)** absorption spectrum of **2** on addition of TFA and **D)** the corresponding emission spectral changes.

Further, the changes in the intensity of absorption/emission for **1** and **2** were plotted against the equivalents of TFA added (Figure 4.6). These Figures clearly indicate that the intensity reaches saturation at higher molar equivalents of TFA (> 60 equivalents). It was already reported that on addition of protons, 2,2'-bipyridines initially form a monopotonated species which is stabilised by the weak

N-H$^+$--N hydrogen bonding. Di-protonation will take place only at very low pH and this will result in a hypsochromic shift in absorption.

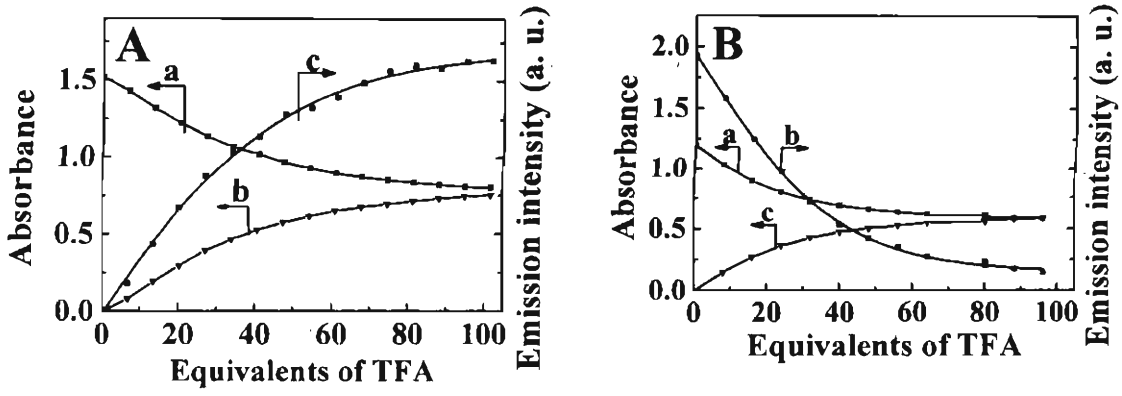

Figure 4.6. Plot of the absorption/emission intensity for **1** and **2** versus the equivalents of TFA added. **A)** absorption monitored at 299 nm (a) and 350 nm (b) and the emission at 514 nm (c) for **1** and **B)** absorption monitored at 323 nm (a) and 378 nm (b) and the emission at 418 nm (c) for **2**.

It is reported in the literature that Zn^{2+} ions form luminescent complex with 2,2'-bipyridine. We have further examined the effect of addition of Zn^{2+} ions on the absorption and emission properties of **1** and **2** and the spectral changes were similar to that observed for TFA (Figure 4.7). The quantum yield of fluorescence of **1** in presence of Zn^{2+} ions is much higher than the monoprotonated form. For example, in the presence of 10 equivalents of Zn^{2+}, ϕ_f is estimated as 0.33 (Figure 4.7B). As in the previous case, addition of Zn^{2+} ions to **2** results in decrease in emission intensity. In the presence of 10 equivalents of Zn^{2+}, ϕ_f is estimated as 1.6×10^{-3} (Figure 4.7D). Changes in the intensity of absorption and emission were plotted against the equivalents of Zn^{2+} ions and a sigmoid type plot was observed (Figure 4.8).

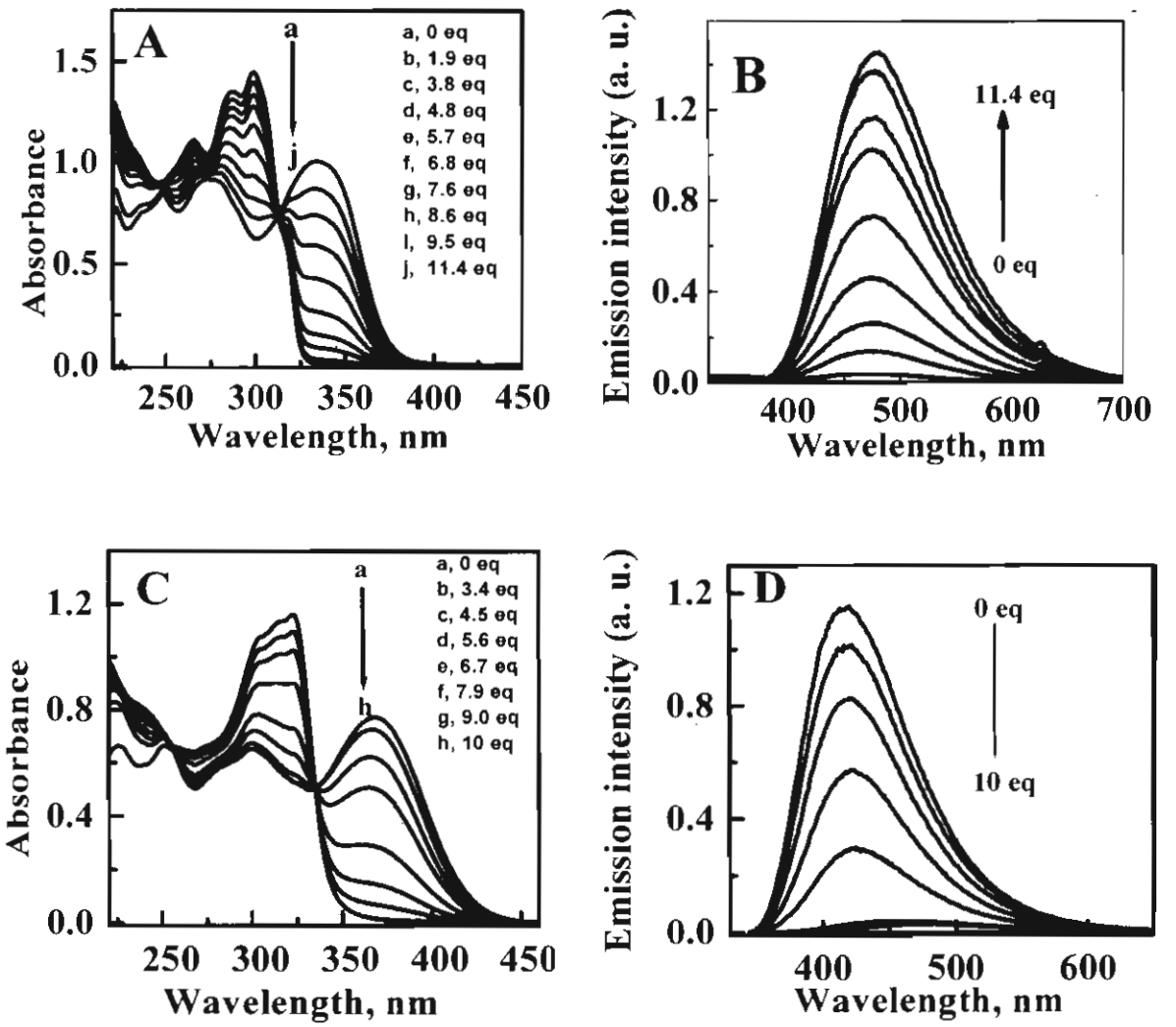

Figure 4.7. Absorption/emission spectral changes upon addition of Zn^{2+} ions to a solution of **1** and **2** in acetonitrile: **A)** absorption spectra of **1** on addition of Zn^{2+} ions and **B)** the corresponding emission spectral changes; **C)** absorption spectrum of **2** on addition of Zn^{2+} ions and **D)** the corresponding emission spectral changes.

Fluorescence lifetimes of **1** and **2** were measured by adding 100 equivalents of TFA and 10 equivalents of Zn^{2+} ions. The lifetimes were found to be much higher when coordinated to proton and metal ions. Fluorescence maximum (λ_{max}),

quantum yield (ϕ_f), and lifetimes (τ_s), of **1** and **2** in the absence and presence of H^+/Zn^{2+} ions are presented in Table 4.1.

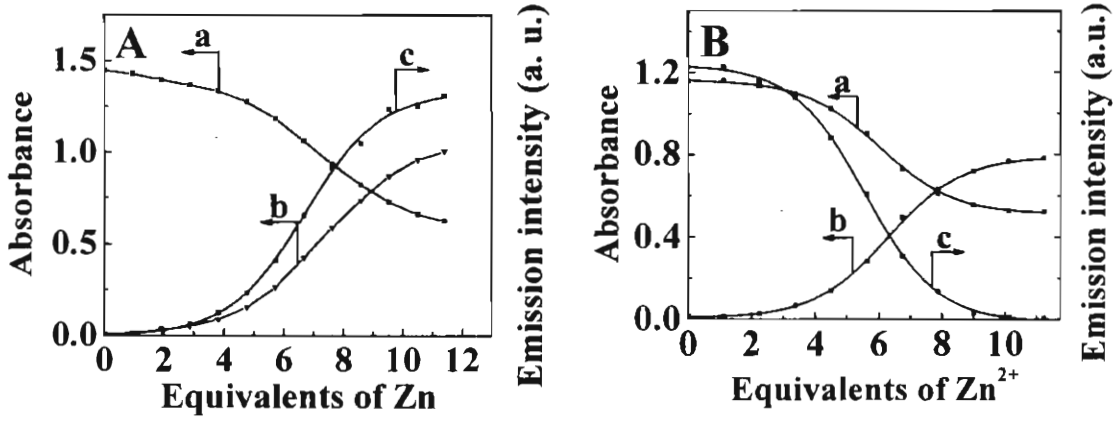

Figure 4.8. Plot of the absorption/emission intensity for **1** and **2** versus the equivalents of Zn^{2+} ions added. **A)** absorption monitored at 299 nm (a) and 335 nm (b) and the emission at 478 nm (c) for **1** and **B)** absorption monitored at 323 nm (a) and 378 nm (b) and the emission at 420 nm (c) for **2**.

Table 4.1. Photophysical properties of 1 and 2 in the absence and presence of H^+/Zn^{2+} ions in acetonitrile.

	λ_{em},(nm)[a,d]		ϕ_f[b,d]		τ_f(ns)[c,d]	
	1	**2**	**1**	**2**	**1**	**2**
-	360	423	2.4×10^{-3}	0.12	1.5	2.3
H^+ (100 eq.)	512	431	0.13	2.8×10^{-3}	3.5	1.7
Zn^{2+} (10 eq.)	484	494	0.33	1.6×10^{-3}	3.1	3.2

[a] fluorescence maxima; [b] fluorescence quantum yield; [c] fluorescence lifetimes; [d] error limit < 5%.

Theoretical studies clearly indicate that compounds **1** and **2** in acetonitrile exist in its *trans* conformation and the absorption originate from a π-π^* transition (Section 4.4.4.). Also we have confirmed from the theoretical studies that the

monoprotonated forms of **1** and **2** exist in its *cis* conformation, stabilized by a cationic hydrogen bond. The intensity of π-π^* transition decreases on addition of H^+/Zn^{2+} ions with the formation of a new band, absorbing in the red region (Figure 4.5A,C and Figure 4.7A,C). The clear isobestic point observed in the absorption spectra of **1** and **2** on addition of H^+/Zn^{2+} ions indicate the existence of the complexed as well as uncomplexed forms. The new band formed at the long wavelength region on addition of H^+/Zn^{2+} ions may be attributed to the polarization due to the complexation as well as conformational changes.

Emission yield of the monoprotonated as well as Zn^{2+} complexed forms of **1** is much higher than the non-protonated form. The non-protonated form of **1** exists mainly in its *trans* conformation in its ground state and several conformations are possible in its excited state. However, the monoprotonated form of the molecule exists in a locked *cis* conformation through N-H^+--N bonding. The high emission yield of the *cis* conformation is attributed to its rigid structure which prevents the deactivation through non-radiative channels.

Interestingly, methoxy substituted compound (**2**) possess higher quantum yield of emission ($\phi_f = 0.13$) compared to unsubstituted compound **1** ($\phi_f = 2.4 \times 10^{-3}$) and can be explained on the basis highly emissive charge transfer state for **2**. The charge transfer from methoxy to pyridyl moiety in the excited state leads to an emissive state, which is not possible in unsubstituted system **1**. Yamaguchi et al. have developed a general concept for developing (*p*-phenyleneethynylene)s based

emitters by introducing appropriate donor and acceptor groups.[37] Authors succeeded in the creation of highly efficient light emitters by suitable end modification such as introducing a methoxy-substituted benzene moiety as donor and a pyridine moiety as acceptor on OPE based molecules. They concluded that the emission efficiency depends on the existence of the dipolar structure in its excited state. In the present case, upon addition of H^+/Zn^{2+} ions, the emission yield of **2** decreases. Interestingly a nonemissive charge transfer state was observed in the case of **2** on adding H^+/Zn^{2+} ions, the excited state charge transfer ability of donor-acceptor increases for methoxy substituted compound and emission yield decreases due to enhanced decay through nonradiative channels.

The excitation spectra of both the compounds **1** and **2** were recorded in the absence and presence of H^+/Zn^{2+} ions in acetonitrile. Figure 4.9 shows the excitation spectra of **1** containing 10 equivalents of Zn^{2+} ions and 100 equivalents

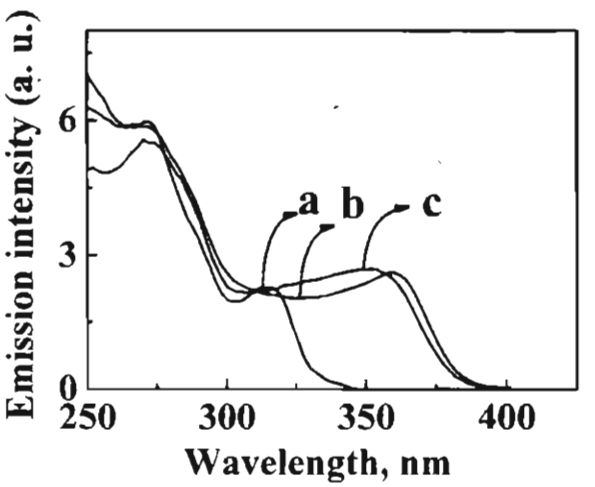

Figure 4.9. Excitation spectra of **1** in the absence and presence of TFA/Zn^{2+} ions: (a) **1** monitored at 370 nm; (b) **1** in the presence of 100 equivalents of TFA monitored at 500 nm; (c) **1** in the presence of 10 equivalents of Zn^{2+} monitored at 480 nm.

of TFA (in comparison with **1**). The excitation spectra recorded are similar to the corresponding absorption spectra (Figure 4.5A and Figure 4.7A) indicating that the emission originates from the complexed form.

Fluorescence and phosphorescence at low temperature in presence of TFA and Zn^{2+} ions. Fluorescence and phosphorescence spectra of **1** and **2**, in the presence of TFA (100 equivalents) and Zn^{2+} ions (10 equivalents), were recorded at low temperature in acetonitrile (Figure 4.10). We have observed a bathochromic shift of 50 nm for compound **1** in acetonitrile (from 360 nm to 410 nm) on decreasing the temperature to 77 K. In the presence of 100 equivalents of TFA, compound **1** emits at 512 nm (Figure 4.5B) which is blue shifted to 435 nm on decreasing the temperature to 77 K. Thus for **1** at 77 K, we observe a red shift in fluorescence whereas its protonated form show a blue shift. More detailed spectroscopic characterization is required, at low temperatures, for understanding this behavior.

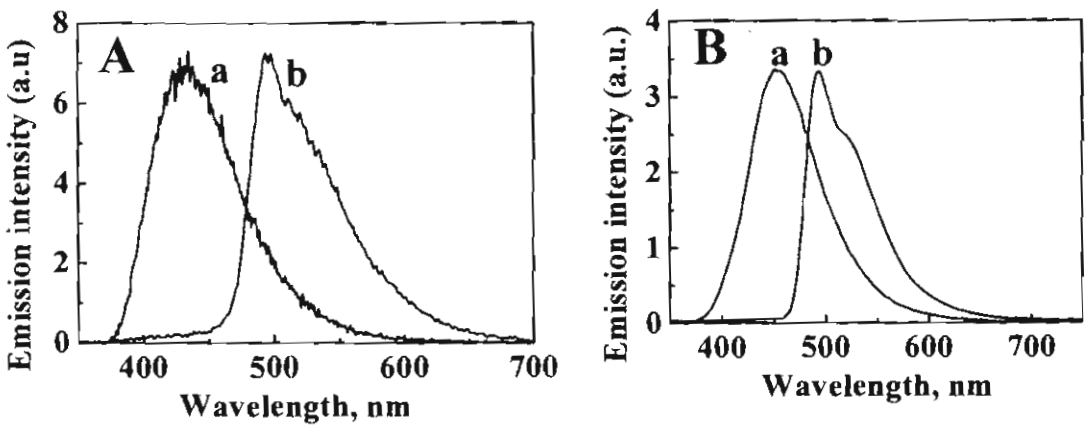

Figure 4.10. Fluorescence (a) and phosphorescence (b) spectra of **1** recorded at low temperature (77 K) in presence of: **A)** 100 equivalents of TFA **B)** 10 equivalents of Zn^{2+}.

Further we have compared the low temperature fluorescence and phosphorescence spectra of **1** and **2** in the presence of H^+/Zn^{2+} ions. In the presence of H^+/Zn^{2+} ions, the fluorescence (at 77 K) and phosphorescence band of **1** are well separated whereas in the case of **2** both the bands are close lying (Figures 4.10 and 4.11). These results indicate that both monoprotonated as well as the Zn^{2+} complexed forms of **2** have close lying S_1 and the T_1 energy levels (Figure 4.11).

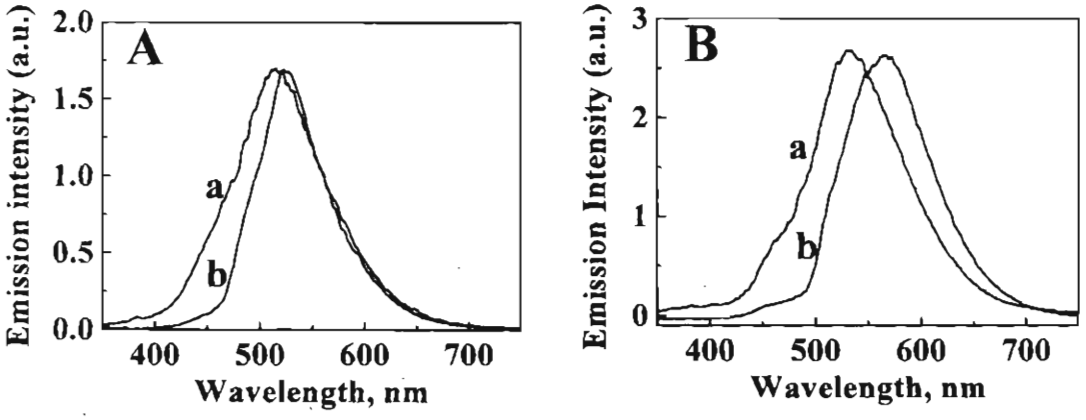

Figure 4.11. Fluorescence (a) and phosphorescence (b) spectra of **2** recorded at low temperature (77 K) in the presence of: **A)** 100 equivalents of TFA **B)** 10 equivalents of Zn^{2+}.

4.4.3. Photophysical characterization of $Ir(Phbpy)_2Cl_2$ complex

The photophysical properties of $Ir(Phbpy)_2Cl_2$ complex were characterized using steady state and time resolved spectroscopy. The absorption spectra of the $Ir(Phbpy)_2Cl_2$ and compound **1** (for comparison) were recorded in acetonitrile and presented in Figure 4.12A. The complex possesses two high energy bands at 285 nm and 322 nm and a low energy band at 415 nm. The spectral features of $Ir(Phbpy)_2Cl_2$ complex were compared with similar iridium complexes[33,43] and the

absorption spectrum of the ligand (**1**). Based on the comparison, the high energy bands are attributed to π-π^* transition of the ligand which is red shifted due to binding with the iridium. The weak absorption band at 415 nm is attributed to the metal to ligand charge transfer (MLCT) transition originating from the filled metal d orbitals to π^* orbital on the ligand, which is a forbidden transition.

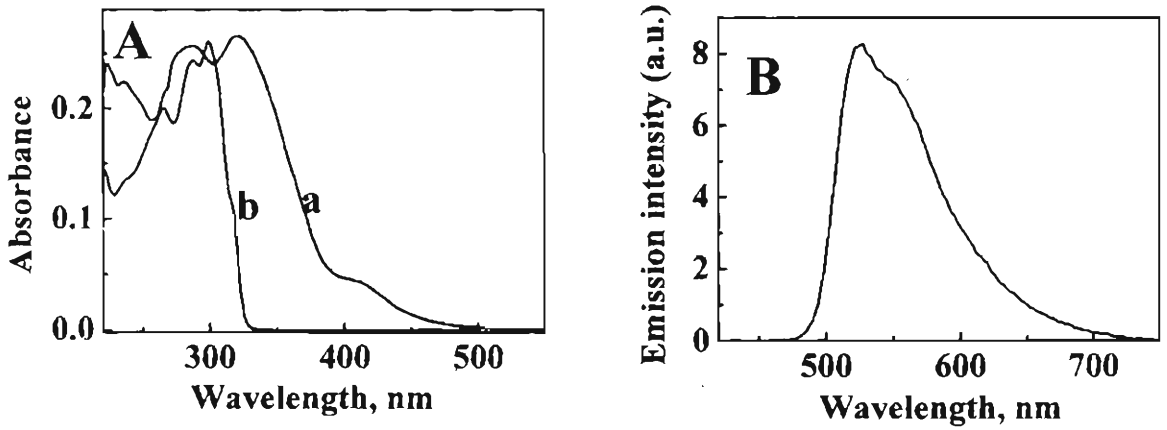

Figure 4.12. A) Absorption spectra of $Ir(Phbpy)_2Cl_2$ complex (a) in comparison with **1** (b) and **B)** the emission spectrum of the $Ir(Phbpy)_2Cl_2$ complex recorded in acetonitrile (degassed) at room temperature.

The emission spectrum of the complex is presented in Figure 4.12B and the maximum of the emission band appears at 528 nm. The quantum yield of luminescence of degassed solution of the $Ir(Phbpy)_2Cl_2$ in acetonitrile at room temperature is found to be high ($\phi_L = 0.30$) compared to the corresponding iridium complex with 2,2'-bipyridine (ϕ_L of $Ir(bpy)_2Cl_2$=0.075).[33] The luminescence lifetime collected by exciting at 400 nm is found to be high (0.9 μs). By considering the previous reports on similar systems,[43,44] luminescence of

$Ir(Phbpy)_2Cl_2$ complex may be ligand centered originating from the $^3(\pi\text{-}\pi^*)$ of the ligand.

The spectral features of the excitation spectrum (Figure 4.13A) of the complex collected at 528 nm were similar to the absorption spectrum. The phosphorescence spectrum (trace b in Figure 4.13B) of $Ir(Phbpy)_2Cl_2$ complex possesses a maximum at 600 nm. This transition may be originating from the triplet state of the MLCT band. The phosphorescence lifetime measurements showed the presence of two components; short lifetime component of 0.054 ms and long lifetime component of 0.27 ms.

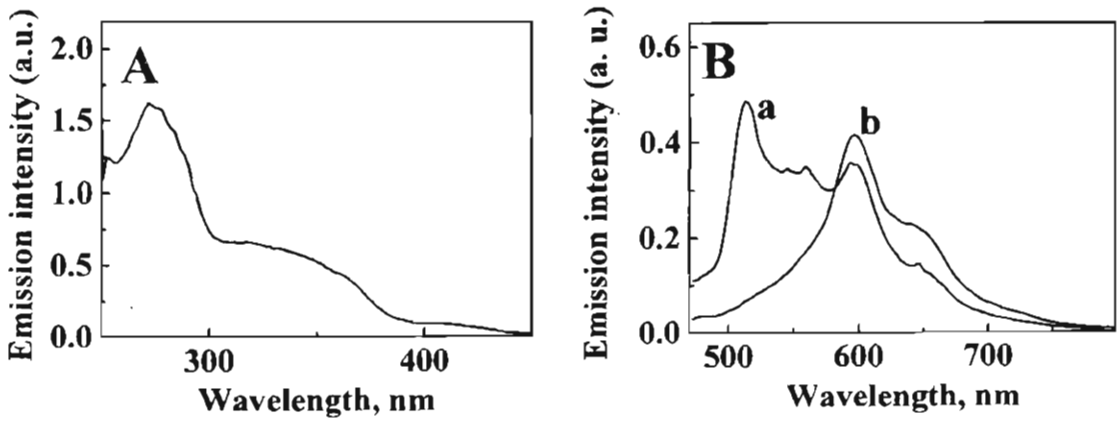

Figure 4.13. A) Excitation spectrum of $Ir(Phbpy)_2Cl_2$ collected at 524 nm in acetonitrile **B)** Emission (a) and phosphorescence (b) spectrum collected at 77 K in acetonitrile.

The emission spectrum of $Ir(Phbpy)_2Cl_2$ collected at low temperature is more or less an additive spectrum of phosphorescence (trace 'b' in Figure 4.13B) and room temperature luminescence (Figure 4.12B). At room temperature, the emission from the lowest emissive state can be predominant; however with decrease in temperature, emission from other states will also contribute due to lack

of solvent reorganization. More detailed spectroscopic characterization is required, at low temperatures, for characterizing various transitions.

4.4.4. Theoretical investigation

Phenyleneethynylene based bipyridine systems (**1** and **2** in Scheme 4.1) were optimized at B3LYP/6-31G* level density functional theory (DFT) methods.[45,46] The basic photochemical properties of these systems were investigated by means of quantum chemical calculations employing mainly the time-dependent density functional theory (TDDFT) formalism[47-49] as well as Zerner's intermediate neglect of differential overlap (ZINDO/S) method.[50] For all the calculations, Gaussian03[51] suit of programs were used.

It has been reported that bipyridines exist in nearly *trans* planar conformation in the solution and the X-ray crystallographic studies have revealed more or less similar arrangements in the solid state.[23] Repulsion between the lone pair on nitrogens destabilize the *cis* conformation of the bipyridines. A non planar conformation is obtained as local minimum for the *cis* conformation of both **1** (**1_cis**) and **2** (**2_cis**) with a carbon-nitrogen-nitrogen-carbon (CNNC) dihedral angle of around 34°. The energy difference between the most stable planar *trans* conformer and the non planar local minima of the *cis* conformer is calculated to be 3.5 kcal/mol for both the compounds (Figure 4.14).

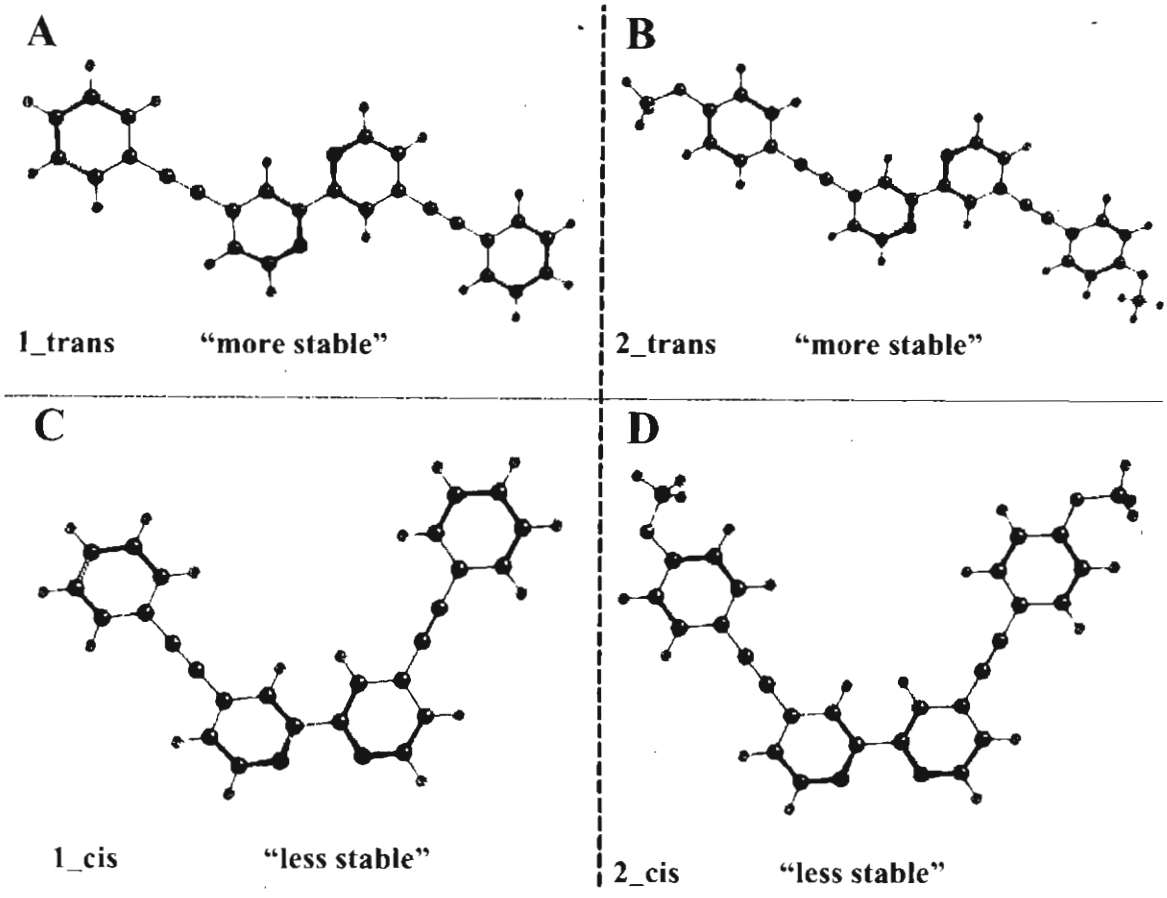

Figure 4.14. More stable *trans* conformers of **A) 1** and **B) 2** and local minimum structures obtained for **C) 1** and **D) 2** by B3LYP/6-31G* method in acetonitrile.

Conformational analysis of 2,2'-bipyridines also gave similar results with twisted geometry for the *cis* isomer and a completely planar conformation for *trans* bipyridine.[20] Solution state dipole moment measurements indicated a twist angle of 20° for bipyridines in the *trans* form.[23] The same deviation can be expected for phenyleneethynylene based systems **1** and **2** since the substituents at the 4,4′ positions do not influence the conformation of the molecule.

The conformational analysis of the monoprotonated form of **1** and **2** were also investigated using B3LYP/6-31G* method and the results were similar to that

of monoprotonated 2,2'-bipyridine.[20] Out of the two stable planar conformations of the monoprotonated form (**1_cis_H, 1_trans_H**), the most stable conformer is the *cis* conformation (**1_cis_H**). The energy difference between the *cis* and *trans* conformers is found to be about 3.4 kcal/mol. The energy required to overcome the repulsion of *ortho* hydrogens is gained from the extra stability attained by the --N-H^+--N- hydrogen bonding. This is more evident from the structural features of monoprotonated forms of **1** and **2** (Figure 4.15A), where the –N1-C1-C3- bond angle on the *cis* conformer is shorter with a value of 116° than the C2-C1-C3 bond angle (126°).

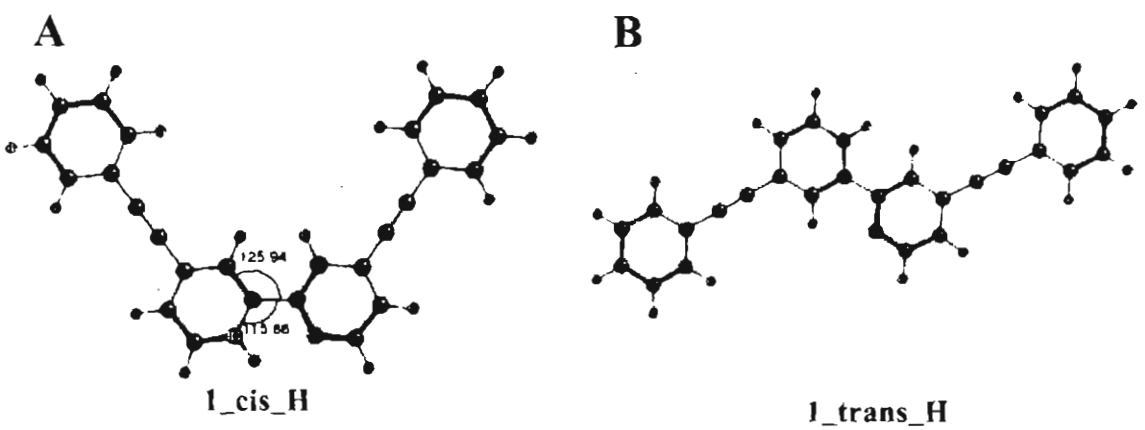

Figure 4.15. A) More stable cis conformation of protonated **1** and **B)** less stable trans conformer.

Using optimized geometries obtained by B3LYP/6-31G* level, the first 20 lowest lying excited states have been calculated at TDDFT and ZINDO/S levels. Calculated wavelength of transitions for **1** and **2** obtained by TDDFT method were in good agreement with the experimental values. For the protonated compounds (**1_cis_H** and **1_trans_H**) the TDDFT calculations were not in agreement with the

experimental values. The results obtained at the ZINDO and TDDFT level of theory were in good agreement for all the systems.

Analysis of the molecular orbitals eliminated the possibility of any charge transfer transition from the lone pair of nitrogen to π^* orbital (n-π^* transition). The transitions in the molecules are mainly π-π^* in nature. The molecular orbitals participating in the transitions of **1_trans** are depicted in Figure 4.16. The lowest allowed transition is from HOMO-1 to LUMO and the band appears at 318 nm with oscillator strength of 0.9640. Next higher energy absorption band is from HOMO to LUMO+1 which appears at 309 nm. The molecular orbital features of HOMO and HOMO-1 are similar in nature and they are very close in energy.

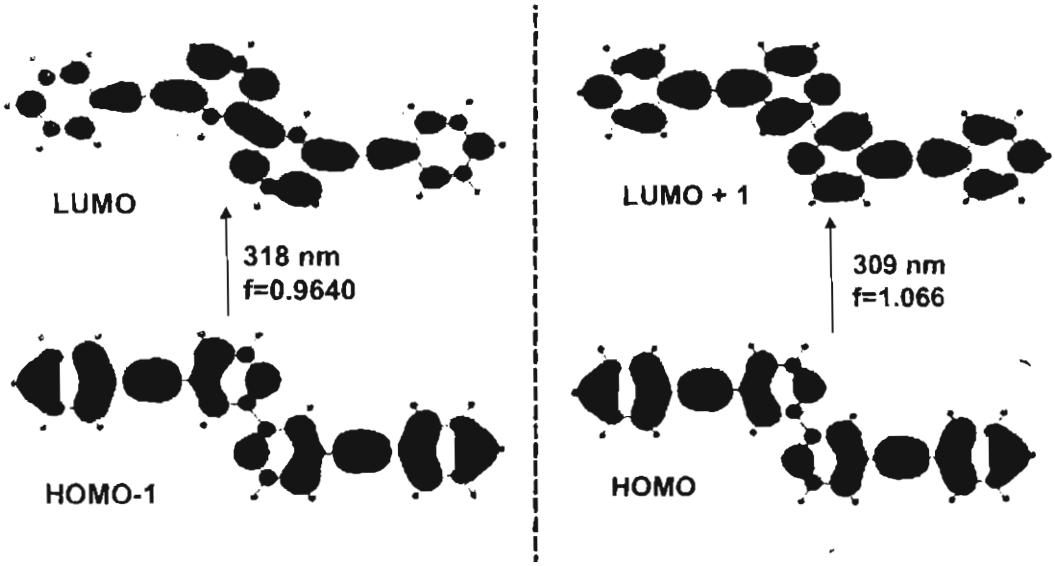

Figure 4.16. Molecular orbitals involved in the transition of **1_trans**.

The experimental absorption spectrum of **2** has a broad band with maximum at 324 nm. The calculated absorption spectrum possesses three peaks; lowest energy band appeared to be from HOMO-LUMO, with very weak

oscillator strength. Two other peaks with considerable oscillator strength appear at 337 nm and 326 nm respectively. The orbitals involved with the corresponding oscillator strength are shown in Figure 4.17.

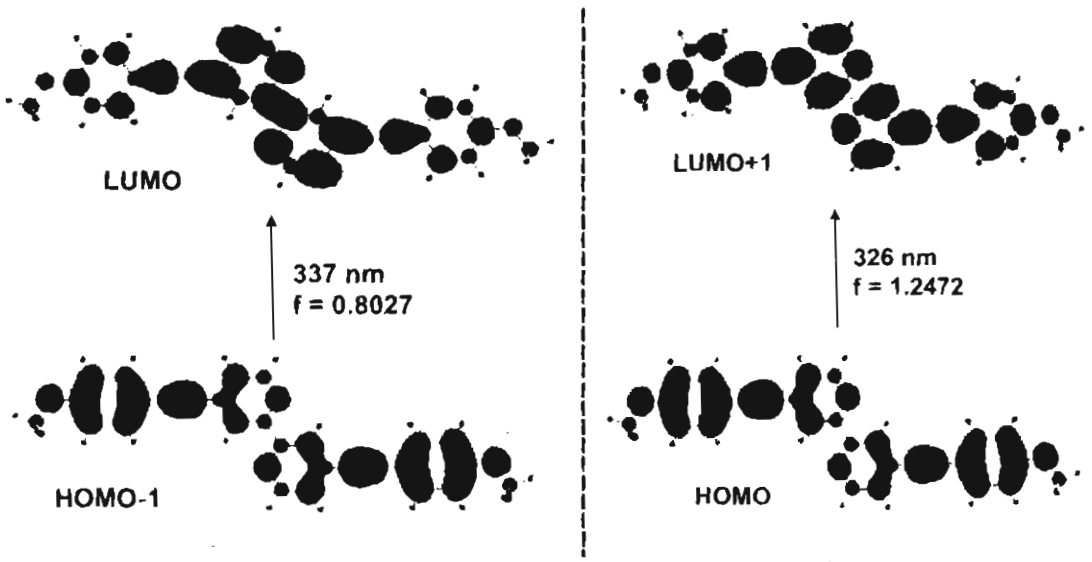

Figure 4.17. Molecular orbitals involved in the transition of **2_trans**.

From the molecular orbitals involved in the transition of both **1_trans** and **2_trans**, it can be seen that the excitation of the molecules causes a shift in the electron density from the phenyl rings to the bipyridine ring. But there is no complete charge transfer as observed in the case of push-pull donor-acceptor systems. The features of the HOMO and HOMO-1 in both the molecular systems are very similar and the energy difference between the MOs is very less. In both the cases the transition from HOMO to LUMO is less preferred with low oscillator strength. Comparing the molecular orbitals involved in the transition, it is evident that both the molecules behaves similarly and there is no involvement of the n-π^* orbitals in the transition.

Further to obtain an insight on the reversal of emission behavior of both the compounds in presence of TFA, molecular orbitals involved in the corresponding transitions were investigated for **1_cis_H** and **2_cis_H** (Figure 4.18). The transition energies obtained for the protonated form of both the systems are not in concordance with the experimental value. The TDDFT method showed a deviation of around 50 nm from the experimental value for the first transition. The four transitions originate from both HOMO and HOMO-2 out of which two transitions were of very low oscillator strength. These transitions showed a charge transfer nature which involves a complete transfer of electron density from the phenylethynyl arm towards the bipyridine core. Similar orbital features were observed for both the compounds **1_cis_H** and **2_cis_H**.

Further the probabilities for the existence of the triplet states were also analyzed by theoretical methods. As we know that the intersystem crossing becomes more efficient when the singlet and triplet states have comparable energies. In all the molecular systems under study, the triplet state exists in close proximity with the singlet state and the difference in emission behavior in both the cases could not be rationalized conclusively using theoretical techniques. From the molecular orbital analysis, we could eliminate the possibility of interplay of n-π^* and π-π^* transitions.

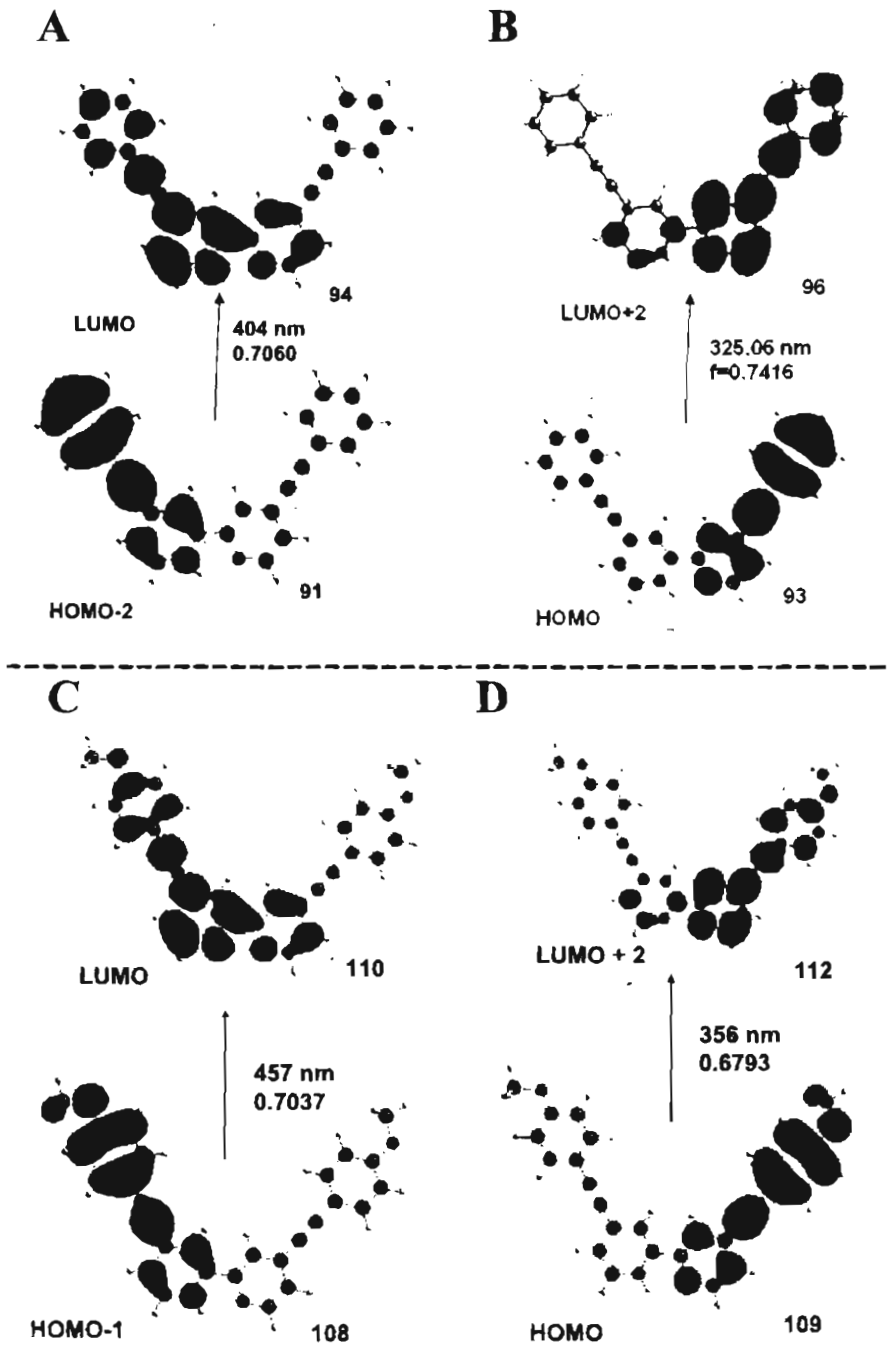

Figure 4.18. Molecular orbitals involved in the transition of **1_cis_H** and **2_cis_H.**

Transition state analysis. Recently, Grummt et.al. have reported the barrier of intramolecular proton transfer from one pyridine ring to another in the gas phase as 46.3 kJ/mol.[22] The transition state of monoprotonated forms, namely **1_cis_H** and **2_cis_H,** were determined and the distance of the proton from each pyridine ring was calculated to be 1.3 Å, in both cases. The energy barrier of proton transfer in both cases is around 44.7 kJ/mol and 44.8 kJ/mol, respectively. The structure of the proposed transition state for **1_cis_H** is shown below.

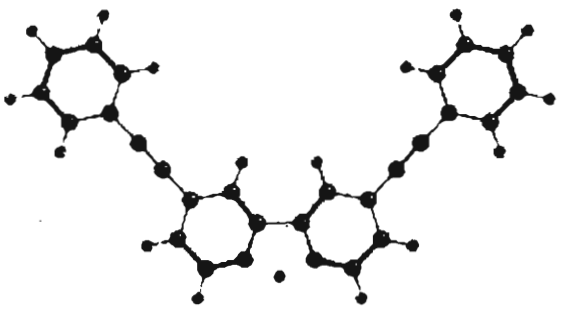

Figure 4.19. Transition state obtained for **1_cis_H.**

4.5. Conclusions

Two bipyridine derivatives bearing substituted phenyleneethynylene units (**1** and **2**) were synthesized and investigated their photophysical properties. Based on various experimental and theoretical investigations, we have concluded that the absorption in these systems originate from π-π* transition and any involvement of n-π* transition is ruled out. The high emission yield of methoxy substituted compound, **2** (ϕ_f = 0.12) compared to unsubstituted compound **1**, (ϕ_f = 2.4 x 10^{-3}) is attributed to the highly emissive charge transfer state of **2**. The intensity of π-π*

transition of **1** and **2** decreases on addition of H^+/Zn^{2+} ions along with the formation of a red shifted band. The newly formed band at the long wavelength region may be attributed to the polarization due to the complexation as well as conformational changes. Complex of **1** with H^+/Zn^{2+} ions is highly emissive due to the existence of a locked *cis* conformation that prevents the deactivation through non-radiative channels. The newly synthesized iridium complex ($Ir(Phbpy)_2Cl_2$) possesses excellent luminescent properties ($\phi_L = 0.30$; $\tau_L = 0.9$ μs) having potential application in optoelectronic devices.

4.6. References

1. Bredas, J. L.; Beljonne, D.; Coropceanu, V.; Cornil, J. *Chem. Rev.* **2004,** *104*, 4971.
2. Kido, J.; Okamoto, Y. *Chem. Rev.* **2002,** *102*, 2357.
3. Katsis, D.; Geng, Y. H.; Ou, J. J.; Culligan, S. W.; Trajkovska, A.; Chen, S. H.; Rothberg, L. J. *Chem. Mater.* **2002,** *14*, 1332.
4. Hima S. Joshi; Jamshidi, R.; Tor, Y. *Angew. Chem. Int. Ed.* **1999,** *38*, 2721.
5. Viau, L.; Bidault, S. b.; Maury, O.; Brasselet, S.; Ledoux, I.; Zyss, J.; Ishow, E. n.; Nakatani, K.; Bozec, a. H. L. *J. Am. Chem. Soc.* **2004,** *126*, 8386.
6. Renouard, T.; Bozec, H. L.; Brasselet, S.; Ledouxb, I.; Zyssb, J. *Chem. Commun.* **1999**, 871.

7. Tao, W. A.; Cooks, R. G. *Angew. Chem. Int. Ed.* **2001,** *40*, 754.

8. Kalyanasundaram, K.; Grätzel, M. *Coord. Chem. Rev.* **1998,** *177*, 347.

9. Ward, M. D.; White, C. M.; Barigelletti, F.; Armaroli, N.; Calogero, G.; Flamigni, L. *Coord. Chem. Rev.* **1998,** *171*, 481.

10. Balzani, V.; Juris, A.; Venturi, M.; Campagna, S.; Serroni, S. *Chem. Rev.* **1996,** *96*, 759.

11. Ulrich Knof; Zelewsky, A. V. *Angew. Chem. Int. Ed.* **1999,** *38*, 302.

12. Belser, P.; Bernhard, S.; Jandrasics, E.; von Zelewsky, A.; De Cola, L.; Balzani, V. *Coord. Chem. Rev.* **1997,** *159*, 1.

13. Kotlicka, J.; Grabowski, Z. R. *J. Photochem.* **1979,** *11*, 413.

14. Henry, M. S.; Hoffman, M. Z. *J. Phys. Chem.* **1979,** *83*, 618.

15. Henry, M. S.; Hoffman, M. Z. *J. Am. Chem. Soc.* **1977,** *99*, 5201.

16. Castellucci, E.; Angeloni, L.; Marconi, G.; Venuti, E.; Baraldi, I. *J. Phys. Chem.* **1990,** *94*, 1740.

17. Harriman, A. *J. Photochem.* **1978,** *8*, 205.

18. Buntinx, G.; Naskrecki, R.; Poizat, O. *J. Phys. Chem.* **1996,** *100*, 19380.

19. Oresmaa, L.; Haukka, M.; Vainiotalo, P.; Pakkanen, T. A. *J. Org. Chem.* **2002,** *67*, 8216.

20. Howard, S. T. *J. Am. Chem. Soc.* **1996,** *118*, 10269.

21. Ould-Moussa, L.; Castell`a-Ventura, M.; Kassab, E.; Poizat, O.; Strommen, D. P.; Kincaid, J. R. *J. Raman Spectrosc.* **2000,** *31*, 377.

22. Grummt, U.-W.; Erhardt, S. *J. Mol. Str.: THEOCHEM* **2004,** *685*, 133.

23. Cheng, C. L.; Murthy, D. S. N.; Retchie, G. L. *J. Chem. Soc. Faraday Trans. 2* **1972,** *68*, 1679.

24. Wang, B.; Wasielewski, M. R. *J. Am. Chem. Soc.* **1997,** *119*, 12.

25. Montali, M.; Credi, A.; Prodi, L.; Gandolfi, M. T. *Handbook of Photochemistry, Third Edition* **2006,** 619.

26. Zhao, Q.; Jiang, C. Y.; Shi, M.; Li, F. Y.; Yi, T.; Cao, Y.; Huang, C. H. *Organometallics* **2006,** *25*, 3631.

27. Lo, K. K. W.; Ng, D. C. M.; Chung, C. K., *Organometallics* **2001,** *20*, 4999.

28. Lo, K. K. W.; Chan, J. S. W.; Lui, L. H.; Chung, C. K., *Organometallics* **2004,** *23*, 3108.

29. Di Marco, G.; Lanza, M.; Mamo, A.; Stefio, I.; Di Pietro, C.; Romeo, G.; Campagna, S. *Anal. Chem.* **1998,** *70*, 5019.

30. DeSimone, R. E.; Drago, R. S. *Inorg. Chem.* **1969,** 2517.

31. Kahl, J. L.; Hanck, K. W.; DeArmond, K. *J. Phys. Chem.* **1978,** *82*, 540.

32. Rasmussen, S. C.; Richter, M. M.; Yi, E.; Place, H.; Brewer, K. J. *Inorg. Chem.* **1990,** *20*, 3926.

33. Yoshikawa, N.; Sakamoto, J.; Matsumura-Inoue, T.; Takashima, H.; Tsukahara, K.; Kanehisa, N.; Kai, Y. *Anal. Sci.* **2004,** *20*, 711.

34. Jung, S.; Kang, Y.; Kim, H.-S.; Kim, Y.-H.; Lee, C.-L.; Kim, J.-J.; Lee, S.-K.; Kwon, S.-K. *Eur. J. Inorg. Chem.* **2004**, 3415.

35. Kim, K. Y.; Farley, R. T.; Schanze, K. S. *J. Phys. Chem. B* **2006**, *110*, 17302.

36. Sun, Y. H.; Zhu, X. H.; Chen, Z.; Zhang, Y.; Cao, Y. *J. Org. Chem.* **2006**, *71*, 6281.

37. Zhao, Q.; Liu, S.; Shi, M.; Wang, C.; Yu, M.; Li, L.; Li, F.; Yi, T.; Huang, C. *Inorg. Chem.* **2006**, *45*, 6152.

38. Martin, B.; Waind, G. M. *J. Chem. Soc.* **1958**, 4282.

39. C. M. Flynn, J.; Demas, J. N. *J. Am. Chem. Soc.* **1974**, *96*, 1959.

40. Sullivan, B. P.; Meyer, T. J. *J. Chem. Soc. Chem. Commun.* **1984**, 403.

41. Birckner, E.; Grummt, U. W.; Goller, A. H.; Pautzsch, T.; Egbe, D. A. M.; Al-Higari, M.; Klemm, E. *J. Phys. Chem. A* **2001**, *105*, 10307.

42. Kavanagh, P.; Leech, D. *Tet. Lett.* **2004**, *45*, 121.

43. Collin, J. P.; Dixon, I. M.; Sauvage, J. P.; Williams, J. A. G.; Barigelletti, F.; Flamigni, L. *J. Am. Chem. Soc.* **1999**, *121*, 5009.

44. Ayala, N. P.; Flynn, C. M.; Sacksteder, J. L.; Demas, J. N.; DeGraff, B. A. *J. Am. Chem. Soc.* **1990**, *112*, 3837.

45. Lee, C.; Yang, W.; Parr, R. G. *Phys. Rev. B* **1988**, *37*, 785.

46. Axel, D. B. *J. Chem. Phys.* **1993**, *98*, 5648.

47. Stratmann, R. E.; Gustavo, E. S.; Michael, J. F. *J. Chem. Phys.* **1998,** *109*, 8218.

48. Bauernschmitt, R.; Ahlrichs, R. *Chem. Phys. Lett.* **1996,** *256*, 454.

49. Mark, E. C.; Christine, J.; Kim, C. C.; Dennis, R. S. *J. Chem. Phys.* **1998,** *108*, 4439.

50. Zerner, M. C.; Gilda H. Loew, R. F. K.; Mueller-Westerhoff, U. T. *J. Am. Chem. Soc.* **1980,** *102*, 589.

51. Gaussian 03, V., Frisch, M. J.; Trucks, G. W.; Schlegel, H. B.; Scuseria, G. E.; Robb, M. A.; Cheeseman, J. R.; Montgomery, Jr. J. A.; Vreven, T.; Kudin, K. N.; Burant, J. C.; Millam, J. M.; Iyengar, S. S.; Tomasi, J.; Barone, V.; Mennucci, B.; Cossi, M.; Scalmani, G.; Rega, N.; Petersson, G. A.; Nakatsuji, H.; Hada, M.; Ehara, M.; Toyota, K.; Fukuda, R.; Hasegawa, J.; Ishida, M.; Nakajima, T.; Honda, Y.; Kitao, O.; Nakai, H.; Klene, M.; Li, X.; Knox, J. E.; Hratchian,H. P.; Cross,J. B.; Adamo, C.; Jaramillo, J.; Gomperts, R.; Stratmann, R. E.; Yazyev, O.; Austin, A. J.; Cammi, R.; Pomelli, C.; Ochterski, J. W.; Ayala, P. Y.; Morokuma, K.; Voth, G. A.; Salvador, P.; Dannenberg, J. J.; Zakrzewski,V. G.; Dapprich, S.; Daniels, A. D.; Strain, M. C.; Farkas, O.; Malick, D. K.; Rabuck, A. D.; Raghavachari, K.; Foresman, J. B.; Ortiz, J. V.; Cui, Q.; Baboul, A. G.; Clifford, S.; Cioslowski, J.; Stefanov, B. B.; Liu, G.; Liashenko, A.; Piskorz, P.; Komaromi, I.; Martin, R. L.; Fox, D. J.; Keith, T.; Al-

Laham, M. A.; Peng, C. Y.; Nanayakkara, A.; Challacombe, M.; Gill, P. M. W.; Johnson, B.; Chen, W.; Wong, M. W.; Gonzalez, C.; Pople, J. A., Gaussian, Inc., Pittsburgh PA, 2003.